

NASA TECHNICAL TRANSLATION

NASA TT F- 12,731

Page One Title

**SCHLIEREN METHODS
AND THEIR APPLICATIONS**

H. Schardin

Ergebnisse der Exakten Naturwissenschaften
Vol. 20, pp. 303-439, 1942

Cover Page Source

(b1)

FACILITY FORM 800

N70-25586

(ACCESSION NUMBER)

(PAGES)

(NASA OR OR TXN OR AD NUMBER)

(THRU)

(CODE)

(CATEGORY)

NATIONAL AERONAUTICS AND SPACE ADMINISTRATION
WASHINGTON, D. C. 20546
APRIL 1970

Even

Roman

Odd

SCHLIEREN METHODS AND THEIR APPLICATION

H. Schardin

Cover Page Title

ABSTRACT: This paper presents an exhaustive review of the schlieren method and its applications. The author starts out with the historical development and description of similar methods. He describes applications and techniques used in such areas as geology, physics, chemistry, etc. Many examples are given and explained in detail with pictures of actual exposures of schlieren and associated phenomena in a multitude of materials and their practical application. Extensive use is also made of rigorous mathematical proof to determine the validity of equations and their operators.

Cover Page Source

1. The Definition of a Schlieren

/304*

If there are points in a translucent homogeneous medium at which the index of refraction varies somewhat from its nominal value, these points are called "schlieren". Light falling upon the medium is deflected at small angles. The magnitude of the deflection depends not only on the change Δn of the schlieren refraction index, but also on its shape. Light deflection can also occur if there is no change in the refraction index, e.g. if the surface of a glass plate deviates slightly from its nominal value. Contrary to the definition of schlieren commonly found in glass technology, where only points where the refraction index is changed are considered as schlieren, our concept of schlieren will include a larger area:

The cause of any light deflection restricted to a small area will be considered a schlieren.

In this sense a moving sound wave intensive enough to cause an appreciable light deflection is a schlieren.

Striations in machine glass, based only on a change in glass thickness, are also to be considered schlieren. However, if a pane of glass has a wedge defect, meaning that both sides are smooth but not parallel to each other, it is not a schlieren despite the slight deflection of light, since the deflection is not confined to a small area.

Other examples of schlieren are: air rising from heaters; inhomogeneities in salt solutions or in a mixture of two gases; head and tail waves; and the turbulent wake of a flying projectile.

NASA

*Numbers in the margin indicate pagination in the foreign text.

2. The Nature of the Schlieren Method

Schlieren methods are used at the present time to visualize, observe, photograph or make photoelectric records and measure small light deflections. In the past they could be used only to identify the existence and position of schlieren, but today we are able to measure quantitatively the amount of light deflection and in some cases to deduce the physical condition of the schlieren from this.

In addition, schlieren methods can be advantageously used to record small light deflections, e.g., to investigate the deformation of a reflecting surface by reflecting light under the influence of certain forces.

3. Seeing Schlieren with the Naked Eye

The concept of schlieren is an outgrowth of normal experience. Schlieren can be seen with the naked eye in a windowpane, above a heater or above railroad tracks on a hot summer day; there are also other examples of them. It is not always necessary to use a physical instrument to recognize them. What does seeing schlieren with the naked eye depend upon? Let us pick up a piece of glass plate with streaks and try to hold it so that the schlieren can be seen most distinctly. If we look through the glass plate toward the uniform light of the sky, we do not discern anything; however, some leisurely experimenting can place the glass plate at the boundary between a light and a dark surface. With the glass plate in this position it is easy to recognize schlieren because the light deflection of the schlieren will show light spots against the dark background and dark spots against the light background (Figure 1). If the glass plate is moved back and forth, the schlieren can easily be seen on the entire surface of the plate. Because of the light deflected in the schlieren, straight lines become distorted when seen through the glass plate. This is often unpleasantly noticeable in windowpanes. Seen through a window with gross flaws, a straight flag pole looks as if it has buckled (Figure 2). When the eye is moved, the pole appears to move because the light rays forming the image in the eye pass through continuously changing spots in the glass and this causes various degrees of light deflection. In this way schlieren become very noticeable; however, good pictures of them cannot be taken for two reasons: it is impossible to concentrate upon the object and the plate glass at the same time; the presence of schlieren can be recognized only in a few places from one eye position.

Hot air schlieren rising from a hot object are recognized by background distortion. In this case schlieren movement produces a shimmering effect even though the eye is at rest.

Although coarse schlieren can be observed with the naked eye, the construction of special instruments is necessary for more accurate observation, particularly if quantitative measurements are required.

NASA

/305

/306

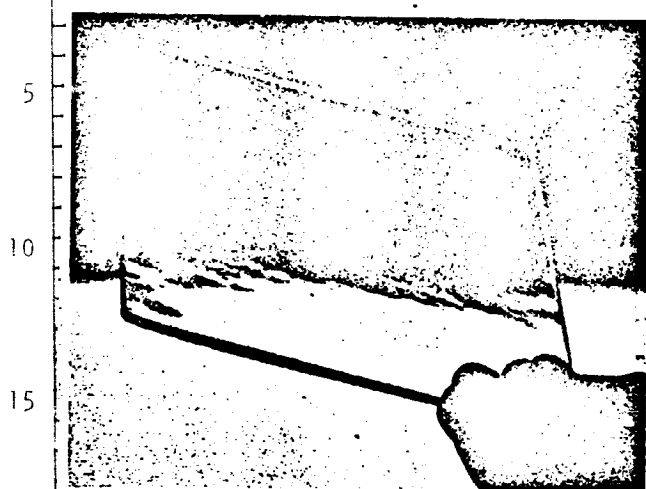


Figure 1. To Observe Schlieren in a Glass Plate, Hold the Plate Between the Eye and the Boundary of a Light and a Dark Surface.

1. Schlieren Methods with Optical Representation of the Schlieren

4. Schlieren Method Number 1

In addition to the Toepler schlieren method and the Dvorak shadow method, which have generally been considered the schlieren methods up to the present time, quite a number of other methods are available for visualizing schlieren. They will be numbered consecutively in this paper. Not all of these methods are of great importance, but there will occasionally be cases where a particular method is especially suitable because there are so many applications the schlieren methods. Moreover, for systematic reasons it has seemed inadvisable to list them all here because many of them have not been published elsewhere.

Imitation of the method described above for recognizing schlieren with the naked eye leads to the following arrangement (schlieren method number 1).

In Figure 3 S represents the schlieren under investigation; objective O produces its image on S'. Light coming from illuminating surface L passes through it. B is a straight edge which restricts the light source to the optical axis, so that only light above it can shine freely. The camera Ka corresponds to the eye and B to a dark patch in front of the bright sky (L). What kind of image can be expected in S'? The lower half in S' will appear bright because it receives light from L, but the top half will be dark. The transition is not very sharp because B must be represented without sufficient depth as a result of the limited aperture of the image. If a slit diaphragm B' is placed in front of O, the transition can be sharpened by narrowing the diaphragm. But now, a light deflection shows up in the schlieren, i.e., the light-dark transition in the image is not a straight line, but is more or less bent according to the kind of schlieren; dark spots will be present in the light part and vice versa, light spots will be present in the dark part. As an example, the image of point P of the schlieren will lie in the dark part, because the latter lies in front of diaphragm B. If a light deflection occurs in P by an angle ϵ , light from light source L will still contribute to the image of this point and it will appear bright. In the light-dark transition zone the schlieren therefore becomes visible. Figure 1 was obtained by this method. By limiting this narrow but long region with a diaphragm B'' and moving B'' with B, so that both rotate around the internal perspective center of the lens, the schlieren of the object becomes successively visible. The

movement of the diaphragms is identical to scanning a schlieren with the naked eye, as described above. A photograph of fixed objects could easily be made with this method. For stationary observation of the entire surface, movement would have to take place so fast that the eye would receive a stationary impression; this could certainly be achieved by using an electrical motor.



Figure 2. View Through Window Glass With Distortion Shows Straight Lines as Bent. (Left Side-Window Open, Right Side-Through Double Glass).

streaks which are more or less bent. There will be cases where this simple arrangement can be applied directly. Figures 5a and 5b represent two pictures taken by this method. In it the defects in a glass plate and in a water glass can be distinguished very well [126].

The following process can be used to bring out the streaks: in the same arrangement, but without schlieren, a photographic plate is exposed; after being developed and dried, this is used to cover the streaks of light and is placed carefully in the camera; the plate to be exposed is placed against it, emulsion to emulsion. In this way complete darkness without schlieren is obtained. The schlieren will bring out the light over the dark streaks of the coverplate and brightness will be found at these spots. The same result can

With moving phenomena the diaphragms must move appropriately faster. However, this requirement can only be fulfilled up to a certain speed of the phenomena occurring in the object under observation.

5. Schlieren Method Number 2

In schlieren method number 1 we worked with a light-dark edge, by means of which the schlieren along a narrow strip were made visible. Investigation of the complete image field could be achieved by moving the lighted edge and limiting the diaphragm field. Instead of this, it seemed that a large number of individual edges could be used (Figure 4).

In this arrangement the schlieren would become visible along each edge, as described in the previous section. The field of vision is crossed by

be obtained in copying by using the coverplate with the streaks between the original negative and the photographic paper.

/309

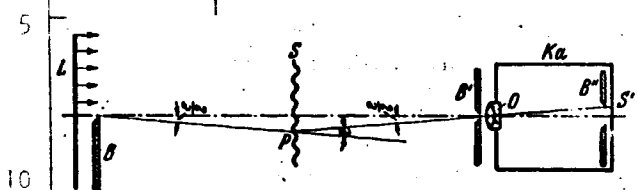


Figure 3. Schematic for the Observation of Schlieren with the Naked Eye (Schlieren Method Number 1).

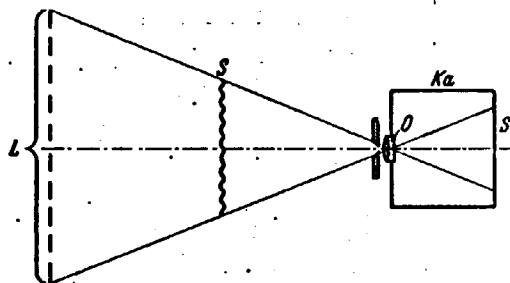


Figure 4. Schematic Arrangement for Schlieren Method Number 2.

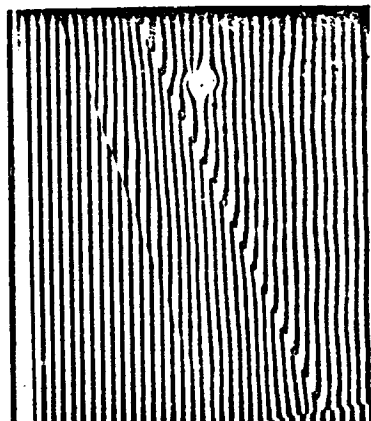


Figure 5a.

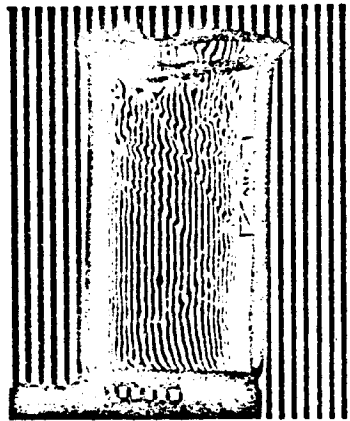


Figure 5b.

Figures 5a and b. Photographs With Schlieren Process Number 2: a, Plate Glass; b, Water Glass.

However, if the deflection is larger than the width of a streak, the deflected light must again be stopped down. This must be taken into account in discussing the pictures obtained, as must the fact that no steady pictures of schlieren are taken.

6. Schlieren Method Number 3

The construction principle of schlieren method number 2 also provides another way of making schlieren visible. In Figure 6 let a represent a surface radiating white light, while b' , b'' , c' , c'' , etc. represent surfaces which radiate light of different colors. As seen from B , specimen S should not be so large that it exceeds surface a . For the sake of uniformity, let distances LS and SB be of the same magnitude ($= t$). Now for instance, if the center of the schlieren deflects the incident light by angle ϵ , the center of

/310

object as seen from B contains light from surface b', and therefore appears in colored light. In this way every color corresponds to a definite light deflection in the object. If there is a definite expansion of the object, surface a radiating white light should be twice as large in accordance with Figure 6; moreover, if a definite sensitivity of arrangement is required (i.e. the first color in the object must appear at a definite angle ϵ), distance t is found. In principle it would be possible to use this arrangement for large objects and great sensitivity, but then the light would have to travel extremely long distances.

For example, if

$$d = 25 \text{ cm,}$$

$$\epsilon = 0.00291 - 10 \text{ min.}$$

are required, then

$$t = \frac{3.25}{0.00291} \text{ cm} = 258 \text{ m.}$$

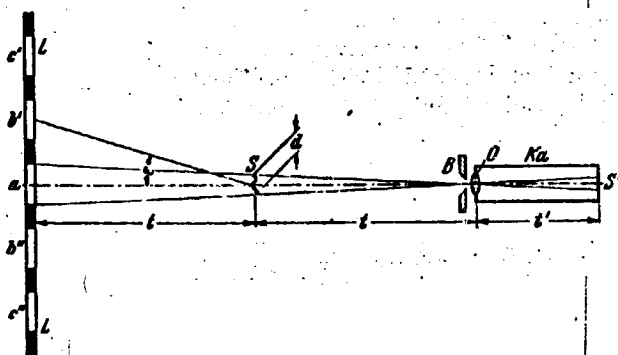


Figure 6. Diagram of the Arrangement for Schlieren Method Number 3.

dark at all spots where the irregular deflections exceed a definite value (around $1/2^\circ$ = angle of vision of the sun). The surface of the sun corresponds to surface a in Figure 6.

A similar case occurs if the reflections of the sun in waves are observed from a boat. A moving picture film of these reflection phenomena could be used to measure the shape of the waves.

The colored photograph of a glass plate with strong schlieren taken by this method is given as Figure 7 in Table 1. There it is compared with a photograph of the same glass plate taken with the lattice diaphragm method (see §13).

[Note: Figure 7 is on page 134]

This is practically the same arrangement as in a phenomenon of daily life. If, for example, a city is approached by car at twilight, the windows of houses are illuminated in the reflected sunlight. If a window appears with an angle of vision smaller than the angle of vision of the sun (i.e. if the distance is large enough), all of the window would be equally bright if the reflecting glass surface were sufficiently smooth; the windowpane would appear

7. Schlieren Method Number 4

The object was presented optically in the three schlieren methods described above. The schlieren were made visible by lighting the object with an illumination surface divided into different areas of brightness or color to cause the difference in brightness or color to become apparent in the object. However, sufficient sensitivity can only be achieved with a relatively small lens opening. Now, in reference to schlieren method number 2, apparatus will be described which for the first time introduces the principle of the so-called "schlieren diaphragm". In the structure of Figure 4 the field of vision was crossed by streaks which are deformed according to the deflection in the object. The streaks not deflected can be masked in front of the ground glass plate. However, the following better method is also possible: the light surface L and the object S are pictured at different distances by the lens O; in this way the regular rays can be screened out in the image plane of L(L') (see Figure 8); in this case the diaphragm is called a "schlieren diaphragm". If it is exactly negative to the light surface L, no light would reach the image plane S, if there were no refraction in lens S. Every light deflection of a point P in S, however, produces another position in L' of the rays going through this point, so that part of these rays may contribute to the reflection of the point in S'. Point P appears light on a dark background. Every deflection perpendicular to the streaks of light surface L result in a brightening of the image S' of the object. The greatest brightening occurs when the lighted streaks from L coincide exactly with the spaces between the lattice diaphragm at L'. In this case the light deflection ϵ in the schlieren has the value

$$\epsilon_1 = \frac{e}{2(l-t)} \quad (1)$$

With still greater deflection another darkening occurs; for

$$\epsilon_2 = \frac{e}{l-t} \quad (2)$$

and

$$\epsilon = \frac{k \cdot e}{l-t} \text{ (wo } k = 2, 3, 4 \dots) \quad (3)$$

all of the light is cut off again. Thus, curves of uniform brightness (isophots), appear in the image of the object; these curves are identical with the curves of constant light deflection perpendicular to the streaks from the light surface. With sufficiently large light deflection, this method is very well suited for quantitative evaluation. For a light deflection producing a change in brightness to actually occur for every point in the object, the following condition must be fulfilled:

$$\frac{D}{l} \geq \frac{e}{l-t} \quad (4)$$

NASA

Even

Roman

7

/311

X312

where D is the free opening of the image-forming lens O , l and t are distances corresponding to Figure 8 and e is the lattice constant of the light surface L . If we imagine D to be small and e to be large, the entire surface S would not be illuminated. The lattice constant e must at least be so small that the light rays originating in two successive edges (separated by e) of light source L just touch each other at the position of schlieren S . With D , l and t being given, equation (4) permits the necessary lattice constant e to be computed at the same time.

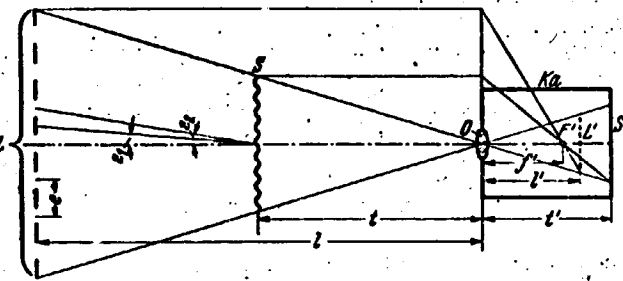


Figure 8. Schlieren Method Number 4. Application of a "Schlieren Diaphragm" in the Image Plane of L .

In the arrangement described, the field of vision (without schlieren) is dark, and every deflection perpendicular to the edges of the lattice diaphragm produces a brightening. However, the adjustment can be made in such a way that the field of view provides a medium brightness, and deflection in one direction produces more brightness while deflection in the other direction produces obscurity. For this purpose the optical images of the bright streaks from

light surface L on one side of the corresponding dark streaks from the lattice diaphragm can be bypassed by an amount $\Delta a'$. A reverse shift of the light by light deflection in the schlieren by the amount $\Delta a'$ would produce complete obscurity. In order to avoid another brightening with stronger light deflection, since then light would fall on the other side of the dark streaks of the lattice diaphragm, the width of the illuminating streaks can be kept narrower than the dark streaks of the diaphragm in the position of the lattice diaphragm.

Figures 9a and 9b represent two applications of this method. Figure 9a shows the photograph of a glass plate with striations and the formation of small bubbles at the surface. (This is the same plate as in Figure 5a). A common round flask was used as the object in Figure 9b. It can be seen from this photograph that the method is very suitable for investigating objects which naturally generate strong light deflections; there is nothing to prevent making light surface L large enough and with enough streaks to light up even the most strongly deflecting parts of the object.

A piece of equipment for the optical measurement of current and voltage, described by J. Malsch, 1937 [123] is closely connected with the method described above and with method number 2. Just as in Figures 4 and 8, Malsch used a light grating L . A lens O also directs this light grating toward L' , where we find a lattice diaphragm which can be produced in the same equipment by photographic exposure. The object is a small sealed volume of air through which a thin heating wire runs. Sending high frequency currents through this wire produces air schlieren whose intensity is to serve as a measurement of

/313

/314

current intensity. Since we are only concerned with the total intensity of the schlieren, an optical image of the object is not necessary; for reasons of maximum sensitivity, the object can be located immediately at lens 0 and the photographic plate can be replaced by a photocell located directly behind the lattice diaphragm L'. In this way we obtain a photocurrent which depends on the charge in the heating wire.



Figure 9a.

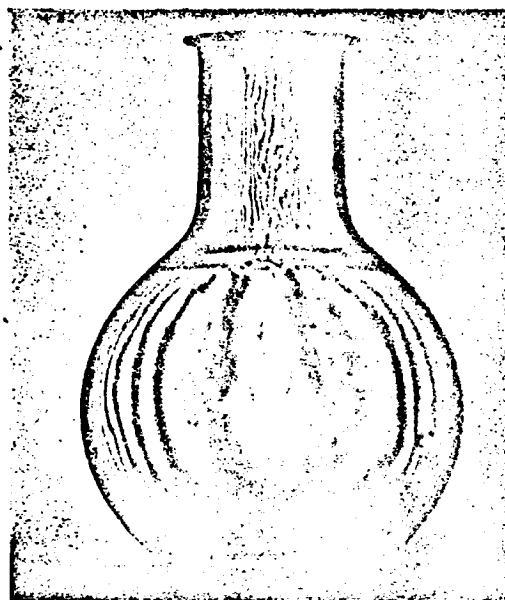


Figure 9b.

Figure 9. Photographs Taken With Schlieren Method Number 4: a, a Flat Pane of Glass; b, a Round Vase.

Another arrangement, similar to method number 4, has been published by F. Fischer [132]. In order to implement a television size projection he used an oil layer, scanned by a modulated electron beam. The electrical charges developing on the surface of the oil produce a corresponding deformation. Thus the oil layer represents a suitable object for the schlieren method. F. Fischer uses a light grating (illuminated by an arc lamp and condensor) for projection. In contradistinction to method number 4--as in the Joeppler method--the representation of the light lattice on the lattice diaphragm and of the object on the projection screen each require a special lens. While F. Fischer uses the lattice diaphragm to increase the brightness of the image, method number 4 was first used by H. Maecker in the Ballistics Institute at the Air War Academy in order to illuminate a larger field of vision.

NASA

8. Schlieren Method Number 5

Application of the schlieren diaphragm principle to schlieren method number 1 leads to the following method:

Let L in Figure 10, as in schlieren method number 1, be an illuminating surface limited on one side by a sharp edge. The object S will be reproduced with the help of lens O in S'. L will now be reproduced in L' by the same lens. Now let a schlieren diaphragm B, limited to a straight line on one side, be introduced into L' in such a way that almost the entire image of light surface L is stopped down. The edge of the aperture and the boundary of the light surface should be exactly parallel and only a narrow strip of light of width a' should pass by the edge of the aperture.

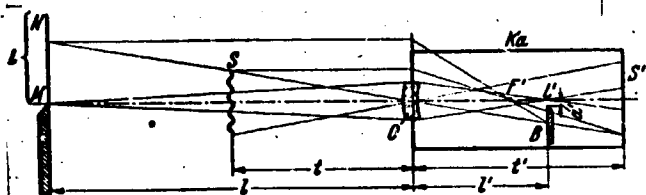


Figure 10. Schlieren Method Number 5.

correspondingly more or less light contributes to forming the image of this particular point P.

If $\Delta a'$ represents the shift of the image of the light source as a consequence of the deflection in the schlieren and Δa represents the corresponding value in the object space,

$$\frac{l}{l'} = \frac{\Delta a}{\Delta a'}$$

and

$$\Delta a = \epsilon(l - l');$$

whence

$$\Delta a' = \frac{l'}{l} \cdot \epsilon(l - l'). \quad (5)$$

$\Delta a'/a'$ is the relative brightening or darkening of point P

$$\frac{\Delta a'}{a'} = \frac{\epsilon}{a'} \cdot \frac{l'}{l} (l - l'). \quad (6)$$

In this way all the points of the object, reproduced in S' and not causing any light deflection perpendicular to the edge of the schlieren diaphragm, will appear in a medium brightness. A deflection ϵ at one point P of the object causes a shift of the image of the light surface in front of the schlieren diaphragm, so that

/315

The larger $\Delta a'/a'$ is for a given ϵ , the greater is the sensitivity of the arrangement. For this reason a' should be made as small as possible at first. If a theoretical setting is made of $a' = 0$, at first only the deflection in one direction would be visible, since then the field of vision ceases to receive any light and further darkening is no longer possible. Still, an increase in light will not provide any useful image of the object at first either, for reasons of diffraction theory. The image of S will appear practically through a slit of width a' , with one edge of the aperture really existing at L' , while the other exists in the image of the straight boundary of the light surface. This causes a lack of sharpness in the reproduction of the object. The picture produced becomes useful¹ only from a definite magnitude of a' on.

It is also advantageous to have a definite surface brightness of the image field at hand.

/316

The sensitivity of the equipment also depends upon the factor

$$\frac{r'(1-t)}{t}$$

It is necessary that t be as small as possible in order to raise the sensitivity. At $t = 0$ the object would coincide with lens O , and for a given ϵ the shift $\Delta a'$ on the schlieren diaphragm would be greatest, but any reproduction of the object would become impossible. In addition L' must be as large as possible. Just as with schlieren method number 1, this method also has the disadvantage that the field of vision is extremely small. At $t = 1/2$, the illuminated height of the objects would be just one half the free opening of the lens. To be sure, the width can be considerably enlarged; it is almost solely dependent on the width of the illumination surface L and at $t = 1/2$ would be half as large as this width.

Just as suggested for schlieren method number 1, an enlargement of the field of sight for stationary or slowly changing phenomena can be achieved by mechanically connecting the edge of the light surface and the schlieren diaphragm and moving them so quickly that a stationary impression is made upon the eye. Caution must naturally be advised in regard to keeping the connection of both movements very precise if the sensitivity of the equipment is not to be worsened. If this precision is reached, the Toepler arrangement for resting and slowly moving objects is completely equaled and the large concave mirror or the large dimension lens, which are absolutely necessary for the Toepler arrangement, can be eliminated.

Before adopting a mechanism of this type, even if no large optical for applying the Toepler method is available, thought should be given to the possibility that schlieren method number 4 might be the proper one.

¹For more details see p. 329.

NASA

A disadvantage of number 4, compared with number 5, is that the individual fields of sight are in contact. They may even partly overlap and the adjustment of sensitivity in the individual fields may be different, so that a reproduction of the schlieren of proper brightness is not immediately guaranteed; this may probably be achieved easier with method number 5.

9. Schlieren Method Number 6: The Toepler Arrangement

The Toepler schlieren method is different from arrangement number 5 by the fact that another optical system is used to reproduce the schlieren and that this second system can be arranged directly behind the schlieren diaphragm. Since then lens O (Figure 10) no longer reproduces the schlieren, it is also possible to make the segment $t = 0$ in order to attain greater sensitivity.

This arrangement is shown in Figure 11. Now, lens K serves only to reproduce light source L which must again be sharply limited on one side. In order to achieve this, it is most practical to produce an intermediate image of the actual light source. In a few cases, e.g., in using an electric spark, it will be sufficient to reproduce it directly. In making an intermediate image the reproduction of the light source can be restricted to any degree with the aid of a diaphragm; the illuminating surface can also be reproduced on a larger scale. Care must naturally be taken to see that the aperture of the illumination system is at least the same as that of the schlieren arrangement. It must even be larger by a definite amount, if the light source has a finite, lateral expansion and dependence is placed upon a uniformly illuminated field of vision for the purpose of possible quantitative evaluation.

The lens K is called the "schlieren head". This must fulfill two basic requirements:

1. The schlieren head must have as large a diameter as possible since the useful field of vision depends upon its size.
2. The schlieren head must be of good optical quality; for it must not possess any original inaccuracies in light refraction or reflection (with concave mirrors) which lie in the order of magnitude of the deflections in the schlieren to be made visible.

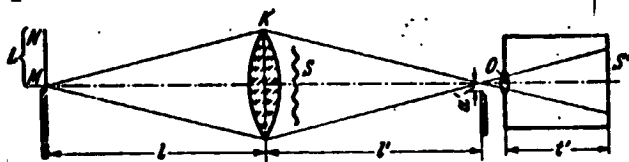


Figure 11. The Toepler Schlieren Method.

If a lens is used as a schlieren head, it must be adjusted as well as possible from a spherical and chromatic point of view; the glass itself must be free of schlieren and bubbles, for all local defects can be seen in the field of vision. Long-focus telegraph lenses, such as those used for astronomical purposes, are most suitable. It would be

best to use them in a rectified condition if two similar lenses are arranged so that a parallel path of rays runs between them. In this case the lenses can simultaneously serve as the end of a space in which the phenomena under investigation take place.

It may be suggested that a front coated concave mirror be used as a schlieren head instead of a lens; the mirror has no color defects and schlieren inside the glass have no effect upon the optical quality; finally, concave mirrors can be produced more easily and cheaply than lenses of the same diameter. It is possible to arrange a concave mirror in a number of ways. In general, a construction like Figure 12 cannot be used because, in the first place, the construction of light source L interrupts the uniform illumination of the image field, and, in the second place, this arrangement produces spherical defects which are too large for reproducing light source L at the place of schlieren diaphragm B. A concave mirror reproduces from midpoint to midpoint with no defect whatsoever. The possibility of using this aplanatic reproduction is provided by the so-called "coincidence method", which was first described by Hans Boas [60] (Figure 13). With the help of condenser C, light source L* is reflected onto the front of a plane mirror located almost exactly at the center of curvature of the schlieren concave mirror. From the plane mirror the light falls on the concave mirror and is reflected back to the plane mirror. Adjustment is carried out in such a way that after the reflection the image of the light source is shifted to the degree that the edge of the mirror functions simultaneously as a schlieren diaphragm. The advantage of this method is, first, that the concave mirror is really used in the most optically favorable way and, second, that the arrangement has high sensitivity since the light rays go through the object twice; thus the light deflections caused by the schlieren are twice as large as with a single light penetration. Naturally, if the angle of deflection of the schlieren assumes too high a value, the light falls onto another part of the object after reflection on the concave mirror. Then the angle of deflection of the light rays is no longer dependent merely upon the particular location of the schlieren. In this case the schlieren image obtained is no longer conclusive.

/318

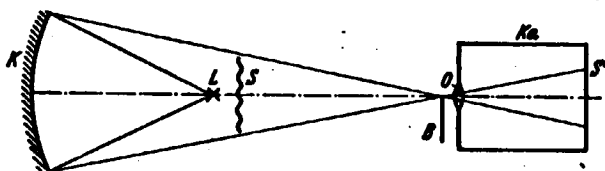


Figure 12. Possible, But Not Very Suitable, Arrangement for Using a Concave Mirror as a Schlieren Head.

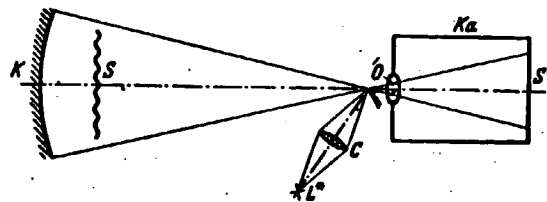


Figure 13. The Coincidence Method.

If a very sensitive schlieren arrangement is necessary, it may be suggested that light be directed through the schlieren several times instead of once or twice. For example, two concave mirrors can be opposed in such a way that their midpoints

almost coincide. Then proper adjustment can direct the light through the schlieren four, six or more times. This arrangement has been constructed by the author. Sensitivity was really increased to a considerable degree, but the complete adjustment is very delicate. Vibrations in the room and currents of air are noticeably disruptive.

The most profitable arrangement for using a concave mirror as a schlieren head is shown in Figure 14. The illumination slit and its image are both at the side of the center of curvature of the concave mirror. The schlieren is located in the reflected beam and far enough from the mirror not to disturb the incident pencil of light. For this reason the complete opening of the concave mirror cannot be used.

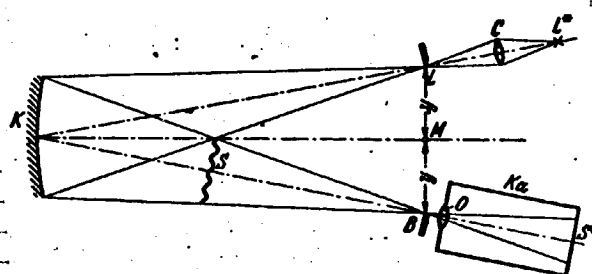


Figure 14. Schlieren Arrangement to Use a Concave Mirror as a Schlieren Head.

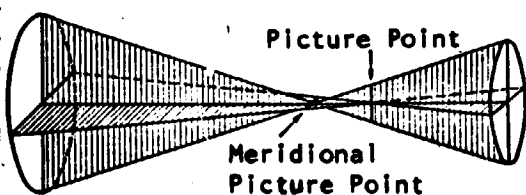


Figure 15. At the Sagittal and Meridional Picture Point the Image of a Point Shaped Light Source is Pulled Apart in Streaks.

atic defect in the light source image, the two sides of the light ray still passing through the schlieren diaphragm do not contribute equally in lighting all points of the field of vision (Figure 15). Thus, if the schlieren diaphragm

As presented here, the reflection of the light source takes place by means of an oblique beam; for this reason astigmatic-image defects occur. However, they have no essential influence, since this only concerns the precise reproduction of the straight boundary of the light source. A shift of the light rays parallel to the diaphragm edge has no effect. For this reason the schlieren diaphragm must be located according to its orientation in the sagittal or meridional image point of the light source (Figure 15). Another requirement is that the edge of the light source with the straight boundary lies exactly in or perpendicular to the plane described by three points: light source--mirror center--light source image. Otherwise no sharply delimited edge of the light source image will appear. The diaphragm edge must also satisfy this condition and run exactly parallel to the edge of the light source. If this is not the case, narrowing the diaphragm will not produce uniform brightness in the image field because, as a result of the astig-

operating in the meridional image point has a component in the direction proper for the sagittal image point, this component will affect the brightness in the image field in the same way as the lack of a schlieren diaphragm in the image plane of the light source (see p. 231). From this it follows that the schlieren diaphragm must have a very exact straight boundary. If the aperture is narrowed, a microscopically saw-toothed appearance would produce a field of vision crossed by dark and light stripes.

/320

The smaller the distance y is (Figure 14), the less will be the effect of a spherical defect in an oblique beam on the quality of the light source image. For normal equipment sizes with a mirror radius of 6 m, a diameter of 30 cm and $y = 50$ cm, the marginal rays suffer a displacement on the schlieren diaphragm on the order of magnitude of $5 \mu (= 0.17'')$. This is about equal to the limiting value of the schlieren sensitivity of the apparatus (p. 339).

It is often necessary to deal with the phenomenon under investigation in a parallel path of rays. The apparatus shown in Figure 16 is used in working with concave mirrors. The object is located between the two concave mirrors. It could be thought at first that the greater the distance s_k of the schlieren from concave mirror K_2 , the greater the sensitivity. However, this is not the case. A thorough optical computation shows that displacement $\Delta a'$, caused by a definite angle of deflection ϵ on the schlieren diaphragm, is completely independent of s_k ; it is

$$\Delta a' = \epsilon \cdot f'. \quad (4'') \quad (7)$$

In reference to the spherical aberration in the oblique beam, it is advantageous to place the light source and the schlieren diaphragm, as shown in Figure 16, on different sides. F Weidert and Stroeble have found by computation and M. Czerny and A. Turner¹ have found by testing that the asymmetry in the meridional segment is removed when the light source and the schlieren diaphragm are on opposite sides; in addition, with equal focal distances of mirrors, the tilt angles can be made equal in size.

The schlieren diaphragm must be located within the image of the light source. If this is not the case, no uniform darkening of the field of vision will occur when the schlieren diaphragm is narrowed. Determination of the side from which darkening comes first immediately indicates the direction the schlieren diaphragm must be moved. When the spot is found where no more unilateral darkening in the direction of the narrowed diaphragm occurs, the diaphragm must be turned in its plane in the presence of astigmatic-image defects until brightness is also equally distributed in the direction perpendicular to it. Up to here we have only discussed illumination surface L with a straight line boundary and a schlieren diaphragm with a straight line boundary. Here the light deflections in the object perpendicular to the edge of the schlieren diaphragm are made visible as brightening or darkening. The object appears as

/321

¹ Z. f. Physik, Vol. 61, p. 792, 1930.

if it were illuminated from one side (e.g., the schlieren image of a burning candle (Figure 17).

Page One Title

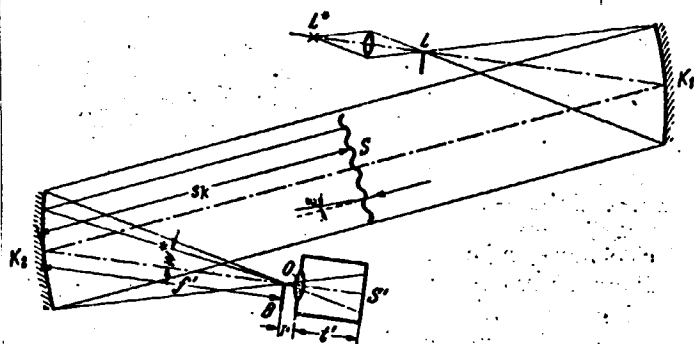


Figure 16. Schlieren Arrangement Using Two Concave Mirrors With Parallel Penetration of the Object.

Cover Page Source

extent is to be determined. If a concave mirror is used as a schlieren head, the circular diaphragm is inappropriate because of the astigmatic-image defects. Th. Fromme (Ballistic Institute of the Air War Academy) found that an astigmatic lens can be inserted into the path of rays to compensate for the astigmatism at the position of the schlieren diaphragm.

With the help of a perforated diaphragm, it is also possible to give the illumination surface a circular form and also to use a circular schlieren diaphragm. In this case deflections in every direction would become visible in the image as changes in brightness. However, this image is ambiguous because such exposures provide the extent of light deflection but not its direction. This arrangement is still appropriate if the direction of light deflection is fixed on the basis of other conditions or if only its extent

/322



A simple achromatic lens of long focal distance is usually used as reflecting lens O . An intermediate image as in Figure 18 can also be formed in order to avoid having to use a long camera extension and to facilitate a rapid change in the image scale. Lens O reproduces the schlieren in the position of field lens O_2 on a smaller scale. The field lens makes sure that all light rays pass through lens O_3 by reflecting O_1 in O_3 . Finally,

Figure 17. A Candle Flame and a Flying Projectile as Objects in the Toepler Arrangement.

O_3 casts an enlarged image from the intermediate image of the schlieren onto the ground-glass or photographic plate. Any desired enlargement can be obtained easily with a slight change in the distances.

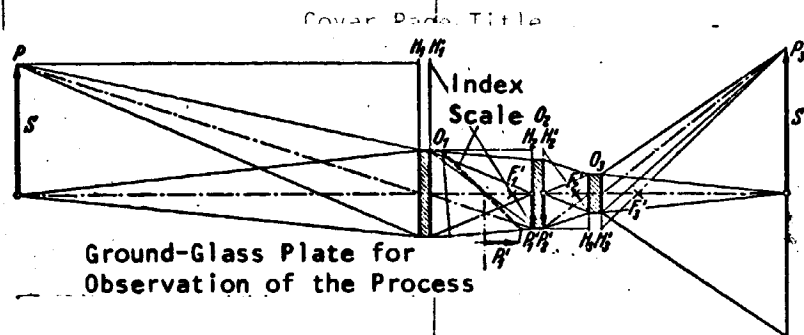


Figure 18. Optical System With an Intermediate Image Instead of a Line With Long Focal Distance.

In investigating an object in a state of change, e.g., a thermohydrodynamic process, it is sometimes desirable to take a photograph at a particular moment. To do this, continuous observation of the schlieren is necessary, even if a photographic plate has already been inserted. As can be seen from Figure 18, this can easily be achieved by casting the intermediate image of the object through an index plate onto a laterally arranged ground-glass plate.

Sharp focus on the ground-glass plate can be obtained by using any kind of test object. The use of light diffraction occurring at the edges of solid objects is very suitable for this, as described on page 330.

In dealing with processes of extended focus, it is still not clear what distance the focus should be set for. The testing apparatus itself provides the best answer to this question. For, if we completely remove the schlieren diaphragm, nothing could be seen of the schlieren, because projection through lens O or (O_1 , O_2 and O_3) makes sure that all beams of light originating from one point in the object, no matter what their direction, are again collected at the corresponding image point. A lack of schlieren in the object on the ground-glass plate is the criterion for correct setting without a schlieren diaphragm. In this way optimal setting is found for spatially extended processes.

If it is a question of a very great deflection in the schlieren, these can be made visible without a special schlieren diaphragm by using the mounting of the image-forming lens O as a schlieren diaphragm. If for some reason or other a regular schlieren diaphragm is not used, e.g., if an electrical spark serves as a light source and takes a different direction from time to time, a somewhat blurred adjustment of the object on the ground plate can be

/323

intentionally accepted; however, precise adjustment of the schlieren is always preferred.

Page One Title

10. Measurement of Light Deflection With the Toepler Schlieren Method

Cover Page Title

The illumination strength E^* of a point in the image field of the objects depends not only on surface brightness B of the light source and of the light losses (designated by the factor η), but also on the magnitudes f' , r , t' , a' , b' and $\cos w^*$ (Figure 16) in accordance with formula

$$E^* = \eta B \left(\frac{f' + r}{f'} \right)^2 \frac{a' b'}{f'^2} \cos^4 w^* \quad (8)$$

where a' is the distance from the edge of the schlieren diaphragm to the sharp edge of light source image L' , and b' is the width of the light source image. Let it be assumed that an arrangement with two concave mirrors K_1 and K_2 (or two lenses) with a parallel path of rays between them is used for the following derivatives. In this way the schlieren diaphragm is located at the focal point of K_2 and the object is located between K_1 and K_2 . If an arrangement as pictured in Figures 11 or 14 is used, it is obvious that f' is to be replaced by the distance between the schlieren and the schlieren diaphragm. If errors up to 1% are acceptable, $\cos^4 w^* = 1$ can be inserted up to a total aperture angle of 8° and r in the presence of f' can also be disregarded. Thus we obtain

$$E^* = \eta B \frac{b'}{f'^2} \cdot a' \quad (9)$$

If now the light for a definite point of the schlieren is shifted by an amount $\Delta a'$ perpendicular to the edge of the schlieren diaphragm,

$$E_i^* = E^* + \Delta E^* = \eta B \frac{b'}{f'^2} (a' + \Delta a') \quad (10)$$

$\Delta a'$ is further described by

$$\Delta a' = \varepsilon \cdot f' \quad (7)$$

where ε is the angle of deflection of a point of the schlieren in the arc and f' is the focal distance of the schlieren head, so that

$$\varepsilon = \frac{f'^2}{\eta B b' f'} E_i^* - \frac{a'}{f'} \quad (11)$$

i.e., the angle of deflection ε at one point of the schlieren, up to a constant amount, is linearly proportional to the illumination intensity in the image of the point in question. An absolute measurement of the brightness in the image

¹See [102].

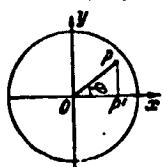
/324

and an evaluation according to equation (11) would be quite involved and too inexact, especially if a photograph had to be taken of moving phenomena. It is more appropriate to project into the image field a "standard schlieren" of which the deflections at individual points are known on the basis of previous calibration. Then a comparison of darkening in the object and in the standard schlieren show up on the photograph and the deflections ϵ are immediately provided. In this case evaluation is made most conveniently by using a recording photometer.

A planoconvex lens of very small curvature is appropriately used as a standard schlieren. Under all conditions it must be located in the parallel path of rays for, in the converging beam of light, a plane-parallel plate would immediately cause a shift in the image of the light force by about $d/3$ (d = plate thickness). As a result of this the schlieren diaphragm would not be located at the right spot and would consequently cause a one-sided darkening of the field of vision within the standard schlieren.

The focal distance F of the biconvex lens used as a standard schlieren must have a value such that the deflection of the marginal rays is somewhat larger than the largest deflection in the process itself. A light ray which falls on the lens 1 cm away from the optical axis is deflected by the angle $\epsilon_0 = 1/F$ (F in centimeters); the corresponding deflection at distance δ from the axis is δ/F . Deflection occurs in the direction of the optical axis. Depending on the position of the schlieren diaphragm, deflection is considered in only one certain direction.

Let the absolute deflection at point P of the standard schlieren (Fig. 19) equal $\epsilon_0 x$. Since deflection increases linearly with the distance from the optical center, the absolute deflection at point P equals $\epsilon_0 \cdot x / \cos \phi$. If the deflection at P is to be determined in the direction of the x axis, the components in the x direction are to be taken from this, and therefore $\epsilon_0 \cdot x / \cos \phi \cdot \cos \phi = \epsilon_0 x$, i.e., the deflection in the x direction is constant at all points with the identical x ; according to this all points of straight lines $x = \text{const}$ have a constant brightness in the schlieren image. Let the lines of constant brightness be designated as "isophots". Then the isophots of the standard schlieren are straight lines parallel to the edge of the schlieren diaphragm.



The absolute value of brightness in the schlieren image depends also on the light losses in the standard schlieren. If only the η -th part of the incident light is transmitted by the schlieren, the brightness in the schlieren image of the standard schlieren is:

Figure 19. Resolution of Deflection in a "Standard Schlieren".

NASA

/325

$$E_n^* = \eta' \cdot \eta \cdot \mathfrak{B} \cdot \frac{b'}{f^2} (a' + \varepsilon_0 \cdot x \cdot f'). \quad (12)$$

Therefore, for two points in the schlieren image of the process in question and of the standard schlieren both of which have the same brightness,

$$\begin{cases} a' + \varepsilon f' = \eta' (a' + \varepsilon_0 x f'), \\ \varepsilon = \eta' \varepsilon_0 x - \frac{a'}{f'} (1 - \eta'). \end{cases} \quad (13)$$

is valid. If the x , for which the same brightness is present as in the outside field of vision (x_0), is found in the schlieren image,

$$0 = \eta' \varepsilon_0 x_0 - \frac{a'}{f'} (1 - \eta')$$

whence

Cover Plate Source

$$\frac{a'}{f'} = \frac{\eta'}{1 - \eta'} \varepsilon_0 x_0$$

inserted in (13)

$$\begin{aligned} \varepsilon &= \eta' \varepsilon_0 x - \frac{\eta'}{1 - \eta'} \varepsilon_0 x_0 (1 - \eta'), \\ \varepsilon &= \eta' \varepsilon_0 (x - x_0). \end{aligned} \quad (14)$$

On the basis of this equation the value for the light deflection ε at one point of the schlieren is found in the following way: first position x_0 of the standard schlieren, which has the same brightness as the outer field of vision, is determined; then position x in the standard schlieren, which exhibits the brightness of the point in question in the process, is found. Then $x - x_0$ is multiplied by the factor $\eta' \varepsilon_0$, which can be taken as the characteristic value of the schlieren; the product provides the value sought for ε (Figure 20).

11. The Sensitivity of the Toepler Schlieren Method

/326

In the previous section we deduced that the illumination intensity at one image point of the schlieren has the following value:

$$E^* + \Delta E^* = \eta \cdot \mathfrak{B} \cdot \frac{b'}{f^2} (a' + \varepsilon f'). \quad (10a)$$

¹Here it is presumed that no absorption takes place in the schlieren itself. This is not always the case, e.g., in colloidal solutions.

Here E^* is the normal illumination intensity of the image field, and ΔE^* is its modification because of deflection at one point of the schlieren with angle of deflection ϵ . Since n , B and b' can be considered constants,

$$\Delta E^* = \text{const} \cdot \frac{f'}{t'^2} \cdot \epsilon \quad (15)$$

thus

proportional to f' and
inversely proportional to t'^2
for constant ϵ .

This means that in order to obtain a large absolute modification of brightness f' must be made as large as possible and t' as small as possible. If, at the same time, it is required that the size of the image of the schlieren be equally large in all cases, the following condition applies, under the assumption that the object is located near the second concave schlieren mirror ($s_k \rightarrow 0$):

$$f' = \text{const} \cdot t'; \quad (16)$$

and then

$$\Delta E^* = \text{const} \cdot \frac{1}{t'}, \quad (17)$$

i.e., in this case the focal distance f' must be chosen as small as possible.

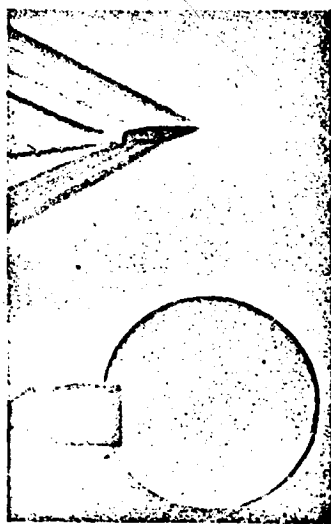


Figure 20. Schlieren Exposure of a Flying Projectile and Simultaneous Projection of a Standard Schlieren. (From VDI-Forsch.-Heft, Vol. 367). NASA

The absolute modification of brightness in the image of the schlieren, just considered, is important if the image of the schlieren is not seen with the eye or photographed, but is recorded with the aid of a photocell. Then the possibility exists of compensating for the steady current caused by the brightness of the field of vision. A practical example of application, where an arrangement of the type in question occurs, is research on the mode of oscillation of a membrane. The membrane is coated and the parallel path of rays between both schlieren heads are allowed to reflect on it. Every deformation of the mirror surface, which is perfectly plane at rest, will then act as a schlieren. The angle of deflection ϵ is twice as large as the angle of inclination to the surface at the point considered.

Shifting the photocell in the schlieren image and recording the

photocurrent easily provides the mode of oscillation of any individual point of the membrane.

When the schlieren image is observed by eye, the absolute modification in brightness ΔE^* is not the most important consideration; this is the $\Delta E^*/E^*$ ratio (Weber-Fechner law). Based on equation (10), this is:

$$\frac{\Delta E^*}{E^*} = \frac{f'}{a'} \cdot \epsilon. \quad (18)$$

In order to achieve high sensitivity in this sense, the fraction f'/a' must be as large as possible. This can be achieved by making a' , the width of the beam of light bypassing the schlieren diaphragm, very small. The following reasons oppose making a' arbitrarily small:

1. Light diffraction, which becomes noticeable when a' is too small, results in a blurry image of the items in the object and an uneven distribution of light in the image field. This is explained in more detail below.

2. The requirement, that light deflections in both directions be made visible and that both brightening and darkening occur in the image field of the schlieren, demands a certain minimum size of a' .

If we let ϵ_{\max} be the greatest deflection causing darkening, a' must at least be equal to $\epsilon_{\max} \cdot f'$.

If this is introduced into (18),

$$\frac{\Delta E^*}{E^*} = \frac{f'}{\epsilon_{\max} f'} \cdot \epsilon = \frac{1}{\epsilon_{\max}} \cdot \epsilon, \quad (19)$$

i.e., the relative sensitivity of the schlieren arrangement in meeting this requirement is independent of focal distance f' .

3. In observing with the eye, it is nice to have a definite minimum brightness in the field of vision independent of the requirement just described; this also leads to an a' which should not be lowered any further.

Here is a numerical example of this:

Let an arc lamp with a light density of 15,000 stilbs serve as a light source. 10 lux = 10^{-3} phots are required for the illumination intensity in the image. If a format 9×12 cm is to be illuminated, the use of a concave mirror of $f' = 6.5$ m focal distance and 30 cm diameter as a schlieren head produces a value of 212 cm for t' . Let the width of the light source image be 1 cm. The light losses should amount to 50%, i.e., $\eta = 0.5$. If this value is inserted into equation (9), then

$$10^{-3} = 0,5 \cdot \frac{15000 \cdot 1}{212^2} a',$$

whence

$$a' = 6 \cdot 10^{-3} \text{ cm} = 60 \mu.$$

For this value of a' , as long as there is still visible a modification in the ratio of $\Delta E^*/E^*$ of 5%, the smallest detectable angle of deflection ϵ_{\min} comes from

$$\frac{\Delta E^*}{E^*} = \frac{f'}{a'} \cdot \epsilon_{\min} \quad (18a)$$

and, with $f' = 650 \text{ cm}$ and $a' = 6 \cdot 10^{-3} \text{ cm}$, becomes

$$\epsilon_{\min} = \frac{\Delta E^*}{E^*} \cdot \frac{a'}{f'} = \frac{0,05 \cdot 6 \cdot 10^{-3}}{650} = 0,46 \cdot 10^{-6},$$

$$\epsilon = 0,22 \text{ sec}$$

and

$$\Delta a' = 3 \mu.$$

The brightness increases with the width b' of the light source image (see cf. equation (9)). This depends on the extent of the light source. In the example above $b' = 1 \text{ cm}$. If considerably more brightness is necessary, e.g., in order to illuminate a large projection screen, the light source in L can be subdivided by a suitable lattice diaphragm into several superposed strips. In this case the schlieren diaphragm should also be replaced by a lattice diaphragm (see cf. p. 314). The sum of the individual width of the strips of light in L' produces b' . However, if the deflection at some points of the object is larger than the free opening in the lattice diaphragm, the illumination intensity of the image field is no longer proportional to the deflection. More details are given in §13 about the use of an arrangement of this type to measure light deflection.

Let us ask the question of how the focal distance f' should be chosen in order to obtain maximum relative sensitivity of the equipment with a constant illumination intensity in the image field and constant image size.

Valid for the illumination intensity E^* is

$$E^* = \text{const} \cdot \frac{a'}{f'^2}. \quad (9a)$$

The relative sensitivity is then

$$\frac{\Delta E^*}{E^*} = \text{const} \frac{f'}{a}. \quad (18)$$

Cover Page Title

In order to maintain constant image size, it is necessary that

$$f' = \text{const} \cdot l' \quad (16)$$

(assuming that s_k is smaller than f').

Then

$$\frac{\Delta E^*}{E^*} = \text{const} \frac{f'}{l'} = \text{const} \cdot \frac{1}{f'}. \quad (20)$$

This means that if a constant illumination intensity of the image field and constant image size are required, the smallest possible focal distance f' of the schlieren head must be chosen to achieve high relative sensitivity.

However, the following point-of-view also plays an essential role in deciding the best dimensions for a schlieren arrangement: the object under investigation has a predetermined dimension. For this reason the schlieren head must have a certain minimum diameter. If the focal distance f' is selected as very small, the proportion of the opening becomes correspondingly large and with it the image defects, found in projecting the light source onto the schlieren diaphragm, increase. If f' is too small, e.g., if one or two spherical concave mirrors are selected as a schlieren head, the image defects in projecting the light source could equal the order of magnitude of the light deflections ϵ under investigation. In this case the arrangement would be unusable. In reference to the image defects, it would be most favorable to keep the proportion of opening as small as possible; this is the case when the focal distance f' is selected as large as possible.

In this way we have recognized the contradictory requirements for the size of focal distance f' . These were:

Case 1: f' can be arbitrarily chosen,

Case 2: f' should be as small as possible,

Case 3: f' should be as large as possible.

How can a schlieren head be chosen with a compromise among these conditions?

First of all, the given dimension of the object determines the diameter. If this is larger than about 30 cm, work can be done practically only with spherical concave mirrors. The proportion of opening is then chosen so small, and the focal distance so large, that the shifts caused on the schlieren diaphragm by the image defects are somewhat smaller than those caused by the

/329

still invisible deflections in the schlieren. f' need not be larger, but must not be smaller; in this way cases 3 and 2 are compromised with each other, and at the same time take care of case 1.

Testing the diffraction phenomena described in the next section still has to demonstrate whether the greatest sensitivity required can even be achieved because of basic principles.

Sensitivity and the sensitivity boundary will be discussed in more detail with an example at the end of these considerations (p. 337).

12. The Diffraction Phenomena Occurring in the Toepler Schlieren Arrangement

In the object space are found mostly opaque objects which diffract the light coming from light source L at their edges, i.e., from their edges light rays go in practically all directions which are perpendicular to the diffracting edge and lie in the direction of the light. Therefore this diffracted light partially goes past the schlieren diaphragm, even if the direct light is completely stopped down. Now, since the image-forming lens O again assembles at the corresponding image points all of the light rays coming from the object in any direction, the edges of all objects which are not exactly perpendicular to the schlieren diaphragm must be circumscribed by a bright margin (Figure 21a). This kind of diffraction does not interfere with visualization of the schlieren, because the diffraction margin lies right at the edge of the opaque bodies.

/330



Figure 21a. Diffraction Margin at the Contours of a Rifle. The Direct Light is Completely Stopped Down.

This phenomenon is very well suited for focusing the schlieren sharply. If a slit is used as a light source and if the direct light is stopped down in the position of the schlieren diaphragm by a special aperture, so that the diffracted light passes both sides of this aperture symmetrically, all edges will be circumscribed by a double margin as long as the ground-glass plate has not been sharply adjusted for the object (Figures 21b and 22); the margin is single only if the focus is very sharp.

This adjustment is so sensitive because the image-forming line of light in the object space is to be considered infinitely narrow. Its width in the image plane S' is only conditioned by the projection defects of lens O (in addition to part of the schlieren head, if this is located between the object and the schlieren diaphragm). Thus under certain circumstances measurement of the width of the diffraction margin can be used to determine the projection defects of lens O.



Figure 21b. Double Diffraction Margin at the Contours of a Rifle With the Setting of Figure 22 I or III.

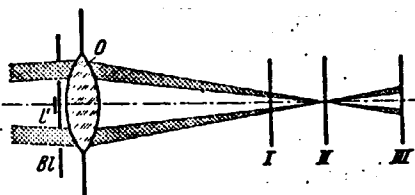


Figure 22. The Diffraction Margin Can Be Used for Sharpening the Image. L', Image of the Light Source. Bl, Diaphragm Which Cuts Down the Direct Light but Allows Two Symmetrical Pencils of the Diffracted Light to Pass Through. The Margins are Single Only in Position II, and Double in Positions I and III; cf. Figure 21b.

(See §19 for the derivation of this).

In this way two images, L' and L'' from the edge of light source L , appear next to each other in the position of the schlieren diaphragm. Image L' is produced by light rays which do not go through the schlieren while L'' only by light rays which go through the area with variable n .

The openings of the diaphragm (Figure 22) must be wide enough for the diffraction occurring at the openings to have no effect. However, it is very illustrative to indicate the refraction of the light which has already been diffracted once. For this purpose monochromatic light must be used, one slit in Figure 22 completely covered and the other almost closed. Then the multiple diffraction maxima shown in Figure 23 are obtained from the contours of the rifle. The primary diffraction at the edges of the object eliminates the need for a narrow light slit otherwise required for such a diffraction image.

In addition we should consider the sharpness (caused by the diffraction phenomena) with which the edge of the light source in the position of the schlieren diaphragm is projected by light rays deflected by schlieren in the object [134].

In Figure 24 along segment z there should be a region with an altered refraction index which extends from the center of the image field to the bottom margin; the refraction index should be constant in the light direction but become perpendicular to it within a segment dy by the value dn . If we assume that $dn/dy = \text{const}$ within this area, the angle of deflection for all rays passing through this region

$$\epsilon = z \cdot \frac{dn}{dy} = \text{const} \quad (21)$$

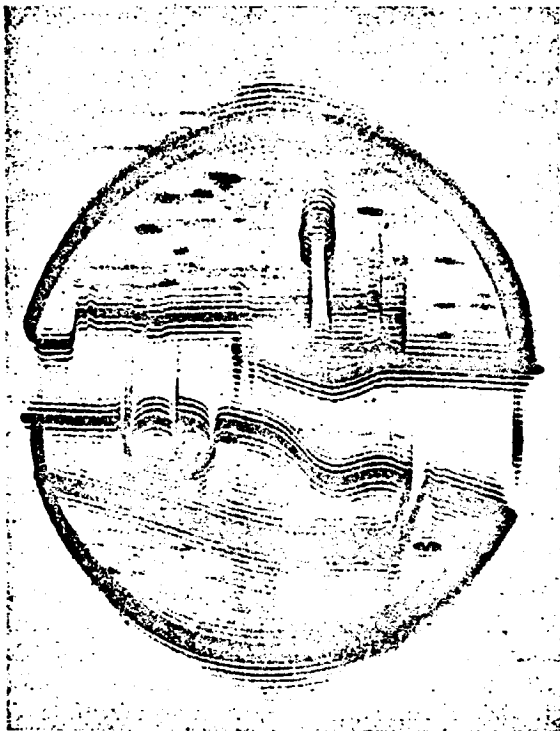


Figure 23. Diffraction of Light Already Diffracted Once at the Edges of a Rifle by a Slit in Front of the Image-Forming Lens (Negative for the Purpose of Better Reproduction). Monochromatic Light.

almost the entire increase in brightness takes place within an area $2\pi d/\lambda \cdot \epsilon = 2\pi$, i.e.,

$$\epsilon_u = \frac{\lambda}{d} \quad (22)$$

thus ϵ_u is the angle at which the fuzziness of the edge appears in the image of the light source from the object. The fuzziness u of the edge of the light source image itself is then

$$u = \frac{\lambda \cdot f'}{d} \quad (22a)$$

(Numerical example: $\lambda = 6 \cdot 10^{-4}$ mm; $d = 300$ mm; $\epsilon_u = 2 \cdot 10^{-6} = 0.42$ for $f' = 5$ m, and then $u = 10 \mu$).

No projection, even in the absence of geometric and optical projection defects, is ideal because of diffraction phenomenon. If the monochromatic light source L were an infinitely narrow slit perpendicular to the drawing plane, distribution of brightness in image L' would have an appearance like that of curve I in Figure 25. The distance of the first minimum from the center of the diffraction image is equal to

$0.61 \cdot \lambda f' / d$ (f' is the focal distance, d is the diameter of the schlieren head and λ is the length of the light wave). However the light source is an extensive illumination surface with a straight boundary. Now it is important to know how steeply the increase in brightness rises at the edge of the light source image. This can be found out by superimposing the diffraction images produced by every point of the light source, since the individual points of the light source are not coherent. The result has been plotted in Figure 25 as curve II. This shows that

/333

NASA

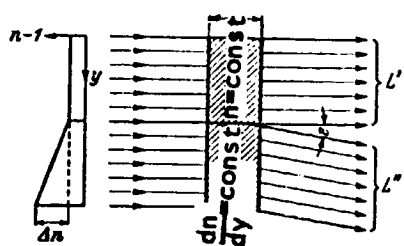


Figure 24. The Object is a Plane-Parallel Plate; In the Upper Half $n = \text{const}$, In the Lower Half $dn/dy = \text{const}$.

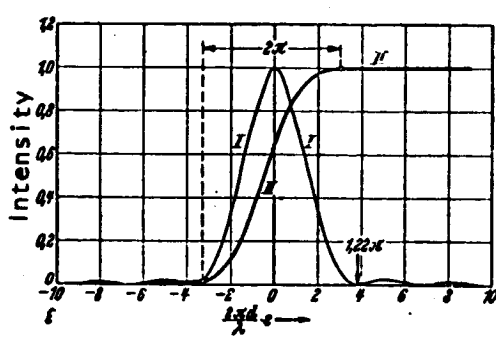


Figure 25. Diffraction Image of a Slit (I) and a Straight Edge (II) Projected Through a Circularly Described Lens.

If we now transpose this result to the arrangement shown in Figure 24, we can introduce the width of each of the two light pencils for d according to size. This furnishes the sharpness with which the edges of both light source images L' and L'' are bordered. It is still possible to shift the two images toward each other by a value which amounts to ξ times the sharpness of the edge (therefore by $\xi u = \xi \lambda \cdot f'/d$). In order to decide which value factor ξ may have, let us first consider the case in which a schlieren of diameter d is located in a very large field of vision. In this case the edge of the light source image projected across the schlieren-free field of vision is practically arbitrarily sharp, while the edge projected over the schlieren is blurred by an amount $u = \lambda f'/d$. Now if the schlieren diaphragm is inserted in such a way that the schlieren, without diffraction, would produce a modification in brightness by α times the brightness of the field of vision (i.e., $\alpha \cdot a' = \epsilon \cdot f'$), we can see from Figure 26 that the presence of refraction causes practically no alteration in the brightness ratio as long as fuzziness $u < 2(\epsilon \cdot f'/\alpha)$. Then we may directly get

$$u = \frac{\lambda f'}{d} = 2 \frac{\epsilon f'}{\alpha}, \tag{23}$$

i.e.,

$$\epsilon = \frac{\alpha}{2} \cdot \frac{\lambda}{d} = \frac{\alpha}{2} \cdot \epsilon_u. \tag{23a}$$

Thus the factor would be

$$\xi = \frac{\alpha}{2}. \tag{23b}$$

If, for example, the schlieren causes a variation in brightness of 5%, i.e., $\alpha = 0.05$, $\xi = 0.025$.

NASA

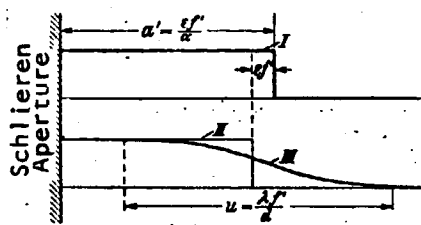


Figure 26. Curve I: Distribution of Brightness in the Image of the Light Source Projected Over the Entire Schlieren Head (Practically Without Diffraction). Curve II: Brightness Distribution in the Image of the Light Source Projected Over a Schlieren Without Diffraction; II Compared With I is Displaced By the Value $\epsilon \cdot f'$. Curve III: Brightness Distribution in the Image of the Light Source Projected Over a Schlieren of Diameter d .

In this case, then, the blurring angle ϵ can be 40 times as large as the deflection angle ϵ to be detected, without a noteworthy alteration in the brightness distribution in the image of the schlieren occurring because of this diffraction phenomenon. If we forego reproduction of brightness, a still smaller ϵ could be detected.

If we are not concerned here with the detection of a smaller schlieren in a large field of vision, but with the comparison of two equally large fields, as in Figure 24, the ratios do not change to any important degree.

Therefore we posit the still-to-be-detected

$$\epsilon = \xi \cdot \epsilon_u = \xi \cdot \frac{\lambda}{d} \quad (24)$$

and the corresponding shift on the schlieren diaphragm

$$u = \xi \frac{\lambda \cdot f'}{d}, \quad (24a)$$

where ξ is a factor which is essentially determined by equation (23b). If we make $\xi = 1$, as has been done in some of the following examples, the limit set by the diffraction is considered too unfavorable. If we now solve dn/dy , which is still to be detected, the result from

$$\epsilon = \xi \frac{\lambda}{d} = z \cdot \frac{dn}{dy} \quad (\text{eq. 21})$$

is

$$\frac{dn}{dy} = \xi \cdot \frac{\lambda}{d \cdot z} \quad (25)$$

(Numerical example:

For a) $\xi = 1$, $\lambda = 6 \cdot 10^{-5}$ cm, $d = 1$ cm, $z = 1$ cm: $\frac{dn}{dy} = 6 \cdot 10^{-5}$ cm $^{-1}$.

b) $\xi = 1$, $\lambda = 6 \cdot 10^{-5}$ cm, $d = 10$ cm, $z = 10$ cm: $\frac{dn}{dy} = 6 \cdot 10^{-7}$ cm $^{-1}$.

NASA

The smaller the wavelength used and the larger the depth z of the object and the extension d of the area with variable dn/dy , the smaller will be detectable dn/dy .

Since dn/dy was assumed to be constant, $\Delta n/\Delta y$ can also be written for it if Δn means the difference in the value of the refraction number for both sides and Δy means the width of the pencil. Then if Δy is introduced into equation (24) for d ,

$$\frac{\Delta n}{\Delta y} = \xi \cdot \frac{\lambda}{\Delta y \cdot z},$$

whence

$$\Delta n = \xi \frac{\lambda}{z}. \quad (25a)$$

This means that if λ and z are given, only the difference Δn of the refraction number on both sides of the light pencil concerned is of importance. The smaller the pencil, the larger must be the gradient of the refraction number, caused by the diffraction phenomena, by which the light deflection in question can just be made visible. However, this fact must not lead one to believe that the sensitivity of the schlieren method depends on the magnitude of the n -gradient perpendicular to the light direction and not absolutely on Δn , as is the case with interference refractors which can be used for similar purposes. In order to make this clear let us think of the schlieren in the schlieren method with a constant dn/dy extended over the entire field of vision. Then the light deflection caused by the schlieren will be equally large everywhere and in an extreme case can still be made visible if the difference in the refraction number at both boundaries of the field of vision amounts to $\Delta n = \xi \cdot \lambda / z$.

If an interference refractor is used, an alteration in optical distance by the value $\Delta n \cdot z$ is found for an alteration in the refraction number by an amount Δn . If $\Delta n \cdot z = \lambda$, the interference reading shows a shift of one interval in the interference band. If ζ is the part of a band interval still to be measured, the Δn to be determined is computed by

$$\Delta n = \zeta \cdot \frac{\lambda}{z}. \quad (26)$$

If we make ξ and ζ approximately equal in size, and follow the above example, the interference method would just show on the extreme edge of the field of vision the value Δn , necessary for detection, so that for this example variation in brightness lies above the minimal value in the entire field of vision according to the schlieren method, while according to the interference

/335

NASA

method the band displacement everywhere within the field of vision lies below the minimal value necessary for resolution.

Still another refraction phenomenon must be considered. The object S is projected into image plane S' with lens O by the light bypassing the schlieren diaphragm. This projection occurs practically through a slit where the schlieren diaphragm is a real edge, while the other projection is the result of the straight boundary of light source L. In order to determine the diffraction caused by this slit, let us first imagine an illuminating point in the object. Its image on the ground-glass plate S' would be a light shape similar to that in Curve I of Figure 25. In order to obtain the light shape coming from an illuminating surface, the diffraction image of the point must be appropriately shifted and the intensities added everywhere. In this way a light distribution corresponding to Curve II of Figure 25 is obtained.

/336

Essentially the same light distribution will be present if an object in S surrounded by fixed diaphragms² gets its light from light source L.

The slit imagined has a width a which may be k -times that just resolvable because of diffraction, so with equation (24a)

$$a' = k \cdot \xi \cdot \frac{\lambda}{a} \cdot f'. \quad (27)$$

The new diffraction occurring in the split will now blur every boundary in the object by an amount u perpendicular to the edge of the schlieren diaphragm.

Very sensitive adjustment of the schlieren, at which the schlieren diaphragm is almost completely closed, makes this phenomenon extremely inconvenient. A dark shadow runs perpendicularly to the edge of the schlieren diaphragm into the field of vision from the edges of all objects which are in the light path in the position of the schlieren; at the same time things outside become brighter. Turning the schlieren diaphragm and moving the edges of the light source at the same time also turn the diffraction shadows. The amount of influence which this diffraction has is given by

$$u = \xi' \cdot \frac{\lambda}{a} \cdot f'. \quad (28)$$

The opposite occurs if, e.g., a flat plate is introduced into the parallel path of rays of the schlieren arrangement or of the interference refractor. This does not cause any effect at all in the schlieren arrangement, but causes such a great band displacement with the interference refractor that special measures must be taken in order to measure it. For this reason it is not possible to compare the sensitivity of the schlieren method and of the interference refractor immediately.

² If necessary, this may be the mount of the mirror or of the lens.

Inserting the value for a' from equation (27)

$$u = \frac{\xi r d}{k \cdot \xi \cdot f'} \quad (28a)$$

If we make $\xi' = \xi$, the ratio of the angle u/t' , in which the disturbed area of brightness lies, to the vision field angle d/f' is given by

$$\frac{u}{t'} \cdot \frac{f'}{d} = \frac{u}{\xi} = \frac{1}{k} \quad (29)$$

(d' is the diameter of the schlieren in the image).

If $k = 1$, i.e., if the most sensitive setting is chosen, the brightness of the entire image field is also disturbed by the diffraction at the schlieren diaphragm; the larger k is compared with 1, the less noticeable will be this diffraction phenomenon.

These considerations are not only valid for d as the diameter of the entire image field, but correspondingly also for d as the diameter of a single schlieren in the object.

With a very narrow diaphragm, especially if the direct light is completely cut off, it can be observed that there is a reversal in the brightness of the light distribution caused by the diffraction phenomenon just described (Figure 27). How does this occur? The secondary diffraction at the edge of the schlieren diaphragm of the light forming the diffraction margin and already diffracted once by the edges of the object is to be considered responsible for this (cf. Figure 25; naturally with white light no individual streaks are present).

Let an example summarize below what has been said about sensitivity and diffraction. Let the focal distance f' of the concave mirror (or lens) used for the schlieren arrangement be 5.15 m.

The relative sensitivity is computed with equation (18). In Figure 28 it is plotted for value $\epsilon = 1.939 \cdot 10^{-5} = 4$ sec. At the same time angle of deflection ϵ , still to be made visible, is given in the schlieren if we assume $\Delta E^*/E^* = 5\%$.

First let the edge of the schlieren diaphragm be 5 mm from the edge of the light source image. In this position an angle of deflection of 10 sec. still produces a change in brightness of 5%. If the schlieren diaphragm is now narrowed, the relative sensitivity is only altered a little at first; i.e., the appearance of a schlieren with a definite ϵ (e.g., 4") remains approximately the same (cf. the left-hand scale in Figure 28). However, more and more fine details appear; for every ϵ just becoming visible is, according to

equation (18), directly proportional to a'

Page One Title

$$\epsilon = \frac{\Delta E^*}{E^*} \cdot a' \quad (18a)$$

Cover Page Title

With values from this example
($\Delta E^*/E^* = 0.05$, $f' = 5.15 \cdot 10^3$ mm) we
get

$$\epsilon \text{ (In sec)} = 2a' \text{ (In mm)} \quad (18b)$$

a simple relationship which easily provides the sensitivity of the adjustment at all times in the present case.

If the aperture has been narrowed to $a' = 1$ mm, angles of deflection of 2 sec become visible. Now schlieren caused by air of different temperatures in the room become unpleasantly obvious. A good criterion for a sensitive adjustment is the visibility of schlieren near a hand held in the path of rays. At room temperature light deflection caused in this way lie as high as 5 sec (Figure 29b).

/338

Figure 27. The Effect of Diffraction at the Side of the Schlieren Diaphragm on the Appearance of the Field of Vision When the Diaphragm is Almost Closed.

any more narrowing of the aperture. A small adjustment in the schlieren diaphragm is now enough to considerably change the contrast in the image.

However, the diffraction phenomena also become obvious now. The fuzziness at the edge of the light source image deflected by a schlieren depends on the extent of the schlieren and is given by equation (22) or (22a). Table 1 has been computed by using $\lambda = 6 \cdot 10^{-4}$ mm and $f' = 5.15 \cdot 10^3$ mm.

If the schlieren diaphragm is narrowed to the extent that $a' = u$, the brightness of the schlieren in question, compared with the amount which would be present without diffraction, is practically unaltered. According to equation (23), narrowing the diaphragm even to $u = a'/2$ would be permissible. In this case $\epsilon = \xi \cdot \epsilon_u = \alpha \cdot \epsilon_u$; $\alpha = 1/20$ th. This value is introduced into Figure 28 as the upper limit set by diffraction. Therefore it still has a factor of certainty. Consequently the following demonstration is also possible (cf. Table 2).

/339

Cover Page Source

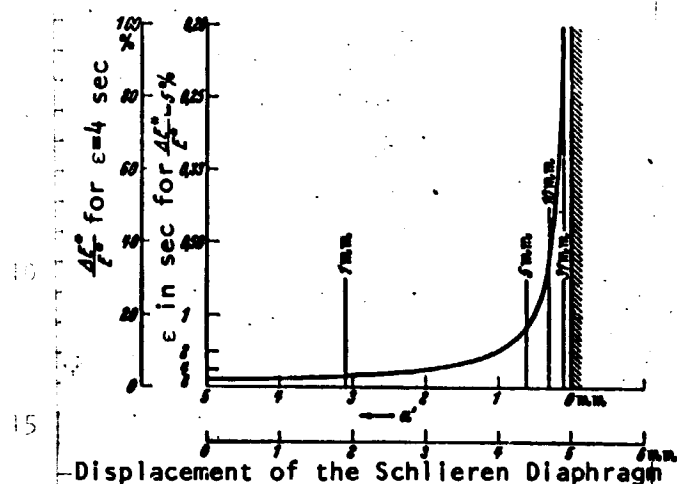


Figure 28. Representation of the Sensitivity and the Limits Set by Diffraction Depending on the Position of the Schlieren Diaphragm.

In this case we have considered only the alteration in brightness of a schlieren caused by diffraction taking place in the object itself. As was indicated on p. 336, however, the "diffraction shadow" caused at the edge of the schlieren diaphragm by the diffraction is given by the same values; the numbers 1, 5, 10 and 31, introduced in Figure 28, refer simultaneously to the approximate lengths of the diffraction shadow emanating from the edges of solid materials and transmitted to the object.

Some practical reproductions of the example just cited are given in Figure 29. In this case the schlieren was located

TABLE 1.

Diameter of the Schlieren d	Blur u	$\epsilon_u = \frac{1}{d}$
1 mm	3.09 mm	$6 \cdot 10^{-4} = 2 \text{ min}$
5 mm	0.62 mm	$1.2 \cdot 10^{-4} = 24.8 \text{ sec}$
10 mm	0.309 mm	$6 \cdot 10^{-5} = 12.4 \text{ sec}$
20 mm	0.154 mm	$3 \cdot 10^{-5} = 6.2 \text{ sec}$
50 mm	0.062 mm	$1.2 \cdot 10^{-5} = 2.5 \text{ sec}$
100 mm	0.031 mm	$6 \cdot 10^{-6} = 1.24 \text{ sec}$
500 mm	0.006 mm	$1.2 \cdot 10^{-6} = 0.25 \text{ sec}$

TABLE 2. DETECTABLE LIGHT DEFLECTION $\epsilon = 1/20 \epsilon_u$.

d in mm	ϵ in arc scale	ϵ in sec.
1	$3 \cdot 10^{-5}$	6
5	$6 \cdot 10^{-6}$	1.24
10	$3 \cdot 10^{-6}$	0.62
31	$0.97 \cdot 10^{-6}$	0.20

NAS

Tr. Note: Commas indicate decimal points.

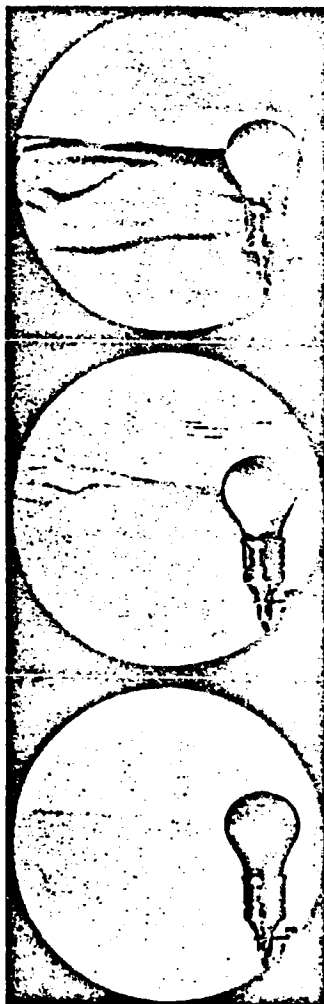


Figure 29a. Object: Incandescent 75 Watt Bulb.

$a' = 4; 2; 1/8 \text{ mm};$
 $a'/f' = 2'40''; 1'20''; 5''.$

Figures 29a through c. The Appearance of Schlieren Images Narrowed Differently. $f' = 5.15 \text{ m}.$

only with considerable mathematical effort.

In Figure 29a and in the next two figures, the object (i.e., the incandescent bulb, the hand or the flask) is lighted at the same time from the front by an auxiliary light source, so that the opaque objects do not appear

in converging pencil of an arrangement as in Figure 14. The distance between schlieren and schlieren diaphragm was 5.15 m , i.e., equal to a focal point $f' = 5.15 \text{ m}$ of the arrangement in Fig. 16, taken as the basis for our primary considerations. In Figure 29a the warm air current coming from an incandescent light is given first. In the first part of the picture the schlieren are just becoming visible; a' amounts to 4 mm . According to equation (18b) this corresponds to a deflection of 8 sec if 5% brightness variation can be considered visible. For instance, the slit method (cf. §13, p. 346) makes it possible to measure simply and immediately the absolute value of light deflection and to determine what percentage of change in brightness must be considered. A corresponding series of tests has shown that in a normal Toepler arrangement with a sensitive adjustment, light alterations of $5-8\%$ are just able to be perceived while alterations of 10% can be perceived well. Part 2 of the picture has $a' = 2 \text{ mm}$, thus an adjustment which is twice as sensitive; Part 3 has $a' = 1/8 \text{ mm}$ and therefore according to (18b) an angle of deviation of $\epsilon = 0.25 \text{ sec}$ should still be visible at $\alpha = \Delta E^*/E^* = 5\%$. To keep this change in brightness undistorted by diffraction, the pertinent schlieren must have at least a lateral extension of about $d = \alpha \cdot (\lambda/\epsilon) = 1/20 \cdot \lambda/\epsilon = 24.8 \text{ mm}$ (cf. Figure 28). The dimensions of the warm air drafts lie within this order of magnitude. However, it should be noted that the above derivations refer only to the case of a constant angle of deflection within the schlieren, while in reality the angle of deflection usually changes from place to place. This general case can actually be handled

only in the shadow contour, as is generally the case with schlieren reproductions. Reproduction of the schlieren is not affected by this at all and a clearer image is obtained. Figure 29b records the warm air schlieren coming from a hand. Because of the lower surface temperature, compared to an incandescent bulb, a more sensitive adjustment is necessary to produce a clear picture. At $a' = 1$ mm not much can be seen, and even at $a' = 1/2$ the image still has the same appearance (corresponding with the progress given in Fig. 28), but at $a' = 1/8$ and at $a' = 1/20$ mm, the schlieren are clearly defined. The sensitivity for the last part of the picture is 0.1 sec, and the pertinent size of the object without any diffraction effect is 6.2 cm.

The third object shown in Figure 29c is an open flask containing ether. The flask is tilted, but not so far that the ether could flow out; nevertheless, even with a relatively coarse adjustment ($a' = 4$ mm; i.e., sensitivity 8 sec) a definite current of ether vapor may be observed flowing out. Therefore the deflections must amount to considerably more than 8 sec. In the last section of Figure 29c the direct light is completely cut off and $a' = -0.5$ mm. Therefore only those parts of the current are visible which have an angle of deviation greater than $\epsilon = 0.5/5.150 = 20$ sec perpendicular to the direction of the edge of the schlieren diaphragm and only in one direction. In this way the successive alteration of $-a'$ can furnish the curves of constant deflection (isophots) in the case of stationary processes (cf. p. 346). /342

These examples should be enough to demonstrate the sensitivity of the Toepler schlieren arrangement. (4")

13. Schlieren Method Number 7 (Lattice Diaphragm Method)

The Toepler schlieren method is used to make schlieren visible where great sensitivity is necessary. A quantitative evaluation is possible by measuring brightness, most appropriately by comparison with a standard schlieren. Now there is a complete gamut of cases in which great sensitivity is not necessary, but where rapid and simple quantitative evaluation is required. The lattice diaphragm method described below is applicable for these cases. The basic arrangement of this method is shown in Figure 30. A slit L, illuminated from light source L^* , is projected in a free opening of lattice B across the optical system K_1 and K_2 . The lattice consists of grid apertures and lattice bars which are generally of equal size¹. If the latter constant is $2a$, a is the width of the bars and of the apertures. Let the image of the slit have a width somewhat smaller than a . The object S in this case, just as in the Toepler method, is projected into S' by lens O. If no light deflection occurs in S, the field of vision is uniformly bright. For a deflection by angle ϵ , just large enough to shift the light to the first lattice bar, complete darkening occurs. In this case

$$\epsilon = a \cdot f'.$$

¹ In many cases it is completely appropriate to make the apertures and bars of different sizes.

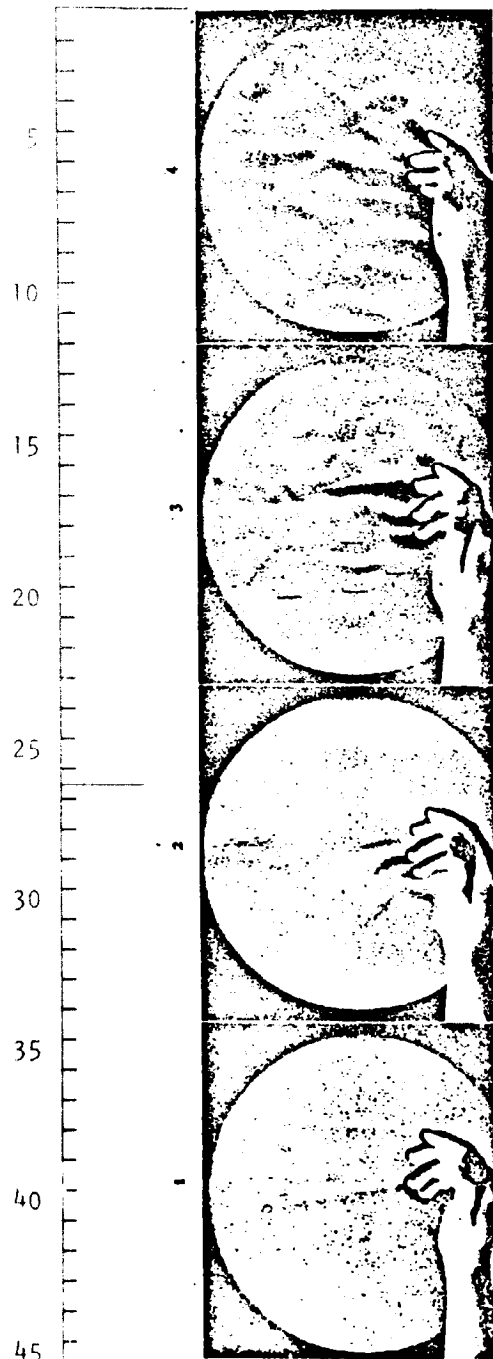


Figure 29b. Object: Hand.

a' = 1; 1/2; 1/8; 1/20 mm;
 a'/f' = 40", 20", 5", 2". NASA

Page One Title

Cover Page Title

Cover Page Source

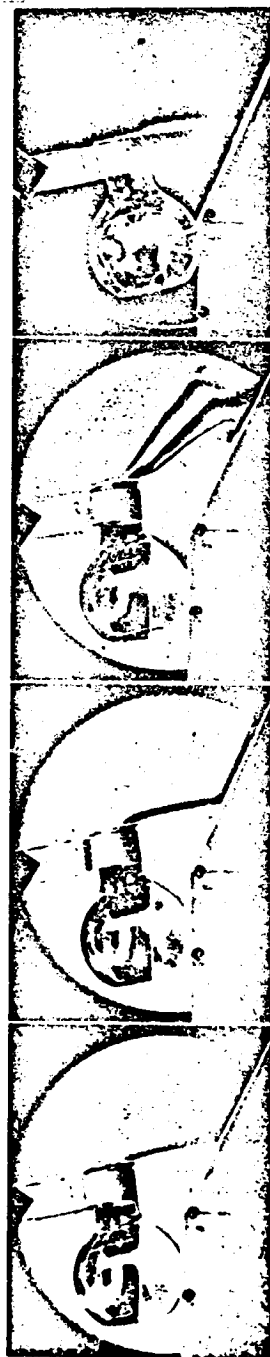


Figure 29c. Object: Open Flask
 Containing Ether.

a' = 4; 1/2; 1/8; -1/2 mm;
 a'/f' = 2'40"; 20", 5", -20".

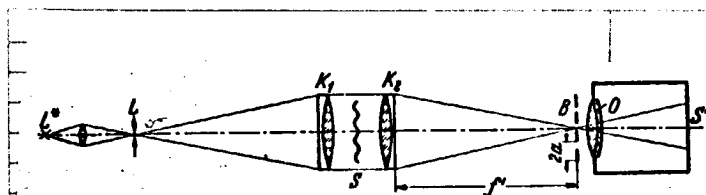


Figure 30. Arrangement for the Lattice Diaphragm Method.

If the deflection is twice as large, the light again falls through the next aperture and brightness occurs, etc. In this way curves of constant deflection perpendicular to the direction of the lattice bars are obtained in the image field. They correspond to the curves of constant brightness in the

Toepler method and can therefore also be designated as isophots. Such an image usually allows immediate determination of the extent of light deflection for one point in the object. (As an example for the use of this method, see Figures 31, 34 and 77) Of course the ordinal number of each isophot must be unambiguously definable, i.e. one must know through which aperture of the lattice diaphragm the light in question has fallen. This is almost always possible if an approximate picture of the course of light deflection in the object can be made on the basis of conclusions made otherwise. But there is also a direct way of determining the ordinal number: the individual apertures of the lattice diaphragm can be provided with color filters differing from one another. A colored image of the object is then obtained; each color corresponds to a very definite ordinal number. The simplest way of preparing such a color lattice is to transfer black and white lattice reproductions drawn in suitable size on a piece of cardboard onto diapositive plates of the desired size. Then the spaces on the plate can be easily colored with filter colors. The colors should be selected so that they are clearly different from one another, not only in colored photographs, but also for the eye. Naturally no value is to be put upon color fidelity in photographing these. This method is very suitable for rapid evaluation of rather large deflections (about $1/2$ min and greater). If the value of the deflections in a definite direction (i.e., perpendicular to the direction of the lattice bars) is not to be recorded, but rather the absolute value of the deflections, this can be done simply by choosing a circular diaphragm at L (see Figure 30) and arranging a circular lattice diaphragm at B.

Figure 32 in Table I gives an example of the application of the colored lattice diaphragm method. This concerns a glass plate with relatively great deflections of light for which a lattice diaphragm was chosen with lattice constants large enough that the photograph of Figure 32 corresponds to the photograph of Figure 7 made by schlieren method number 3. Two color ranges are seen on the image: red and blue-green. Each region corresponds to a definite deflection furnished by the data of the arrangement.

Further examples for this method are provided in Figures 59, 67 to 73 and 113, which are described in more detail at the corresponding places in the text.

NASA



Figure 31a.

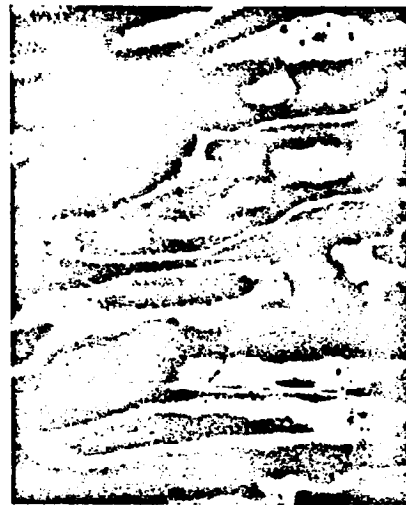


Figure 31b.

Figure 31a and b. Schlieren Pictures of Glass Plates Exhaled Upon. Figure 31a Shows the Lattice Partially Covered in Order to Determine the Ordinal Number.

In investigating how much effect refraction has, one can begin with a light source which just illuminates one slit of the lattice diaphragm. In correspondence with Figure 25, the refraction shape of an image point caused by this illumination has one main maximum and several adjacent maxima¹. The distance of the first minimum from the center of the diffraction shape is equal to

$$u = \frac{\lambda t'}{a} \quad (30)$$

(Example: $\lambda = 6 \cdot 10^{-4}$ mm, $a = 1$ mm, $t' = 1,500$ mm, $u = 0.9$ mm, i.e., the width of the average streak between the two minima amounts to 1.8 mm.)

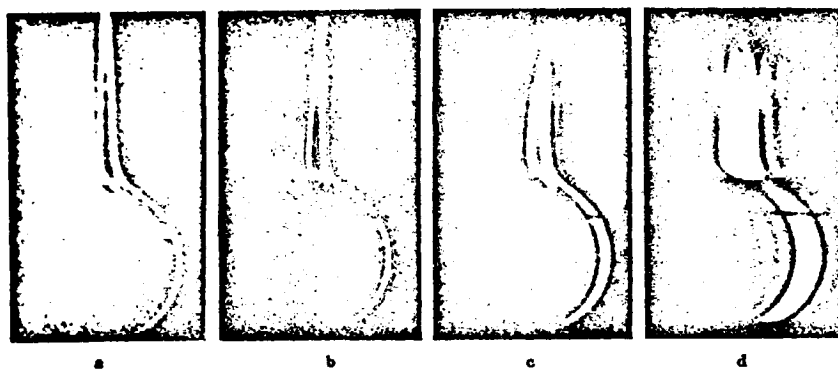
Figure 33 shows exposures made with four slit widths ($a = 0.38$ to 3.27 mm). A horizontal heating pipe served as the object, and a strong lateral deflection was picked out and provided only a narrow line of light in the image of the object. The main and several adjacent maxima can easily be picked out in the exposures. Now the points in the object lie directly next to the projected line at a somewhat smaller or somewhat larger deflection. If the adjacent slit of the lattice diaphragm is cleared, a second line with its adjacent maxima must appear in the image of the object and, under certain

In Figure 25 the diffraction has been plotted on a circular diaphragm, while here we are concerned with diffraction at a slit.

/345

REPRODUCIBILITY OF THE ORIGINAL PAGE IS POOR.

conditions, must lie so close to the one reproduced here that further interference phenomena occur and the main maxima of the two lines become indistinguishable.



Cover Page Source

Figures 33a to d. Diffraction on a Slit Schlieren Diaphragm. Slit Widths: a, 3.27 mm; b, 1.60 mm; c, 0.75 mm; d, 0.38 mm; $t' = 135$ cm.

For this reason a suitable choice of lattice constants and slit widths depends on the object. If the slit is very wide, the diffraction caused by it will be very small, but too large a range of deflections is covered so that the isophots in the image become wide again. The optimum slit width furnishes the narrowest isophot. The lattice constant, i.e., the distance from the next slit, is determined by a condition that the isophots just miss interfering with one another.

Figure 34 shows, again with the horizontal heating pipe as the object, several examples of the effects of slit width and lattice constant.

Pictures a to d were taken with the same lattice constant but with decreasing slit widths. The position and number of isophots should have been the same in these four pictures. Figure 34b must have been the best suited for evaluation, since here the isophots are most easily separated from one another. Figure 34c already shows a very reciprocal blur, while Figure 34d seems to be completely blurred because of diffraction. The lattice constant in Figure 34e is smaller (only 3 mm instead of 5); this leads to considerably disruptive overlapping, so that the photograph can no longer be evaluated.

In order to eliminate the errors caused by overlapping the diffraction phenomenon of several adjacent isophots, only one isophot need be shown on a photograph; i.e., only one slit of the lattice diaphragm should be free at one time and the different isophots should be photographed successively. In this case the slit diaphragm can even be discarded and use made of a simple schlieren diaphragm which can be moved by definite amounts with a micrometer gauge. Then the black-white boundary in the image field would correspond to the

position of the isophots. Still, this method is only useful with stationary processes. Under such conditions, photographing could also be eliminated and the isophots could be measured directly with a measuring microscope in the image field. Vice versa, if one starts at a definite point in the object, he can move either the schlieren diaphragm or the light source slit, in the case of a fixed schlieren diaphragm, by using a measuring screw so that the point to be measured lies exactly on the black-white boundary. This type of application is useful in the ultracentrifuge measuring technology, greatly developed in modern times, and is known there by the name "slit method" [135]. This will be gone into in more detail in §30.

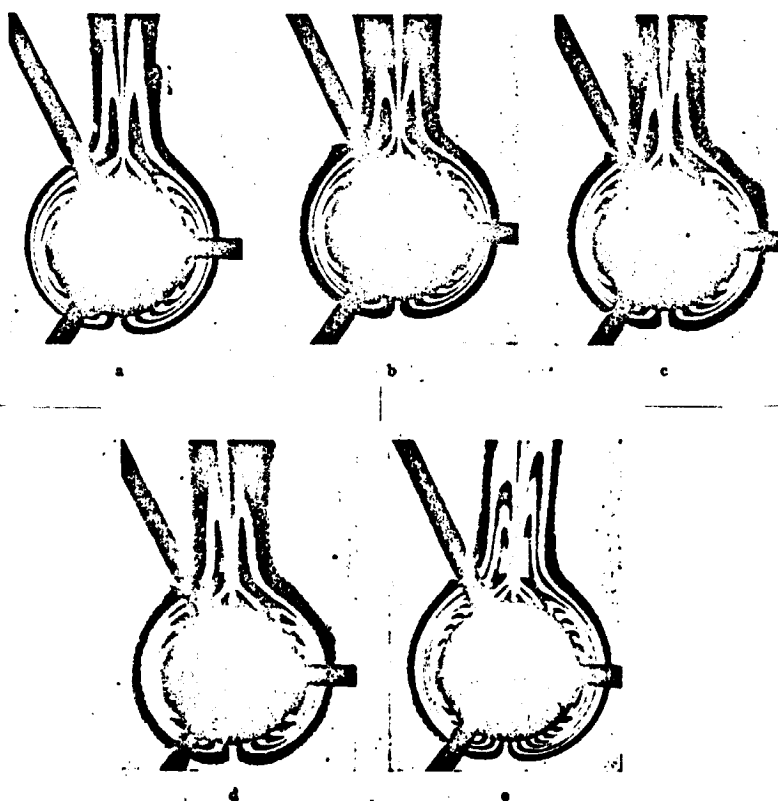


Figure 34 a to e. Photograph of the Temperature Field Near a Pipe Heated to 70°C With The Lattice Diaphragm Method Using Different Slit Widths and Lattice Constants:

Image	:	a	b	c	d	e
Lattice Constant:		5	5	5	5	3 mm
Slit Width	:	2.5	2.0	1.5	1.0	1.5 mm.

NASA

14. Schlieren Method Number 8

Page One Title

In principle, schlieren method number 7 could have been operated in such a way that a series of colored light slits were arranged next to one another in L if a simple slit diaphragm was used at B. This should be the reverse order as schlieren method number 7; naturally, in reference to the kind of slit illumination, it would be somewhat more difficult to carry out. However, this consideration leads to a new principle: a simple slit can be arranged at L, as usual up to now, and illuminated with standard white light; then the light is analyzed for color in a dispersion prism (Figure 35).

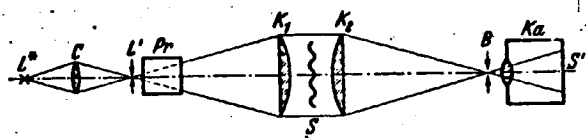


Figure 35. Schematic for Schlieren Method Number 8 (Pr = Direct-Vision Dispersion Prism.)

As a result of the light deflection in the schlieren, a definite amount of color is contributed to the reproduction of the point in question. In this way a colored image of the object is obtained; a very definite ϵ corresponds to each color. An optimum value exists for the dispersion of the prism. With too large a dispersion, color

alternation--and therefore sensitivity, too--is very small for a definite ϵ ; with a smaller dispersion, under certain circumstances, the measuring range required is not filled with color. This colored schlieren method is considerably more sensitive than the lattice diaphragm method; there a displacement by one value of the complete lattice constant had to take place to cause a change in color. The occurrence of diffraction phenomena place a limit on arbitrary reduction of the lattice constant. In using a prism to break down colors, no arbitrarily small slit can be taken in B, either, because of diffraction, but a small displacement of the light in front of the slit diaphragm causes a change in color by itself. In this way schlieren method number 8 corresponds to the Toepler method; the changes in brightness caused there correspond to changes in color here. This arrangement was set up and investigated by G. Stamm, who also took numerous photographs. Figure 36 in Table I shows the hot air rising from a burning match as an example. The background is green; deflections in one direction--which would cause more brightness in the Toepler method--here produce color variations from yellow to red. From a certain deflection on, complete blackening begins. In the other direction--corresponding to the darkening in the Toepler method--the colors here appear from blue to violet. Figures 64 and 65 provide two other exposures made with the prism method.

Schlieren method number 8 would correspond to the lattice diaphragm method if a light source were used which radiated only limited wavelengths. Decomposition with the prism provides several colored light slits practically adjacent to one another. With a suitable distribution of wavelengths, these could lie at a desired and constant distance from one another. Under certain conditions this can be very useful for the simple evaluation and assignment of colors.

/347

15. Further Possibilities for Schlieren Arrangements with an Optical Projection of the Object

Page One Title

The basic principle of the arrangements described to this point is the combination of an optical projection of the object with a determination of the light deflection in its image. In general the brightness of a point serves as the measurement of light deflection. It was shown that a color scale can lead to useful arrangements. What other possibilities exist for determining the amount of light deflection? In addition to intensity and color, the direction of polarization is also characteristic of a beam of light. It would be completely reasonable to use this as a schlieren method. For this purpose one must work with polarized light and use, at the location of the schlieren diaphragm, a device to turn the polarization plane by definite amounts depending on the extent of the light deflection. An analyzer, which makes every desired isophot visible according to its position, is used for observation. However, photographic recording of the entire image field to fix the polarization direction of the incident light is not possible, since suitable photographic material is not yet in existence. If continual reproduction of the object is not necessary and if the object is divided into a series of slits parallel to one another, the deflection for each point can be characterized by a second additional deflection produced parallel to the direction of the slit. For this purpose a reflecting helicoidal surface, against which light is reflected (schlieren method number 9), can be introduced into the Toepler arrangement in the position of the schlieren diaphragm. Then for every downward deflection a proportional deflection to the side will be superimposed at the same time. In this way a series of curves, which immediately represent a graphic illustration of the values for the light deflection, is obtained. The reflecting helicoidal surface was achieved simply by the author by properly bracing a coated steel band.

/348

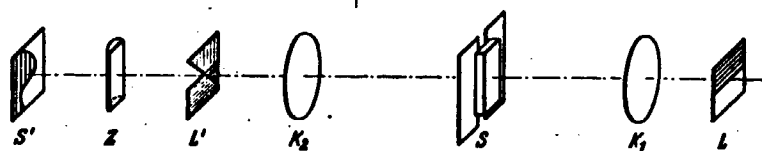


Figure 37. Schematic Arrangement of Thovert's Method.

In some cases of practical application determination of light deflection along 1 slit in the object is sufficient (e.g., in ultracentrifuge measuring technology). Here the arrangement reported by Thovert is useful (schlieren method number 10). It is briefly illustrated in Figure 37. Let light source L be an extensive illuminating surface with a straight limitation going horizontally through the optical axis. It is projected to L' through K_1 and K_2 . S is the object under investigation from which only one vertical streak is permitted to go through a diaphragm. K_2 simultaneously projects S to S' (if we first assume that cylindrical lens Z is not present), and a vertical streak

also occurs there. An oblique diaphragm going through the optical axis is located at L'. Now a cylindrical lens is added at Z and projects horizontal sections from L' to S', while it may be considered as absent from the path of light beams in a vertical direction.

If now a deflection of the light rays occurs in a vertical direction at one point of S, the black-white boundary shifts with the edge of the diaphragm in a lateral (horizontal) direction at L' for this point. This lateral shift is projected true to scale into S' by the cylindrical lens, while vertical correlation with the object is maintained. In this way a curved black-white boundary, whose horizontal ordinate is proportional to the vertical deflection of the point in the object in question, is obtained at S'. A simultaneous light deflection occurring in the horizontal direction in the object has no effect, since it only causes a displacement of the light surface L' parallel to the black-white boundary.

II. Schlieren Methods With No Optical Projection of the Object

16. The Direct Shadow Method (Schlieren Method Number 11)

All of the methods described up to this point for visualizing and investigating schlieren require a greater or lesser use of optical equipment. Dvorak, in 1880, was the first to call attention [6] to the fact that an extremely simple arrangement allows schlieren to be visualized: one need only illuminate the schlieren with a light source of the most extreme pinpoint type and a screen, on which the light falls, will show the presence of a schlieren by an unequal distribution of brightness because of the light refraction.

Let L in Figure 38 be the most concentrated possible source of light and let S be the schlieren. Let light ray c be deflected in the schlieren by angle ϵ . In this way it reaches the screen at a point $\epsilon \cdot g = \Delta a$ away from its origin. The alteration in brightness caused in this way will indicate the schlieren most sensitively if the deflection Δa is as large as possible in relation to the size of the shadow image of the schlieren (d'); now $\Delta a = \epsilon \cdot g$

and $d' = \frac{h}{h-g} \cdot d$, so

$$\frac{\Delta a}{d'} = \frac{\epsilon}{d} \cdot \frac{g(h-g)}{h}. \quad (31)$$

Since ϵ/d is to be considered as an assumed constant of the schlieren, $\frac{g(h-g)}{h}$ should be made as large as possible to attain the greatest sensitivity. If we make $g/h = x$,

$$\frac{\Delta a}{d'} = \frac{\epsilon}{d} \cdot h \cdot x(1-x). \quad (32)$$

$x(1-x)$ has a maximum at $x = 1/2$ (see Figure 40).

/349

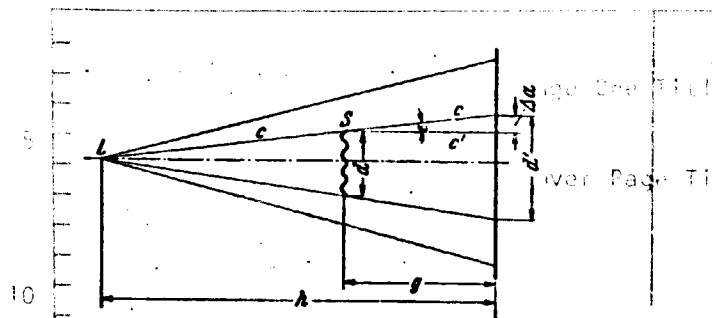


Figure 38. Direct Shadow Method.

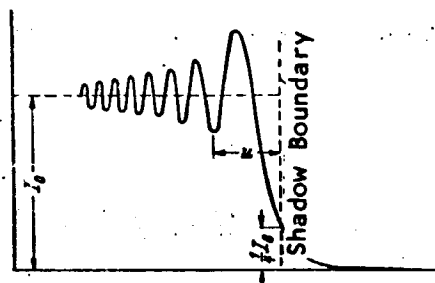


Figure 39. Diffraction of a Straight Edge.

Thus for sensitive adjustment:

1. The total distance h must be as large as possible.
2. The schlieren must be located approximately in the middle of the light source and the screen.

The edge of a schlieren, insofar as the passing light is concerned, can be considered the edge of a diaphragm. Thus it produces a diffraction which blurs the image on the screen of the border between the undistorted field of vision and the schlieren (Figure 39). The distance from the geometrical shadow boundary to the first minimum can be approximately defined as blurred. According to Fresnel, this is proportional to

$$\sqrt{\lambda \cdot g \cdot \frac{1}{\frac{g}{h-g} + 1}} \quad (33)$$

Since the wavelength of the light used can also be considered constant,

$$\begin{aligned} u &= \text{const} \cdot \sqrt{\frac{g(h-g)}{h}}, \\ u &= \text{const} \cdot \sqrt{h} \cdot \sqrt{\frac{g}{h} \left(1 - \frac{g}{h}\right)}. \end{aligned} \quad (34)$$

If we derive again with $g/h = x$,

$$u = \text{const} \sqrt{h} \sqrt{x(1-x)}. \quad (35)$$

The smaller u is in ratio to d' , the less does the diffraction interfere with the identification and eventual evaluation of the schlieren

$$d' = \frac{h}{h-g} \cdot d = \frac{1}{1-x} \cdot d.$$

then

$$\frac{u}{d'} = \text{const} \frac{\sqrt{h}}{d} \cdot \sqrt{x(1-x)^3}, \quad (36)$$

$\sqrt{x(1-x)^3}$ has a maximum at $x = 1/4$ (see Figure 40). Thus, with reference to diffraction, it would be inconvenient to arrange the object right at the distance $g = h/4$.

/351

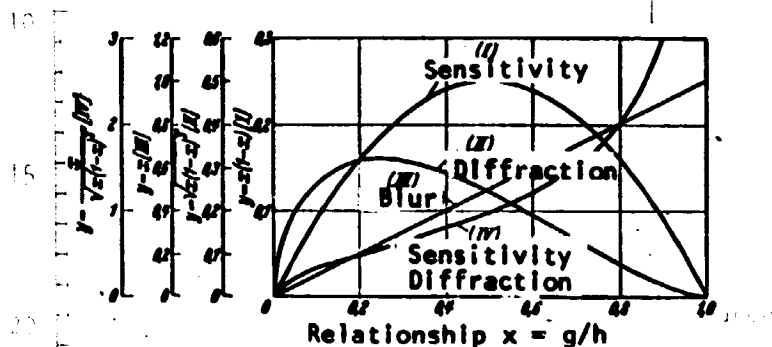


Figure 40. Representation of Sensitivity, Diffraction and Blur As Well As the Sensitivity-Diffraction Ratio as a Function of g/h for the Direct Shadow Method.

Another cause of disturbance for a sharp delineation of the schlieren on the screen is the ever present finite extension of the light source.

Let the diameter of the perforated diaphragm serving as a light source be δ ; let the blur caused by this on the screen be δ' ; again it is important to keep the ratio δ'/d' as small as possible.

$$d' = \frac{h}{h-g} \cdot d = \frac{1}{1-x} d,$$

$$\delta' = \frac{g}{h-g} \delta = \frac{x}{1-x} \cdot \delta,$$

then

$$\frac{\delta'}{d'} = \frac{\delta}{d} \cdot x. \quad (37)$$

This means that the fuzziness caused by the extension of the light source is linearly proportional to the diameter of the perforated diaphragm and the ratio $x = g/h$. With a given perforated diaphragm the object must be as close to the screen as possible in order to attain good delineation.

If we summarize the results to this point, we reach the following specification for carrying out the direct shadow method:

Greatest sensitivity is attained if the distance between the light source and the screen is as large as possible and if the object is located centrally between the two. As curve I in Figure 40 shows, it is not necessary to meet the latter condition exactly, since sensitivity is changed very little with deviations of 0.5 in the ratio $x = g/h$. The diffraction caused at the edges

of the schlieren has a maximum effect upon blur at $x = 0.25$. Increasing the distance h also increases the effect of the diffraction, although only by \sqrt{h} , while sensitivity increases directly with h . If the deflection in the schlieren are so small that the diffraction has a disruptive effect, it is more advantageous to make the ratio $x = g/h$ larger than 0.5 (Curve IV). Naturally with a large x , i.e., with a large interval between the object and the screen, the perforated diaphragm must have a sufficiently small diameter since the blur originating from the finite magnitude of the light source increases as x increases. The greater the extension of the schlieren is, the less obvious becomes the blur caused both by the diffraction and by the geometrical optics.

The shadow method is used very often to make a very rough schlieren visible, e.g., in regular window glass, in bottles or in other common glass objects (see Figures 42, 43 and 44). In this case a very sensitive setting is not important; on the contrary it may even be of considerable disadvantage, as we shall see immediately.

To avoid working in a darkened room, it is preferable to have an image as bright as possible on the screen. For this reason a light source is chosen with as much light intensity as possible, e.g., an arc lamp or a high pressure mercury lamp. This can be used directly or with an intermediate projection with a condenser on a perforated diaphragm to regulate the sharpness better. But in both cases, in order to achieve the desired brightness on the screen, the diameter of the light source is so large that sufficient sharpness is only achieved if x , i.e., g/h is sufficiently small.



Figure 41. Ether Vapor
Escaping from an Open Bottle.
Shadow Method Exposure.
(From Journal *Heizung u.
Lueftung*, December 1932).

The direct shadow method is a schlieren method without optical projection of the object. This has very important consequences: the light deflected by the schlieren falls on some spot on the screen and increases brightness there. In this way the projection of the schlieren contains less light than the normal field of vision. In this way the schlieren can be recognized on the screen as dark spots true to scale. It is different with the light spots. These are not caused by a light deflection in the corresponding points of the object, but rather the light in question comes from any direction not immediately determinable. However, the occurrences of bright light are now much more obvious than the dark spots in the schlieren image. Figure 41, showing a stream of ether vapor escaping from an open bottle of ether and exposed with the shadow method, can serve as an example of this.

First the outlines of the flowing ether vapor can be recognized because they

are darker than the background; these are true to scale. But the light line within the stream and forked at the top is much more striking. It contains all of the interrupted light. The screen was probably located right in the focal plane of the vapor stream representing a cylindrical lens.

Another example is the incandescent light in Figure 42. It is very easily realized that the bright lights need not be an index for the light deflection of any pertinent point in the shadow image of the bulb, because they extend far beyond the outside edges. As already emphasized, only the darker spots of the bulb are conclusive. Where the deflections are not very large, the bright streaks are usually next to the dark ones, or else this can be more or less achieved by a suitable choice of distance g . Then the schlieren have unusual contrasts. This is the case with some of the "glass threads" of Figure 42.

/353

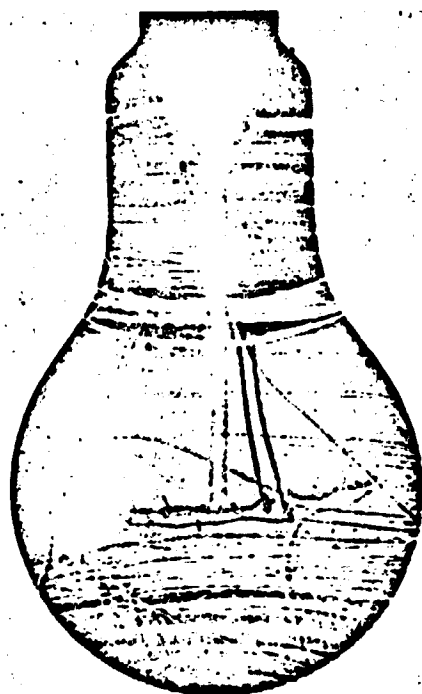


Figure 42. Shadow image of an Incandescent Bulb.

While the change in brightness of light deflection is directly proportional in the Toepler schlieren method, there is an indication of alteration in light deflection with the shadow method (in the case of small deflections). If we imagine two fields of adjacent constant light deflection, differing in strength, these two fields would have a different degree of blackening in a Toepler schlieren image; in contradistinction to this, they would be equally bright in a shadow exposure, and only the transition zone would become noticeable because of a change in brightness.

A field with a light deflection deviating from its outer field will be dark on the one side and surrounded by a bright margin on the other. If the field is narrow, the bright and dark streaks lie next to each other in the schlieren image and, as already emphasized, are particularly striking because of their contrast. Figure 44 is also an example of this: the shadow

/354

image of a glass plate interspersed with numerous "threads". In the four individual images the object to screen distance has been varied at the same time and it is directly obvious that sensitivity increases up to $g = h/2$.

Another illustrative example, again very clearly confirming the above derivation of sensitivity depending on g/h , is Figure 45. Here there are ten

exposures of a glass plate with schlieren at different schlieren-screen distances. The distance from the light source to the screen was 3 m and the perforation diameter of the diaphragm serving as a light source was 0.3 mm. Naturally all images were of different sizes in the original. They had to fit the same format in order to be compared. This was done in Figures 45 and 44.

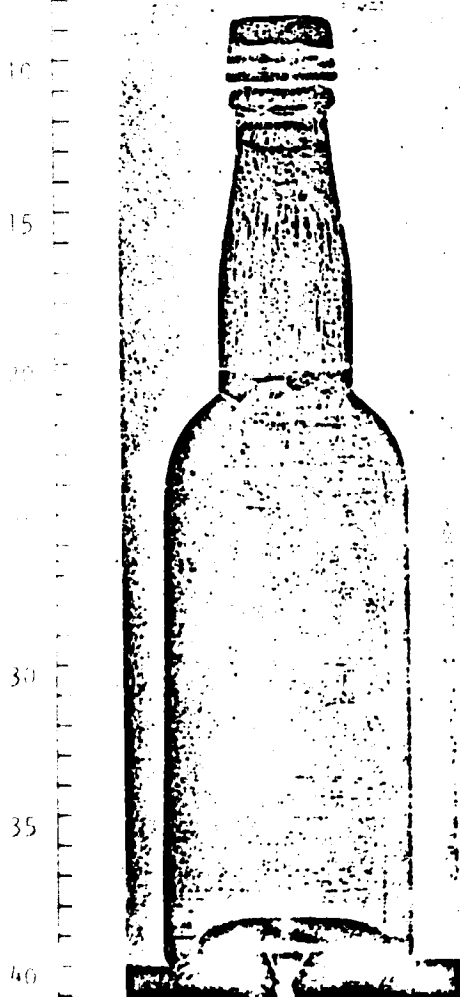


Figure 43. Shadow Image of a Good Bottle But With Perturbations at the Neck.
(From H. Jebesen-Marwedel: *Glastechnische Fabrikationsfehler* [Manufacture Defects in Glass Technology], Berlin, Springer, 1936.).

The first picture is a contact copy of the glass plate in the same arrangement ($g = 0$), so with extremely strong illumination. It shows up all the blisters, scratches and particles of dirt in the glass plate. The next exposure was made 1 cm away from the plate and the effects on it have become much clearer; this increases considerably in the following images (3.5 and 10 cm). At a distance of 25 cm the deflected light already bypasses some spots at the edge of the plate and at other spots, particularly at the corners, the light is deflected inwardly. As was to be expected, the greatest relative deflections occur at $g = h/2 = 150$ cm. If the distance between the schlieren and the screen is enlarged, sensitivity drops again. Therefore the image with $g = 100$ cm corresponds to the one with $g = 200$ cm, and the one with $g = 40$ cm corresponds to the one with $g = 260$ cm, exactly as shown in Curve I in Figure 40.

If the optical condition of the object were known, the distribution of brightness on the screen could be computed definitely on the basis of laws of optics. The reverse, computing the optical condition of the object from the image on the screen is generally impossible; the most important prerequisite for this, a clear correspondence between the size and direction of light deflection at every point in the object, is not available. However, if care is taken with a diaphragm to see that the light from the light source can only fall through certain definite parts of the process, measuring the position of the corresponding dots of light on the screen can show how large angle ϵ is and what its position is for the point of the process in question. This makes further evaluation possible. In many cases it is not even

/355

/358

necessary to introduce special diaphragms, because the type of process itself permits unequivocal measurement and correlation of the light deflection. To clarify this let us present two images taken of the free convection of a horizontal, heated pipe [86] (Figures 46a and b). The pipe had a diameter of 42 mm and was 504 mm long. In a case like this it is necessary to illuminate the process with the most exactly parallel light possible for the sake of simple evaluation. In practice this is partially handled by making h as large as possible in view of the space available, e.g., by using a long hall in the basement of the Institute. With thermo-hydrodynamic processes undesirable air currents may often disturb this process to a considerable degree. In the present case the long light path required was considerably shortened by placing the light source approximately at the focal point of a concave mirror. When such is available, this is the simplest way and, if necessary, precisely parallel light can be produced.

/359

The distance from the end of the heating pipe to the exposure plate was 7.44 mm for Figure 46a. The pipe had a temperature of 76°C while the room temperature was 20.6°C . A number of peculiar lines can be seen in the image. The inner, circular, dark space extending upward does not correspond to the diameter of the pipe which was hatched in later. As already explained, the circular, dark field with the tube shaped extension on top represents the total schlieren area from which the light was deflected. It includes the air warmed by the heat exchange of the pipes. If we now use diaphragms to check the coordination of the other light lines, we find that the incident light streaking directly along the surface of the cylinder supplies the curve which surrounds the central area at a greater distance in the shape of a heart. If a circular diaphragm is used to make sure that only light in the vicinity of the surface of the cylinder can get through, only the heart shaped curve is found.

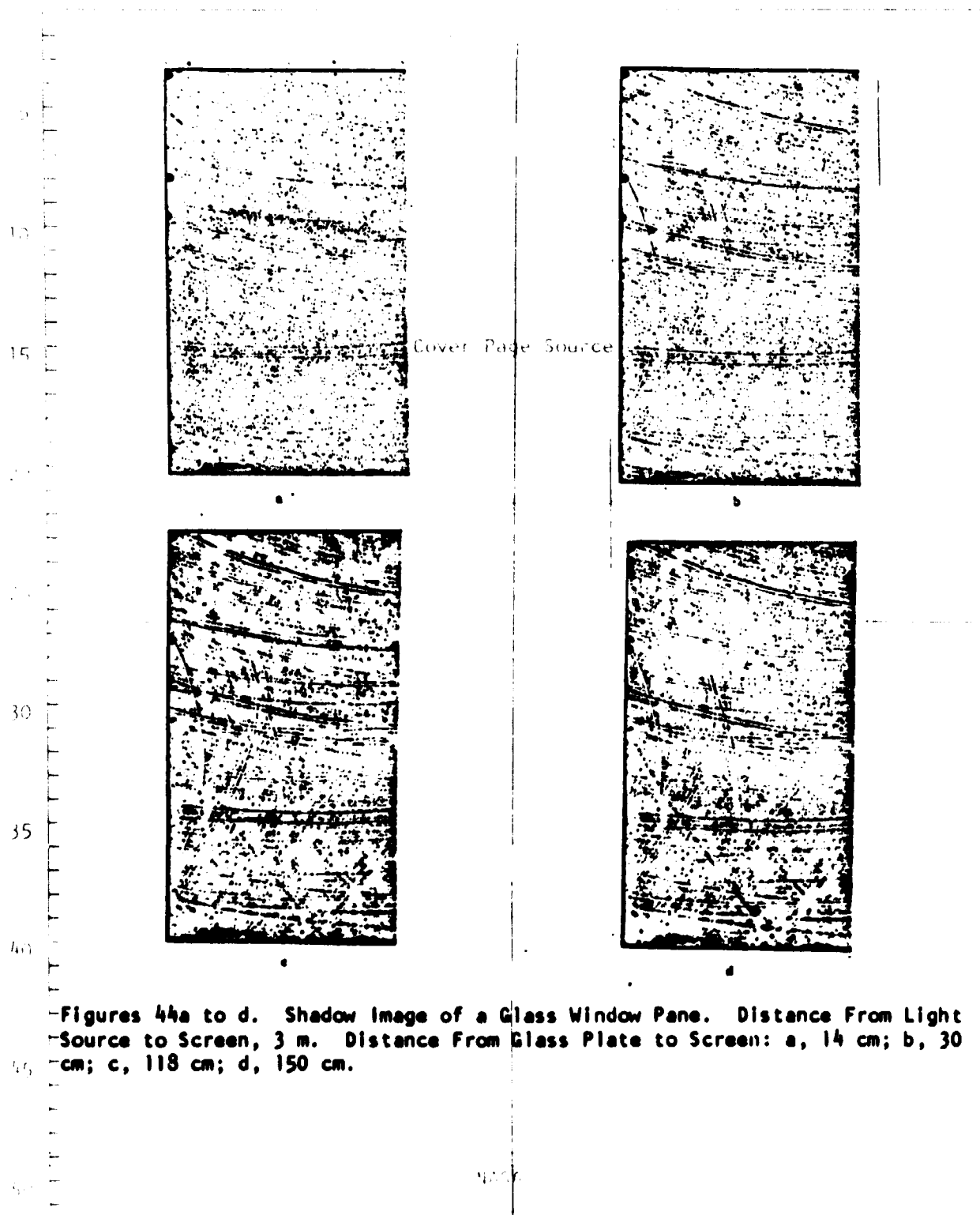
Figure 46b was produced by this method. Here the heart-shaped curves for different pipe temperatures are superimposed. With an increase in pipe temperature, the diameter of the curves increases. Now it is simple to determine the heat transition index for each spot on the cylinder surface from the form of the heart-shaped curve (see p. 387). This agrees well with other measurements.

In some cases the direct shadow method can be used for a direct quantitative evaluation, but this is not generally possible. Therefore it is usually used only for a purely qualitative indication of the presence of schlieren. The great advantage of the direct shadow method is the extremely simple arrangement which does not require any optics and correspondingly allows processes of any extension to be investigated. Still, the use of a condenser to illuminate the perforated diaphragm and, in case of need, a concave mirror or a lens to shorten the path of rays is advantageous.

Some thought should still be given to the most appropriate way of photographing the schlieren image which generally appears on a very large screen.

REPRODUCIBILITY OF THE ORIGINAL PAGE IS POOR.

/355



Even

Roman

51
Odd

/356

&

/357

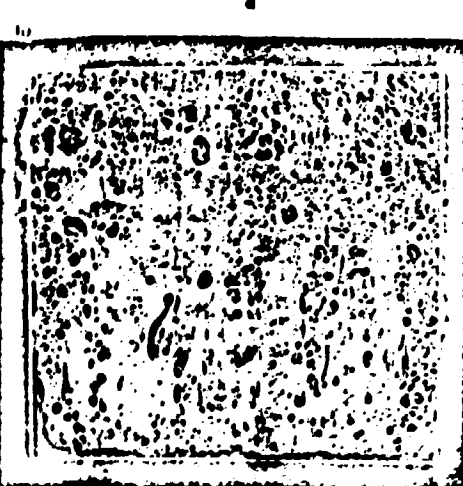
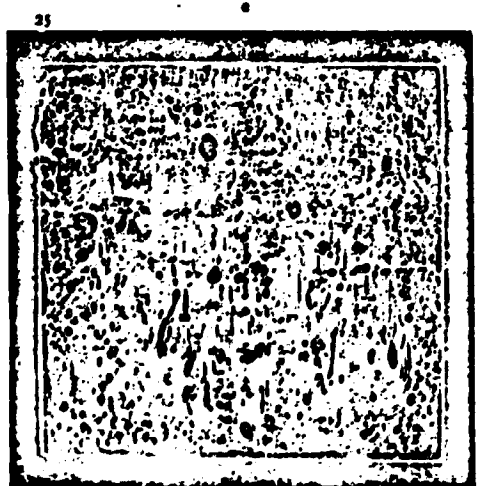
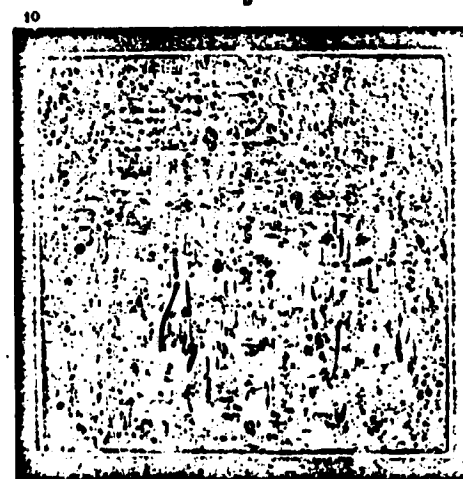
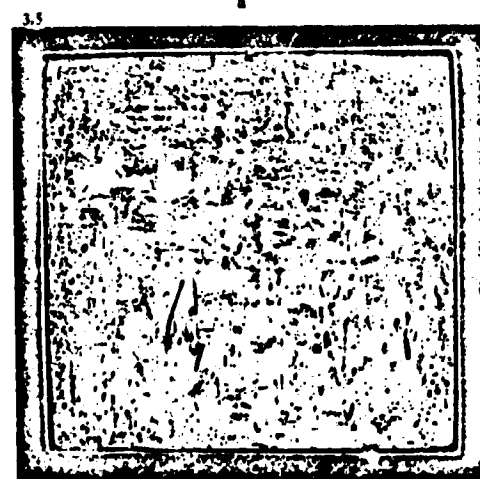


Figure 45. (See Caption on Following Page).

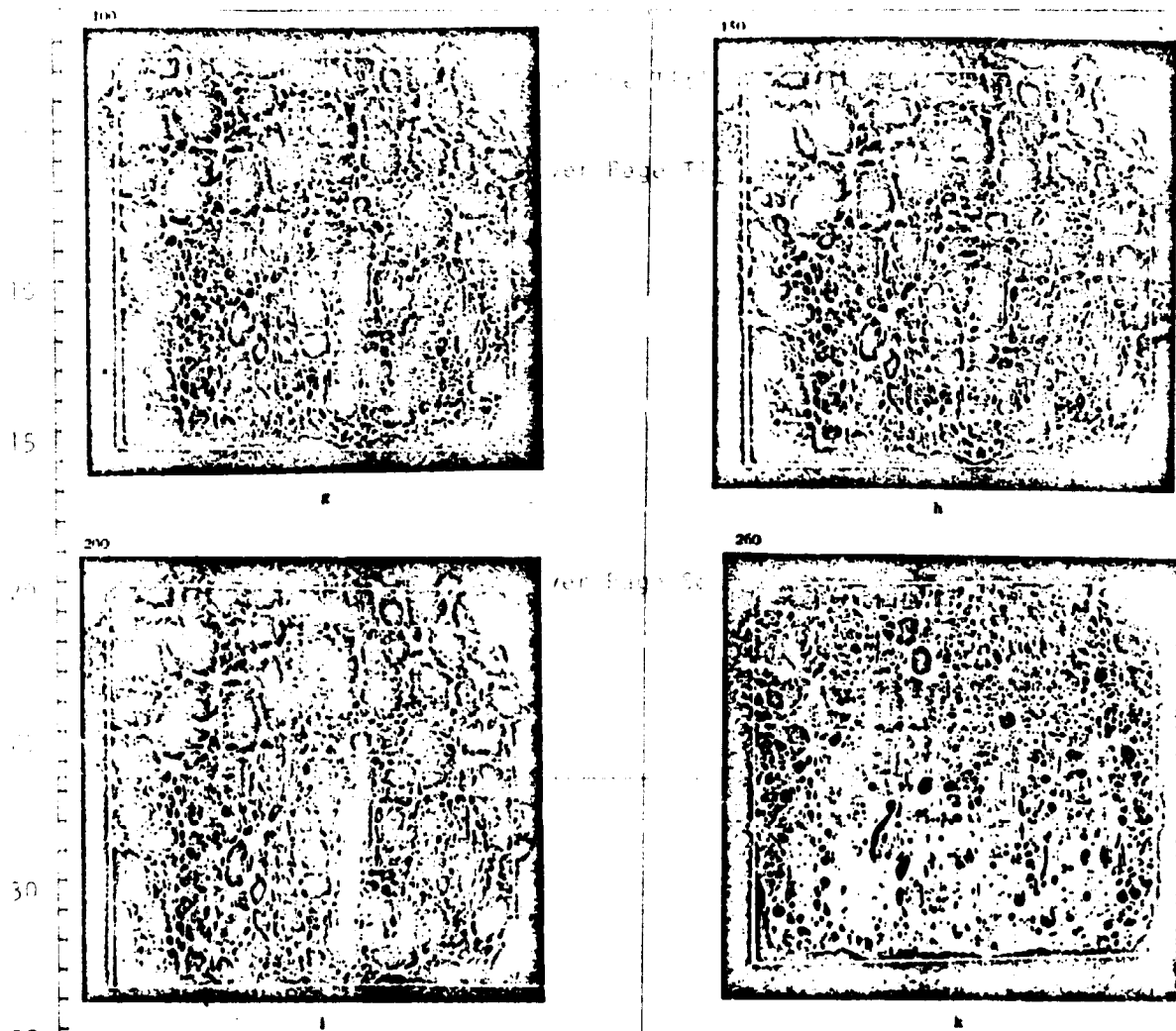


Figure 45a to k (Excluding j). Dependence of the Sensitivity of the Direct Shadow Method on the Position of the Schlieren Between the Light Source and the Screen.

h = 3m, g = 0 1 3.5 10 25 cm,
40 100 150 200 260 cm.

In many cases it will be possible to cover the screen itself with photographic paper and to expose it directly. If objects are too large, the screen image will have to be photographed with a special camera. However, this will be difficult if the screen image is not very bright at a sensitive setting and if the movement of the process does not permit sufficiently long exposure time. Then one will have to be satisfied with observation by eye or use a different method.

/360

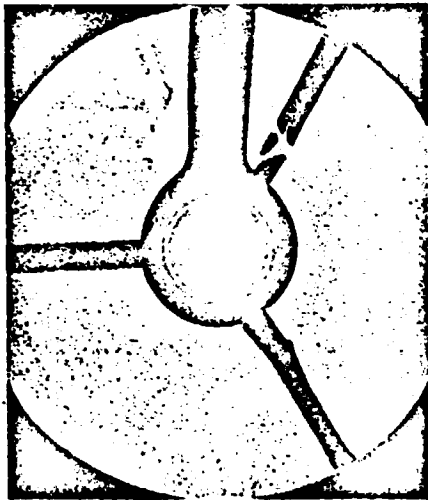


Figure 46a. Shadow Exposure of a Heated Horizontal Pipe. The Three Black Radii are the Shadow Image of the Pipe Fastening. (From *Heizung u. Lueftung* [Heating and Ventilation]).

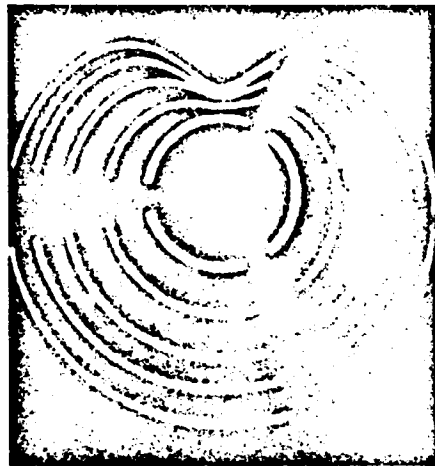


Figure 46b. Deflection of the Light Falling Directly on the Surface of a Heating Pipe in Streaks. Wall Temperature of the Inner Circle 21°C is the Outside Temperature, While for Successive Curves it is 33.0°C; 44.6°C; 56.0°C; 67.5°C. (From *Heizung u. Lueftung*).

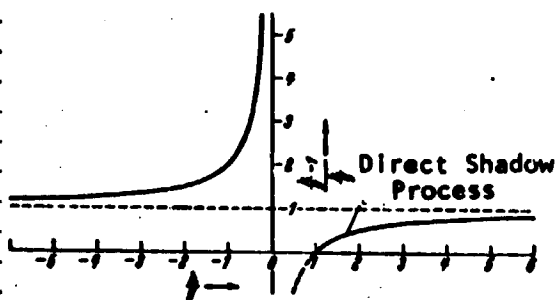


Figure 47. Sensitivity as a Function of Light Source to Screen Distance With the Schlieren at a Constant Distance From the Screen.

17. Schlieren Method Number 12: Reversal of the Direct Shadow Method

In accordance with equation (31), the sensitivity of the direct shadow method was considered proportional to the shift Δa caused by the deflection in the schlieren on the screen in ratio to the size of the shadow image of the schlieren. This sensitivity can be raised theoretically to infinity if it is possible to make the size of the shadow contour of the schlieren arbitrarily small keeping Δa constant. Now let us start with

equation (31) again and write it in another form as follows:

$$\frac{\Delta a}{a} = \frac{a}{d} \cdot \frac{\frac{h}{d} - 1}{\frac{h}{d}}. \quad (38)$$

If we keep g constant and allow h to increase in relation to g , sensitivity will increase from the value 0 at $h = g$ to the value eg/d for $h \rightarrow \infty$. At $h = \infty$, the schlieren is penetrated with parallel light and the shadow contour is as large as the original object. Now if convergent light is used, the projection of the object in question is smaller than the object itself; since here Δa remains essentially constant, the sensitivity correspondingly in-

creases. Figure 47 graphically shows the slope of the function $\frac{\frac{h}{g} - 1}{\frac{h}{g}}$

as a function of h/g .

The right branch of the curve from $h/g = 1$ up to $h/g = \infty$ corresponds to the direct shadow method. The left branch corresponds to the method using a convergent pencil of light. At $h/g = 0$, i.e., $h = 0$, sensitivity would be infinitely large. In this case the point of convergence of the light rays lies directly on the screen and the size of the object diminishes to 0.

/361

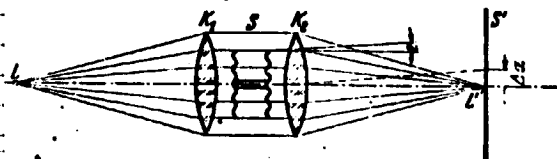


Figure 48. Arrangement for Schlieren Method Number 12.

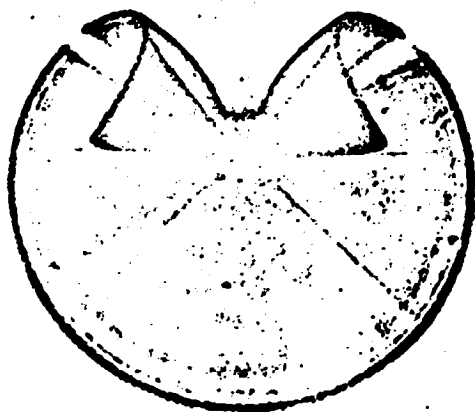


Figure 49. Light Deflections on a Horizontal Heated Pipe as a Radiation Pattern. (Exposure by Schlieren Method Number 12.)

The production of a convergent pencil of rays naturally requires the help of optics which thus removes one great advantage of the direct shadow method. Nevertheless, this method can be used advantageously in certain cases. The horizontal heating pipe can again serve as an example.

In Figure 48 let the phenomenon be arranged in the parallel path of rays between two lenses or concave mirrors. Let light source L be as concentrated as possible. The convergent point L' of the pencil of light will then be located exactly on screen S' . If the photographic paper placed on the screen is now exposed, Figure 49 is obtained. The object itself is concentrated at the center and the deflected rays illustrate the surrounding curves. The deflections are to be measured directly as distances from the center and this practically provides a radiation pattern for the deflections. Still, an exposure of this kind, just as in the direct shadow method, can only be evaluated if

coordination is possible. In the case at hand the maximal deflection corresponds to the layer of air at the immediate surface of the cylinder where the temperature gradient is greatest. The heart-shaped lines shown in Figures 46a and b also originate at this surface.

The arrangement of Figure 48 is identical with the Toepler method, except that here the light deflection at the center of the image of the light source is exposed directly, while in the Toepler method a schlieren diaphragm is introduced here and transposes the value of the deflection into a brightness value in the image of the object. Exposing this phenomenon makes it possible to obtain uniqueness, i.e., the correct coordination of the deflections to the points in the object.

18. Arrangements Which Permit Quantitative Evaluation of the Direct Shadow Method

As described in §16, the images exposed with the standard shadow method are not unambiguous, since the origin of the light cannot generally be determined. This indefiniteness could be bypassed if it were possible to "label" the individual light rays. This is practically possible with the following arrangement (Figure 50): the point-shaped light source L^* is projected with condenser lens C into L where a perforated diaphragm is located. A cross lattice has been set up at B with an image appearing on screen S' through lens O . In this way the divergent pencil of rays LS' is, so to say, subdivided into several light rays. A shift of each light ray caused by an object S can easily be demonstrated by photography with and without schlieren. Figure 51 shows an example of this. This is a reduced reproduction of part of an original exposure. This was produced by projecting a Heidenhain cross lattice with 40 lines/cm onto the wall about 7 m away. In front of the objective stood a 5 mm diameter diaphragm onto which the arc lamp crater was projected. The glass plate being tested was 3.44 m away from the wall so that a shift of 1 mm amounted to a deflection of 1 angle minute. A strip of silver bromide paper was fastened to the wall and two exposures were successively made on it, with and without the glass panel. Evaluation is naturally very tedious, since the shift of every individual point must be measured separately when using a comparator (cf. p. 385).

If a negative of the cross lattice image appearing on the screen is used as an intermediate screen, a lack of light deflection would produce complete darkness, since the screen would be black everywhere where light hit it and vice versa. But now, if a light deflection occurs in the object, complete coverage no longer exists and brightness, proportional to the deflection, appears as long as the maximum possible brightness is not exceeded. According to F. Weidert, if a very narrow cross lattice is used, e.g., a reproduction grid, the shadow image will work like a Toepler schlieren image.

This photograph was furnished through the courtesy of Prof. Weidert, Optical Institute of the Technical University of Berlin.

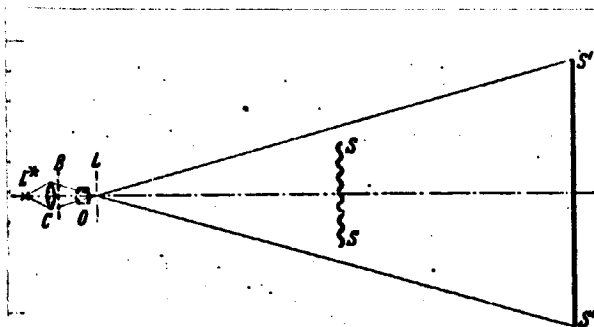


Figure 50. Arrangement for Quantitative Evaluation by the Direct Shadow Method.

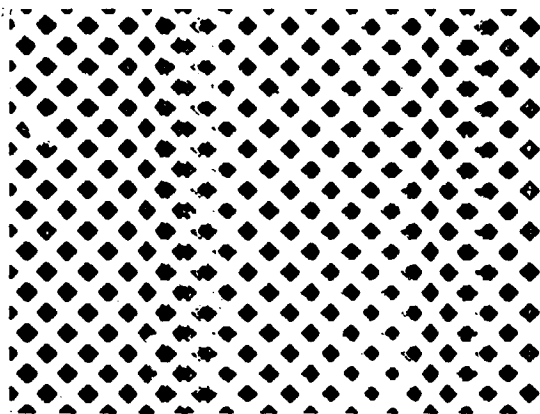


Figure 51. Distortion of the Points of a Cross Lattice According to Heidenhain Through a Glass Plate in the Arrangement According to Figure 50.

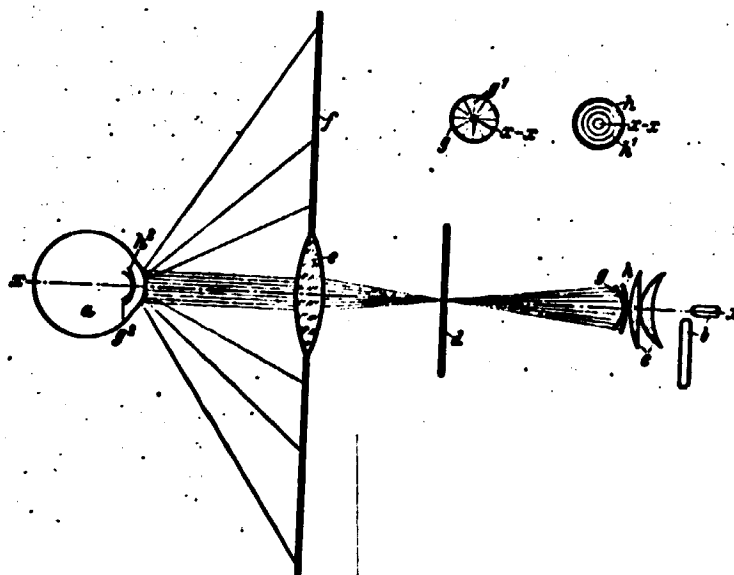


Figure 52. Schematic Arrangement of a Zeiss Device for Testing the Surface Condition of Curved Reflecting Bodies in Reflected Light.

The principle of projecting a grid onto a screen by way of the object being investigated is also mentioned in a Zeiss patent [124] which describes an arrangement for testing the surface condition of the cornea (cf. Figure 52). With the help of condenser c the arc lamp b illuminates two coordinate grids g and h; the light then passes through perforated diaphragm d and is rendered parallel by means of lens e. A reflection occurs at the cornea of eye a and then an illumination of screen f. At the same time lens e projects the coordinate grids g and h onto the screen by way of the cornea. The grids are attached to two surfaces, touching in the optical axis $x...x$, which would be identical to the astigmatic image field surfaces if a projection of plane f occurred in a reversed path of rays. Then if radial lines (g^1) are produced in g and circles (h^1) in h, they both appear sharply at f and form a polar coordinate network. Now if the surface of the cornea is deformed, the points of the network shift measurably and allow deductions to be made about the structure of the cornea. The path of rays between e and h is telecentric in order to be somewhat independent of the distance between the eye and lens e.

The problem becomes simpler if the direction of the light deflection in the object is determined ahead of time. This is, e.g., the case in diffusion processes, in the ultracentrifuge and in machine drawn plate glass. In this case straight slits running perpendicularly to the deflection direction can be used instead of a cross lattice. This arrangement has been used for some time by customs officers to separate mirror and plate glass.

If the state of the object in straight lines is constantly perpendicular to the direction of deflection, the projection of a single oblique slit is enough. In this way O. Wiener investigated diffusion processes as early as 1893 (see §29) [13].

The so-called "scale method" introduced into ultracentrifuge technology can also be used in a similar case. A scale is photographed through an object located in the path of rays; existence of light deflection is determined by a shift in the parts of the scale (cf. §30).

One advantage of the schlieren method is that a rather large field of vision can be observed at one time. If this requirement is eliminated, i.e., if the object is to be studied at one point, the following arrangements can be used:

1. Direct registration of the deflection on a running film in accordance with Figure 53. The image of the slit L is contracted by a cylindrical lens in order to increase brightness. The object being investigated is located directly in front of lens O; this must not have too large an opening, because large deflections of a different magnitude within such an area of the object, which is also illuminated by a beam of light, can make the registration fade. Diffraction phenomena also determine the limit of sensitivity here. F. Weidert tried to increase the available resolution through the use of a slit by producing an overlap of the diffraction of two slits with the aid of a Wollaston prism. The center line thus present has a greater gradient at its

/364

edges and can therefore be measured more exactly than the diffraction image of a single slit.

Page One Title

/365

2. Instead of the direct registration of Figure 53, a photocell can first be more or less strongly illuminated and the registration takes place in an oscillograph. Naturally, care must be taken that when the deflection is changed the light does not always fall onto different parts of the cell coating, since the coating does not have the same sensitivity everywhere. As is done, for instance, in the Toepler arrangement, the light is passed through a diaphragm and the pertinent area of the object is cast onto the photocell with a lens. With the aid of two prisms, F. Weidert separates the light into two separate pencils at the position of the schlieren diaphragm in the Toepler arrangement; each of these strikes a separate photocell. One of the pencils is strengthened by deflection and the other weakened. With an appropriate bridge circuit, greater sensitivity and independence of light source fluctuation can be attained in this way.

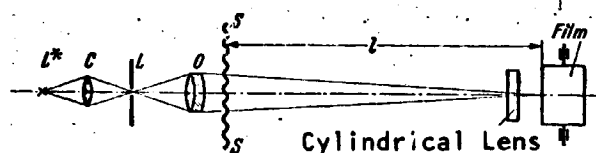


Figure 53. Arrangement for Direct Recording of the Light Deflection.

The F. Kopperschmidt Company (Hamburg) has built a similar piece of apparatus for its own requirements; thorough mechanization makes it possible to investigate a rather large transparent plate relatively fast and to mark the magnitude of the deflection directly on the plate itself in color.

3. Another arrangement has been developed by the Kodak Company (Rochester) by C. Tuttle and R. Cartwright [136]: two beams of light are projected through the test object at a certain distance and unite again on the ground-glass plate. Both light beams are colored and complementary to one another so that their juncture produces white light. Now if a deflection occurs in the glass plate and has a different value for one of the light beams than for the other, two colored streaks will appear next to one another on the ground-glass plate. Sensitivity can be adjusted in such a way that the colors only appear when a certain limit has been exceeded. This method can also be adopted for use with reflection. The deflection is not immediately obvious, but only the difference in the deflection at two points of the objects. This means, for instance, that the inclination of a reflecting surface cannot be determined with this method, but its curvature can be.

III. Theoretical Fundamentals for Quantitative Evaluation

/366

19. Determination of the Refractive Index From Light Deflection in a Schlieren

The quantitative result provided almost always by schlieren methods is the spatial extension and the shape of the schlieren. Valuable results are often derived from this fact alone. Until 10 years ago this method was considered satisfactory for this purpose. As shown above, however, suitable

construction makes it also possible to measure numerically the light deflection undergone by a beam of light after it has gone through the schlieren. Naturally, it is not generally possible to expect any conclusions about the physical state in the schlieren from this fact; this is because the light deflection for a light ray indicates a single value for a generally considerable number of unknowns. A series of other prerequisites must also be fulfilled before the schlieren condition is defined numerically.

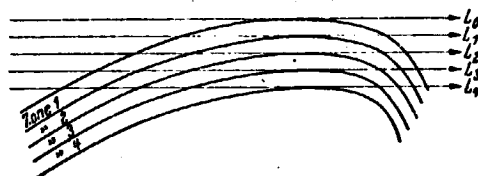


Figure 54. Principle for Quantitative Evaluation.

The most essential of these prerequisites is knowledge of the slope of the curves for a constant n degree. If these are known, evaluation in principle proceeds as follows: in Figure 54 let the light beam L_0 go

straight past the schlieren without being deflected. According to the pure shadow method, darkening of the field of vision would begin to its side, since light rays L_1 ,

L_2 , etc. are deflected. Light ray L_1 should go through a zone which is delineated by two surfaces (in the drawing plane curves) with a constant n degree. The shape of these surfaces must be assumed as known and will be computed within this zone with a uniform n degree. Under these conditions the n degree in the first zone can be computed from the deflection ϵ_1 of light rays L_1 . Light rays L_2 goes through both zone 1 and zone 2; since n degree is now known for zone 1, n degree for zone 2 is obtained from ϵ_2 . L_3 goes through zones 1, 2 and 3, and since n degree for zones 1 and 2 is already known, n degree for zone 3 can be computed from ϵ_3 , until the innermost zone is known.

If the complete gradient of n degree is determined in this way, the refractive index itself can be computed from it by integration.

If the geometrical form of a schlieren is now known at first, it is possible that something may be found by projecting rays through the schlieren from different directions. The basis for the computation of light deflection is afforded by the following equation of theoretical optics:

$$\frac{1}{R} = \frac{n \text{ degree}}{n} \sin \varphi. \quad (39)$$

Here R is the radius of curvature of the light beam, n is the refractive index and φ is the angle between n degree and the direction of the light ray (Figure 55).

NASA

/367

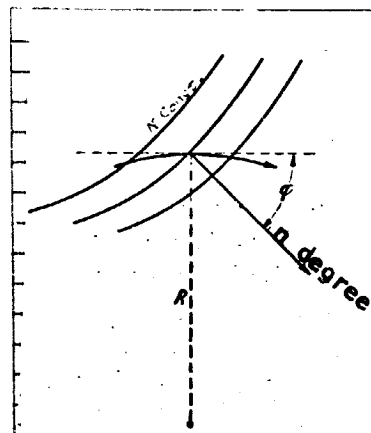


Figure 55. Curvature of a Light Ray in an Inhomogeneous Medium.

In Figure 56 let the direction of the incident parallel beams of light be the z direction. The components of the deflection of a beam of light falling through point x_i, y_k amounts to $(\epsilon_x)_{x=x_i, y=y_k}$ and $(\epsilon_y)_{x=x_i, y=y_k}$.

In Figure 56 below the n degree is plotted for a point P which lies inside the schlieren. With the z direction n degree forms the angle ϕ since the light beam can be assumed as practically a straight direction. If we now imagine a new plane, the η plane, lying through n degree and through the light beam passing through point x_i and y_k , the deflection of the light beam occurs at point P in this plane and gives

$$1. \eta' \ll 1, \quad (40)$$

Since the path of the light ray can be considered almost a straight line,

$$2. \eta'' = \frac{n \text{ degree}}{n} \sin \phi, \quad (41)$$

follows from equation (39), in which $\frac{1}{R} = \frac{\eta''}{(1 + \eta'^2)^{3/2}} = \eta''$ (with $\eta' \ll 1$).

Let the angle of inclination of the η - z plane in relation to the y - z plane be θ ; then

$$\begin{cases} x = \eta \sin \theta & y = \eta \cos \theta \\ x' = \eta' \sin \theta & y' = \eta' \cos \theta \\ x'' = \eta'' \sin \theta & y'' = \eta'' \cos \theta \end{cases} \quad (42)$$

whence

$$\begin{cases} x'' = \frac{n \text{ degree}}{n} \sin \phi \cdot \sin \theta, \\ y'' = \frac{n \text{ degree}}{n} \sin \phi \cdot \cos \theta. \end{cases} \quad (43)$$

From Figure 56 below we get the following relationships:

NASA

$$\begin{cases} n \sin \varphi \sin \vartheta = \frac{\partial n}{\partial x}, \\ n \sin \varphi \cos \vartheta = \frac{\partial n}{\partial y}. \end{cases} \quad (44)$$

By introducing (44) into (43), we get

$$\begin{cases} x'' = \frac{1}{n} \frac{\partial n}{\partial x}, \\ y'' = \frac{1}{n} \frac{\partial n}{\partial y}. \end{cases} \quad (45)$$

In all cases where n occurs as the only factor, we can then usually introduce n_0 , the refractive index before the beginning of the schlieren, with a fair bit of accuracy, so that

$$C \begin{cases} x'' = \frac{1}{n_0} \frac{\partial n}{\partial x}, \\ y'' = \frac{1}{n_0} \frac{\partial n}{\partial y}. \end{cases} \quad (45a)$$

Since the passage of the light ray inside the schlieren is satisfactorily assumed as straight, x'' and y'' depend only on z . The deflections $(\epsilon_x)_{x_i}$, y_k and $(\epsilon_y)_{x_i}$, y_k then produce

$$\begin{cases} (\epsilon_x)_{x_i, y_k} = \int_{x_i}^{x_k} \frac{1}{n} \left(\frac{\partial n}{\partial x} \right)_{x_i, y_k} dz, \\ (\epsilon_y)_{x_i, y_k} = \int_{x_i}^{x_k} \frac{1}{n} \left(\frac{\partial n}{\partial y} \right)_{x_i, y_k} dz. \end{cases} \quad (46)$$

because the deflection angle $(\epsilon_x)_{x_i, y_k}$, for example, is identical with $x' = \partial x / \partial z$ of the light ray at its exit from the schlieren (thus at point $x = x_i$, $y = y_k$, $z = z_2$).

If n were now provided as a function of position, light deflection ϵ could be easily computed from equation (46) (with the assumed condition that the light ray varies only slightly from a straight line inside the schlieren). However, in reality, ϵ is known through the evaluation of a schlieren photograph and n is to be determined as a function of position. Now, the solutions for this problem will be given below for three special cases.

NASA

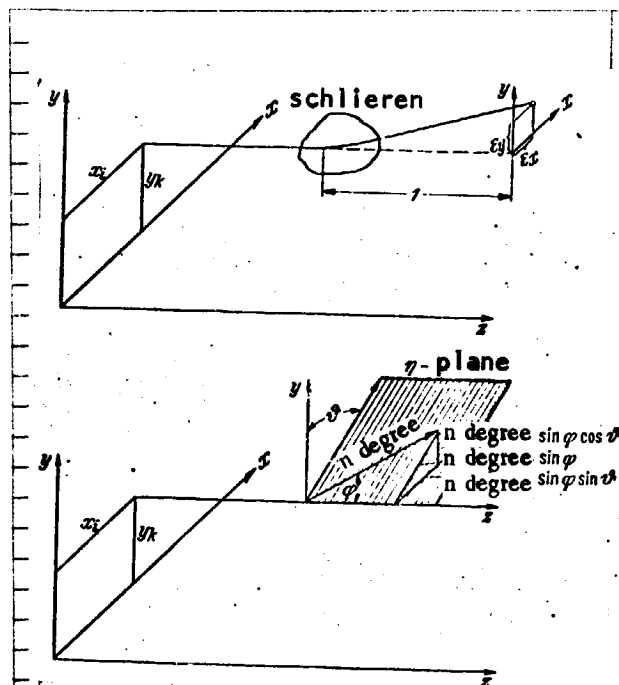


Figure 56. Above: Deflection ϵ_x and ϵ_y For Point x, y of the Schlieren. Below: Resolution of n Degree.

If the process under investigation is bounded by two plane-parallel glass plates, another refraction occurs at the exit where the light beam has been deflected by angle ϵ , so that ϵ^* , which has truly been measured, is related to ϵ in equation (47) or (47a) on the basis of the law of refraction as follows:

$$n\epsilon = n_0\epsilon^* \quad (48)$$

whence

$$\begin{cases} \left(\frac{\partial n}{\partial x}\right)_{x,y} = \frac{n_0}{l_s} \epsilon_x^* \\ \left(\frac{\partial n}{\partial y}\right)_{x,y} = \frac{n_0}{l_s} \epsilon_y^* \end{cases} \quad (49)$$

The refractive index itself is then obtained by integration beginning with the edge of the process

1. Cylindrical Field. If the condition inside the schlieren is constantly parallel to the z axis, n , $\partial n/\partial x$ and $\partial n/\partial y$ are independent of z and therefore can be immediately integrated with equation (46). Each beam of light goes through only one zone with an unknown n degree. Therefore:

$$\begin{cases} \epsilon_x = \frac{1}{n} \left(\frac{\partial n}{\partial x}\right)_{x,y} \cdot l_s \\ \epsilon_y = \frac{1}{n} \left(\frac{\partial n}{\partial y}\right)_{x,y} \cdot l_s \end{cases} \quad (47)$$

or
source

$$\begin{cases} \left(\frac{\partial n}{\partial x}\right)_{x,y} = \frac{n}{l_s} \epsilon_x \\ \left(\frac{\partial n}{\partial y}\right)_{x,y} = \frac{n}{l_s} \epsilon_y \end{cases} \quad (47a)$$

Here l_s means the extent of the schlieren in the z direction.

$$\begin{cases} n_{x,y} = n_0 + \frac{n_0}{l_s} \int \epsilon_x^* dx \\ \text{or} \\ n_{x,y} = n_0 + \frac{n_0}{l_s} \int \epsilon_y^* dy \end{cases} \quad (50)$$

or

$$\begin{cases} \frac{\Delta n}{n_0} = \frac{1}{l_s} \int \epsilon_x^* dx \\ \text{or} \\ \frac{\Delta n}{n_0} = \frac{1}{l_s} \int \epsilon_y^* dy. \end{cases} \quad (50a)$$

2. Axially Symmetrical Field. The curves with constant n should be concentric circles at every point perpendicular to the y -axis, therefore in the x - z -plane, i.e., symmetry prevails with respect to the y -axis. Then,

/370

$$\begin{aligned} \frac{\partial n}{\partial x} &= \frac{\partial n}{\partial r} \cdot \frac{\partial r}{\partial x}, \\ r &= \sqrt{z^2 + x^2}, \quad r dr = z dz + x dx, \\ \frac{\partial r}{\partial x} &= \frac{x}{r}. \end{aligned}$$

Since every ray of light may be practically assumed as a straight line, ($dx = 0$) is

$$dz = \frac{r}{x} dr.$$

Introducing these values into equation (46) produces

$$\begin{cases} (\epsilon_x)_{x_0, y_0} = 2 \int_{r=x_1}^{r_0} \frac{1}{n} \cdot \frac{\partial n}{\partial r} \cdot \frac{x_1}{x} dr, \\ (\epsilon_x)_{x_0, y_0} = 2 \int_{r=x_1}^{r_0} \frac{1}{n} \cdot \frac{\partial n}{\partial r} \cdot \frac{x_1}{\sqrt{r^2 - x_1^2}} dr, \\ (\epsilon_y)_{x_0, y_0} = 2 \int_{r=x_1}^{r_0} \frac{1}{n} \cdot \frac{\partial n}{\partial y} \cdot \frac{r}{\sqrt{r^2 - x_1^2}} dr. \end{cases} \quad (51)$$

In order to evaluate these integrals, let us divide the cross-section into a series of concentric circles (cf. Figure 57) and in each ring posit

$$C \begin{cases} \frac{\partial n}{\partial r} = \text{const} = \mu_\lambda \\ \text{and} \\ \frac{\partial n}{\partial y} = \text{const} = \nu_\lambda. \end{cases} \quad (52)$$

Then, for the deflection which the i^{th} light beam experiences in the λ^{th} circle (n introduced as a factor approximately equal n_0)

$$\begin{cases} (\epsilon_x)_{x_i, y_k} = 2 \frac{\mu_\lambda}{n_0} \int_{r_{\lambda-1}}^{r_\lambda} \frac{x_i}{\sqrt{r^2 - x_i^2}} dr \\ \text{and} \\ (\epsilon_y)_{x_i, y_k} = 2 \frac{\nu_\lambda}{n_0} \int_{r_{\lambda-1}}^{r_\lambda} \frac{r}{\sqrt{r^2 - x_i^2}} dr. \end{cases} \quad (53)$$

are valid.

Both integrals can be solved and give

(4'')

/371

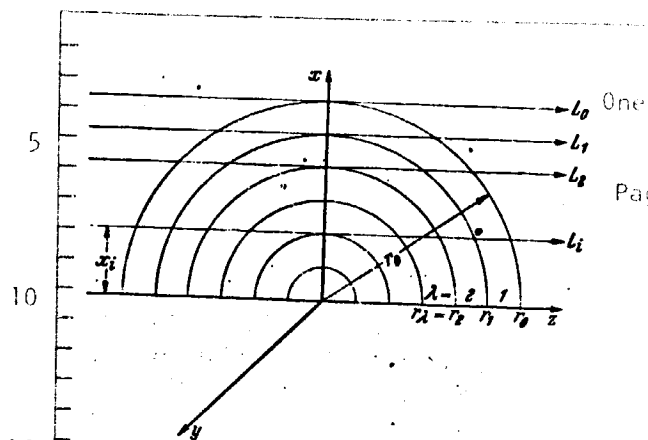
$$\begin{cases} (\epsilon_x)_{x_i, y_k} = 2 \frac{\mu_\lambda}{n_0} x_i \left[\Re(\coth) \frac{r_{\lambda-1}}{x_i} - \Re(\coth) \frac{r_\lambda}{x_i} \right], \\ (\epsilon_y)_{x_i, y_k} = 2 \frac{\nu_\lambda}{n_0} x_i \left[\sqrt{\frac{r_{\lambda-1}^2 - x_i^2}{x_i^2}} - \sqrt{\frac{r_\lambda^2 - x_i^2}{x_i^2}} \right]. \end{cases} \quad (54)$$

The total deflection of the i^{th} light beam may then be written as a sum of the single deflection in each of the different circles

$$\begin{cases} (\epsilon_x)_{x_i, y_k} = 2 \frac{x_i}{n_0} \sum_{\lambda=1}^{L-1} \mu_\lambda \left[\Re(\coth) \frac{r_{\lambda-1}}{x_i} - \Re(\coth) \frac{r_\lambda}{x_i} \right], \\ (\epsilon_y)_{x_i, y_k} = 2 \frac{x_i}{n_0} \sum_{\lambda=1}^{L-1} \nu_\lambda \left[\sqrt{\frac{r_{\lambda-1}^2 - x_i^2}{x_i^2}} - \sqrt{\frac{r_\lambda^2 - x_i^2}{x_i^2}} \right]. \end{cases} \quad (55)$$

Each equation (55) contains its own basis for evaluation. With the ϵ_x (or ϵ_y), measured for each light beam L_1 , μ_1 (or ν_1) is found; equation (55) for light beam 2 then contains only μ_2 (or ν_2) as an unknown, only μ_3 (or ν_3) for light beam 3, etc. until all of the μ (or ν) of the cross-section are determined.

NASA



-Figure 57. Division of a Cross-
-Section Into an Axially Symmetrical
-Field in Concentric Circles. z-Axis =
- = Optical Axis, x-y Plane = Object
-Plane; y-Axis = Symmetrical Axis
- of the Process.

-requires previous evaluation of a larger number

3. Spherically Symmetrical Field. In this field all points with the same radius have the same n . Thus, axial symmetry does not apply to the y-axis alone, but also to the x-axis. Therefore the same relationships which were set up in the axially symmetrical field for the y-axis are correspondingly valid here for the x-axis, too.

In this case evaluation is considerably simplified by the fact that a cross-section going through the center of the spherically symmetrical field clearly determines the condition of the entire spatial field.

Thus, evaluation of such a cross-section according to the first equation (55) is sufficient. The second equation (55) does not apply since the lateral deflections are zero for symmetrical reasons.

Irregularities in the Refractive Index. Sometimes the refractive index in a schlieren does not increase steadily from n_0 but jumps to a certain value of n . This is the case for all explosion and firing phenomena in which a shock wave from the center moves forward with a sudden increase in pressure and refractive index. If a schlieren produced in this way were divided in accordance with methods mentioned above into a series of very narrow zones--practically impossible in most cases--, the infinitely steep rise would always be flattened out into a finite rise across the first zone width. However, with an equal Δn at the same spot of the schlieren, a finite rise produces a greater deflection of the light ray than an explosive rise, as can be seen

The values for the functions in brackets in equation (55) can be computed once and for all for a definite division of the cross-section. The refractive index itself is then found by integrating

$$\left\{ \begin{array}{l} n(r, y) = \int \left(\frac{\partial n}{\partial r} \right)_y dr + n_0 \\ \text{or} \\ n(r, y) = \int \left(\frac{\partial n}{\partial y} \right)_r dy + n_0. \end{array} \right. \quad (56)$$

In practice only the first of these two equations is applied, since these provide for determination of n directly from the evaluation of only one cross-section, while making the other integration number of other cross-sections.

/372

from the above equations and from Snell's law of refraction. Vice versa: if ϵ is given, too small a Δn is obtained from a flat rise, and only a series of steps bring the facts closer to the real Δn . Therefore it is necessary to take Δn directly from the Snell's law of refraction wherever the refractive index change is unstable. The relationships derived for the inside of the schlieren preserve their validity as before.

20. Determining the Other Equations of State

In all materials the index of refraction is in a direct relationship with density ρ , and the formula provided by L. Lorenz and H. A. Lorentz is valid:

$$\frac{n^2-1}{n^2+2} \cdot \frac{1}{\rho} = k. \quad (57)$$

This should be used for processes taking place in fluids. The constant k maintains its value with great precision even in changes of state; it is designated as the specific refractivity of the particular material; multiplied by the molecular weight it produces the molecular refraction.

However, when only processes in gases are concerned, n is not very different from 1 and $n^2 + 2 \approx 3$ can be posited first; this produces the formula of Newton and Laplace

$$\frac{n^2-1}{\rho} = 3k. \quad (58)$$

This can be further simplified by positing $n^2 - 1 = (n + 1)(n - 1)$ and, for $n + 1 \approx 2$, introducing:

$$\frac{n-1}{\rho} = \frac{3}{2}k. \quad (59)$$

This formula was first established by Gladston and Dale on the basis of investigations by Biot and Arago (1806).

The indices for constant k may be taken from Table 3.

The gas formula below is used with gases for computing from density to pressure or temperature:

$$\frac{p}{\rho} = \frac{R}{M} \cdot T. \quad (60)$$

p , ρ , T , R and M represent pressure, density, temperature, gas constant and molecular weight. If p' , ρ' and T' indicate the corresponding data for a

/373

/374

changed condition,

Page One Title

$$\frac{e'}{e} = \frac{p'}{p} \cdot \frac{T}{T'}$$

(61)

Cover Page Title

TABLE 3. SPECIFIC REFRACTIVITY AND MOLECULAR REFRACTION.

Material	Formula	Temperature °C	n_p $\lambda = 0.589 \mu$	ρ g/cm ³	A	Molecular Refraction
Air		0	1.000292	0.001293	0.1505	4.35
Oxygen	O ₂	0	271	1.429	0.1264	4.04
Nitrogen	N ₂	0	297	1.251	0.1583	4.43
Hydrogen	H ₂	0	143	0.090	1.0595	2.14
Carbon Dioxide	CO ₂	0	449	1.977	0.1514	6.65
Methane	CH ₄	0	444	0.717	0.4128	6.62
Acetylene	C ₂ H ₂	0	510	1.171	0.2903	7.55
Water	H ₂ O	18	1.33300	0.9986	0.2060	3.71
Carbon tetrachloride	CCl ₄	18	1.46455	1.5930	0.1734	26.67
Carbon disulfide	CS ₂	18	1.62887	1.2632	0.2813	21.41
Chloroform	CHCl ₃	18	1.45008	1.4483	0.1856	22.16
Methyl alcohol	CH ₃ (OH)	18	1.33001	0.7915	0.2578	8.26
Ethyl alcohol	C ₂ H ₅ (OH)	18	1.36306	0.7894	0.2817	12.97
Acetone	(CH ₃) ₂ CO	18	1.35960	0.7920	0.2784	16.16
Benzene	C ₆ H ₆	18	1.50296	0.8787	0.3364	26.26
Toluene	C ₇ H ₈	18	1.49904	0.8659	0.3391	31.22

To compute the pressure and temperature separately we need more information about the kind of change of state. Let us consider the following cases:

1. Isobaric Process $p' = p$. Then,

$$\frac{T'}{T} = \frac{e}{e'}$$

(62)

This relationship is used, for example, in evaluating all thermo-hydrodynamic processes. In these cases a change in density is caused practically only by a change in temperature, and pressure is to be assumed as approximately constant.

2. Isothermal Change of State $T' = T$.

$$\frac{p'}{p} = \frac{e'}{e}$$

(63)

Tr. Note: Commas indicate decimal points in Table 3.

Free isothermal changes of state in which a change in pressure would have to be measured are practically excluded. However, equation (63) could be used to compute the light deflection in an air lens between glass surfaces if the lens can be filled with measurably adjustable air pressure and maintained at constant temperature. The Zeiss Company suggests using a device of this type as a standard schlieren.

3. Adiabatic Process. With $\frac{p}{\rho^\kappa} = \frac{p'}{\rho'^\kappa}$

$$\frac{p'}{p} = \left(\frac{\rho'}{\rho}\right)^\kappa \quad (64)$$

Small changes in density permit the following transformation:

$$\begin{cases} \frac{p'}{p} = \left(1 + \frac{\Delta \rho}{\rho}\right)^\kappa \approx 1 + \kappa \frac{\Delta \rho}{\rho}, \\ \frac{\Delta p}{p} \approx \kappa \frac{\Delta \rho}{\rho}. \end{cases} \quad (65)$$

In the following table we provide for air, as a function of n and of the change in density as a percentage of density at 0°C :

1. The corresponding temperature for the isobaric process,
2. the corresponding pressure for the isothermal process and
3. the pertinent flow velocity for the adiabatic process, namely
 - a, expansion from an air pressure tank and
 - b, in a sound wave with finite amplitude.

In the first case the flow velocity u is computed according to the air-pressure tank formula of Saint-Venant and Wantzel (1839):

$$u = a_0 \sqrt{\frac{2}{\kappa - 1} \left[1 - \left(\frac{\rho}{\rho_0}\right)^{\kappa - 1} \right]}, \quad (66)$$

where a_0 represents the velocity of sound in the container and ρ_0 is the density in the container.

The flow velocity u' in a sound wave with finite amplitude, corresponding to an adiabatic change of state with the assumption of a linear flow process, follows from equation:

$$u' = \frac{2a}{\kappa - 1} \left[\left(\frac{\rho'}{\rho} \right)^{\frac{\kappa - 1}{2}} - 1 \right]. \quad (67)$$

Cover Page Title

Here a represents the sound velocity characteristic of the state p, ρ, T through which the sound wave passes:

$$a = \sqrt{\frac{\kappa RT}{M}}, \quad (68)$$

and ρ' represents the density of the point with flow velocity u' .

TABLE 4.

Refractive Index n	$\Delta\rho$ in % of the Density at 0°C	Temperature in °C at $\rho = 760$ mm Hg	Pressure in mm Hg at $t = 0^\circ\text{C}$	Velocity in m/sec	
				a	b
1,000292	0	0	760,0	0	0
291	0,354	1	757,4	27,2	1,2
290	0,708	2	754,5	39,8	2,4
289	1,002	3	751,7	48,7	3,4
288	1,416	4	749,0	56,3	4,8
287	1,77	5	746,5	62,9	6,0
286	2,13	6	743,6	68,9	7,2
285	2,48	7	741,1	74,7	8,4
284	2,83	8	738,3	79,8	9,6
283	3,18	9	735,7	84,6	10,8
282	3,54	10	733,1	88,3	12,0

4. Change of State According to the Dynamic Adiabatic Curve. In the case of determining the pressure in an intense shock wave, the change of state at the front of the pressure shock takes place according to Hugoniot's equation

$$(\rho' + \rho) \left(\frac{1}{\rho'} - \frac{1}{\rho} \right) = \frac{2}{\kappa - 1} \left(\frac{p}{\rho} - \frac{p'}{\rho'} \right), \quad (69)$$

whence

NASA

Tr. Note: Commas indicate decimal points in Table 4.

whence

$$\frac{p'}{p} = \frac{\frac{2e'}{\kappa-1} + e' - e}{\frac{2e}{\kappa-1} - e' + e}$$

(69a)

The dispersion velocity of the front of the shock wave w , the flow velocity u and the change in temperature can be similarly computed¹. For a shock wave traveling in air ($p = 1$ Atm., $a = 340$ m/sec), the following relationship holds:

/376

TABLE 5.

Wave Velocity w in m/sec	Flow Velocity u in m/sec	Pressure Jump in Atm.	Temperature Jump in °C	Relative Density Jump $\frac{\Delta \rho}{\rho_0}$	Change in the Refractive Index Δn <small>$n_D = 1,000292$ $(\lambda = 0,589 \mu$ NaD-line)</small>
340	0	0	0	0	0,000000
360	32,3	0,14	10,0	0,102	0029
380	62,0	0,29	21,2	0,202	0059
400	92,2	0,45	28,6	0,307	0090
450	160,2	0,88	58,7	0,561	0164
500	223	1,36	85,3	0,819	0239
750	495	4,52	246	1,968	0574
1000	734	8,96	461	2,814	0822
1500	1181	21,6	1068	3,78	1104
2000	1611	39,3	1910	4,26	1244
2500	2035	62,1	3000	4,50	1314
3000	2460	90,0	4330	4,64	1356
4000	3300	161	7720	4,80	1403
5000	4135	252	12050	4,88	1426

In dealing with fluids, to convert density to pressure in an initial approximation it is sufficient to ignore the influence of a change in temperature and make the change in density proportional to the pressure:

$$\frac{\Delta \rho}{\rho} = \gamma \cdot \Delta p.$$

(70)

Here γ is the compressibility. Its numerical value is given in Tables 6, 7 and 8 for several fluids:

¹See also *Handbuch für Physik* [Handbook for Physics] (Geiger-Scheel), Volume VII, Article by Ackeret.

NASA

Tr. Note: Commas indicate decimal points in Table 5.

TABLE 6. COMPRESSIBILITY $\gamma = \frac{1}{\rho} \frac{\Delta \rho}{\Delta p}$ IN ATM⁻¹ · 10⁶ FOR WATER.
Page One of Table

Pressure in Atm.	0°	10°	20°	40°	60°	80°	100°	200°
1—100	51,1	48,3	46,7	44,9	45,5	46,8	48,3	—
100—200	49,2	46,3	44,3	42,9	43,2	44,9	46,8	81,4
200—300	47,8	45,2	43,3	41,6	41,7	43,4	45,5	76,8
300—400	46,6	44,1	42,3	40,7	40,6	42,1	44,2	72,3
400—500	45,4	42,9	41,3	39,9	39,7	40,9	43,0	68,8
500—1000	41,7	39,8	38,5	37,1	37,0	38,0	39,3	—
1000—1500	36,2	34,8	34,0	32,6	32,8	33,5	34,4	—
1500—2000	32,4	31,3	30,6	29,8	29,9	30,3	30,8	—
2000—2500	29,3	28,7	28,0	27,0	27,0	27,4	27,9	—
2500—3000	26,1	25,7	25,4	24,9	24,9	25,4	25,8	—

TABLE 7. COMPRESSIBILITY $\gamma = \frac{1}{\rho} \frac{\Delta \rho}{\Delta p}$ IN ATM⁻¹ · 10⁶ FOR ALCOHOL.
Cover Page Source

Pressure in Atm.	0°	20°	40°	60°	80°	100°	200°
1—50	96	111	125	—	—	—	—
50—100	90	104	118	136	151	—	—
100—200	84	95	107	121	138	158	—
200—300	78	86	96	107	122	138	333
300—400	73	80	87	96	109	122	258
400—500	68	73	81	89	98	109	216
500—600	64	69	75	82	90	100	182
600—700	60	65	70	77	84	92	156
700—800	57	62	66	72	78	85	140
800—900	55	58	62	67	73	79	129
900—1000	52	55	59	63	68	73	119

Compressibility decreases with increasing pressure, since the individual volume of the molecules becomes much more noticeable; on the other hand, γ increases with rising temperature¹. The prevailing temperature is given by the following formula:

$$\frac{\Delta T}{T} = \frac{\alpha}{\rho \cdot c_p} \Delta p, \quad (71)$$

where α is the cubic thermal coefficient of expansion, ρ is the density and c_p is the specific heat (under constant pressure).

¹Partially abnormal conditions exist in water.

Tr. note: Commas indicate decimal points in Tables.

TABLE 8. COMPRESSIBILITY $\gamma = \frac{1}{\rho} \frac{\Delta \rho}{\Delta p}$ IN ATM⁻¹ · 10⁶ FOR CARBON TETRACHLORIDE.

Pressure in Atm.	20°
1—100	100
100—200	90
200—300	82
300—400	75
400—500	68
500—600	62
600—700	56

21. Determination of the Shape of the Surface of Plate Glass or of Reflecting Surfaces

If it is assumed that the light deflection of the light passing through a plate glass is conditioned only by the shape of the surface and not by alterations in the refractive index, the following simple relationship obtains between the angle of deflection ϵ determined with a schlieren method, and the wedge-shaped angle δ at one spot in the plate (cf. Figure 58):

$$\frac{\delta + \epsilon}{\delta} = n, \text{ whence } \delta = \frac{\epsilon}{n-1}. \quad (72)$$

Here ϵ is the maximum deflection existing for the particular point. If only the deflection in one definite direction is measured, so that

$$\epsilon_x = \epsilon \cos \beta \text{ or } \epsilon_y = \epsilon \sin \beta$$

(β is the angle between the direction of maximal deflection and the X-direction), we get

$$\delta = \frac{\epsilon_x}{(n-1) \cos \beta} = \frac{\epsilon_y}{(n-1) \sin \beta}. \quad (73)$$

The change in thickness Δd is obtained directly by integration

$$\Delta d = \int_{x_0, y_0}^x \delta_x dx = \int_{x_0, y_0}^y \delta_y dy. \quad (74)$$

δ is to be taken as a vector with the components δ_x and δ_y :

$$\begin{aligned}\delta_x &= \delta \cdot \cos \beta \\ \delta_y &= \delta \cdot \sin \beta,\end{aligned}$$

and therefore (with 73)

$$\left\{ \begin{aligned} \Delta d &= \int_{x_0, y_0}^x \delta \cos \beta dx = \frac{1}{n-1} \int_{x_0, y_0}^x \epsilon_x dx \\ \text{or} \\ \Delta d &= \int_{x_0, y_0}^y \delta \sin \beta dy = \frac{1}{n-1} \int_{x_0, y_0}^y \epsilon_y dy. \end{aligned} \right. \quad (75)$$

If the shape of a surface is to be determined alone, the light must be reflected onto it and the light deflection ϵ measured by the reflection. The inclination of the reflecting surface at a definite point in relation to the surface vertical to the incident light beam is then $\epsilon/2$ (Figure 59). The elevations of the reflecting surface are analogous to (74):

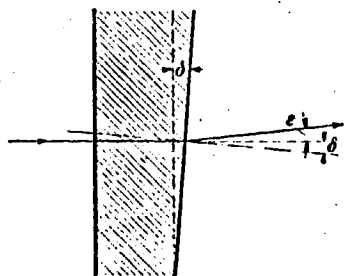


Figure 58. Determining the Wedge-Shaped Angle of Glass Plates.

$$\Delta d = \frac{1}{2} \int_{x_0, y_0}^x \epsilon_x dx = \frac{1}{2} \int_{x_0, y_0}^y \epsilon_y dy. \quad (76)$$

IV. Applications of the Schlieren Method

Possibilities of applying the schlieren methods are extremely versatile. It can be used wherever the condition to be investigated causes a light deflection in a transparent idiom; in addition the shape of a reflecting surface can be investigated by using them. Below we shall not be concerned with an exhaustive report on all applications and results up to the present time, but shall only select a few significant items.

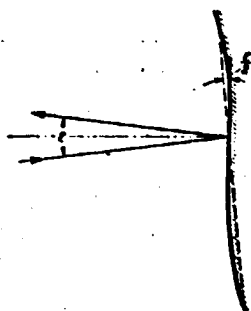


Figure 59. Determining the Shape of the Surface of Reflecting Surfaces. NASA

Previous and following explanations also have the purpose of calling attention to the fact that in many cases the schlieren methods really represent a useful and simple experimental tool which has not been commonly used up to the present.

22. Investigating Lenses and Concave Mirrors

If the schlieren head itself is considered the object in the Toepler arrangement and the ground-glass plate is sharply focussed on it, its spherical and chromatic defects become visible.

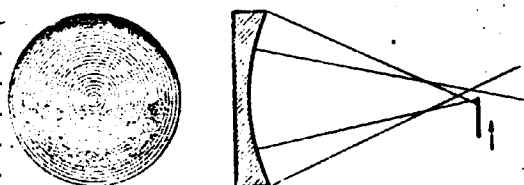


Figure 60. Sketch of a Spherical Concave Mirror in Testing With Foucault's Cutting Method.

In using monochromatic light or concave mirrors (which in principle cannot show up color defects), only the spherical defect is considered. Marginal rays, zone rays and axis rays do not have the same sectional width, so that in practice no position of the schlieren diaphragm can be found at which uniform darkening of the field of vision occurs when the diaphragm is narrowed.

When multicolored light is used, the red, green or blue rays also have sectional width deviating by a definite amount, so that the field of vision appears colored when the diaphragm is narrowed.

As stated in our previous remarks, quantitative determinations of the defects can also be carried out.

The use of the schlieren diaphragm to investigate the correction state of an optic was already mentioned in 1859 by L. Foucault and is known as "Foucault's cutting method". Therefore it can be considered a forerunner of the Toepler schlieren method. Its particular advantage is that optical examination can immediately show at what spots, for instance for astronomical purposes with a concave mirror, there are still defects; this is very essential, especially when correction is done by hand. Figure 60 shows the appearance of a concave mirror upon which the marginal rays deflect too strongly.

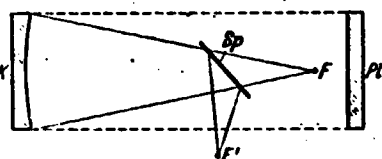


Figure 61. Ritchey's Arrangement for Investigating a Parabolic Mirror.

When the light comes in parallelly, the mirror must be curved parabolically. The arrangement of Figure 61 can be used to test the parabolic shape, but naturally requires the presence of a plane mirror. Just as in the coincidence method (p. 317), the light source and the image lie right next to each other.

23. The Investigation of Flat Glass

A very important area of application of schlieren methods is the investigation of flat glass, such as optically ground plate glass, mirror glass, drawn table glass and plates of plexiglass, and other plastics.

A plane-parallel plate can have the following defects (see Figure 62):

1. The plate can contain blisters or inclusions of foreign bodies (Figure 62a). These spots appear as black specks with the direct shadow method and are indicated very distinctly by the diffraction fringe of the light passing through the completely stopped diaphragm of the Toepler arrangement. This defect does not generally disturb the optical arrangements, but is very annoying when it occurs on photographic plates.

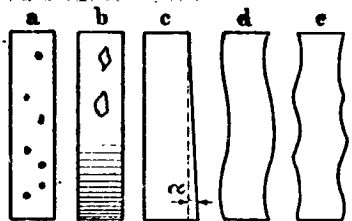


Figure 62a to e. Faults Which May Appear on Flat Glass.

2. The plate shows schlieren in the narrow sense, i.e., it contains places with refractive indices which do not correspond to the nominal value (Figure 62b). The magnitude of the light deflection caused by this depends on the value of the refractive index and on the shape of the schlieren. Even if the refractive index perpendicular to the plate is constant and an n -degree is only parallel to the surface, light deflection occurs (cf. equation (21) and (39)).

The cause of the appearance of schlieren is particularly to be sought in the irregular mixing of the glass melt.

3. The two surfaces of the plate can each be perfectly flat without their being parallel to one another (Figure 62c). In this case the plate shows a wedge-shaped defect which is not generally annoying, if it is of a constant magnitude for the entire plate. Only in special cases, e.g., when sighting through such a plate, is it important to keep the wedge-shaped defect fairly small.

A suitable method of testing is the lattice diaphragm method (or else the prism method or the Toepler arrangement), where attention must always be given to having the plate in question in a parallel beam of light.

4. The two surfaces are not plane, but their deflections run parallel to one another (Figure 62d). If the light goes through without too oblique an incidence, practically no defect is seen on such a plate. However, if the light is allowed to reflect onto the plate, the defects can be abnormally large under some conditions. Therefore a plate must be investigated by either penetrating light or by reflection, depending on the intended application.

NASA

5. Neither surface is plane nor parallel to the other (Figure 62e); defects occur for both penetrating and reflected light.

6. Several of the above-mentioned defects can occur at the same time. The following course of action is to be taken to determine the true condition of a plate under such circumstances: first the shape of each surface is to be investigated quantitatively and a reflection image of them is to be taken for this purpose¹. Since both sides reflect, under certain conditions an evaluation of both sides can be obtained immediately from a single exposure with the lattice diaphragm method. If reflected light from each side cannot be clearly distinguished, care must be taken that only one side reflects. Naturally a mirror coating is always successful. However, the temporary back can also be coated with a black lacquer. Then this will not reflect, since the light in the lacquer layer penetrates almost completely because of optical contact and is absorbed here. In investigating both surfaces successively, clamping the plate a second time should be avoided if possible, because otherwise new deflections could occur and give rise to considerable defects.

/381

An absolute measurement of the thickness should also be made in all cases, since the schlieren methods allow only alteration in density to be evaluated.

With the assumption of a constant refractive index for the plate, a knowledge of the shape of both surfaces allows immediate computation of the defects for penetrating light. Deviations in practical measurements opposed to these values are then to be attributed to the existence of schlieren.

Let us discuss a few practical examples of these facts below.

Figure 63 shows the Toepler schlieren exposure of three optically ground plane plates which are to be used for yellow filters. The topmost one of these has a zonal grinding defect; the plate to the left below has a spherical defect, i.e., either one or both of the surfaces are not plane, but part of a spherical surface of very slight curvature. In this case the distribution of the blackening remains identical when the plate is revolved in its own plane, while a wedge-shaped defect becomes noticeable because of the great dependency of brightness on the orientation of the plate. The lower plate on the right is free of defects (i.e., within the limits of sensitivity of the setting).

/382

Mirror glass is ground and polished mechanically in large sheets. Since the original material is uneven and the grinding process very rough, the plates become bent during the grinding process. In addition, stresses caused by temperature differences during grinding can provoke secondary deformation. As a consequence of this there remain defects which cause deflections of the order of magnitude of several seconds when the mirror sheets are mass produced and

¹The two colored pictures 126 and 127 on Plate I provide as examples the exposures of the surfaces of two distorted glass plates taken with the lattice diaphragm method.

the light penetrates perpendicularly. However, wedge-shaped defects of the order of magnitude of up to 2 minutes can also occur with local deviations usually amounting to only a few seconds.

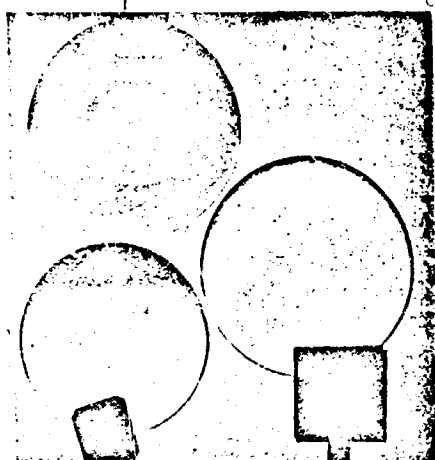


Figure 63. Yellow Filters in the Toepler Arrangement. Upper Plate, Zonal Defects; Lower Left Plate, Spherical Defects; Right Plate, Free of Defects.

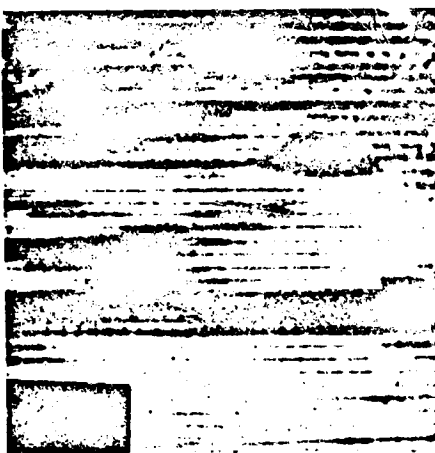


Figure 66. Tempered Glass (Sekurit Safety Glass). Tempered By Blowing Air From Nozzles. Linear Structure of the Surface.

Colored Figure 64 on Table I provides the example of an exposure made with the prism method of a mirror glass plate. The shade of the plate, relatively uniform but very different from the background, is caused by a constant wedge-shaped defect; otherwise the plate has only a few insignificant schlieren. In contradistinction to this, considerable deflections occur in the mirror glass plate in Figure 65 on Table II (up to about 1 minute).

If the glass is tempered during the cooling process, e.g., by a blast of cold air, strong interior stresses occur which give the glass considerable strength against normal outside pressures. Figure 66 shows a Toepler schlieren image of a glass plate of this type. Cooling was carried out by using a rather large number of nozzles from which cold air flowed. The result of the inside stresses built up in this way is a deformation leading to a linear type pattern of the schlieren image.

Today normal sheet glass is either drawn from a nozzle (Fourcault method) or produced by the Libbey-Owens method. Formerly it was blown by mouth, but mouth blown glass plates are hard to obtain today. They may be immediately recognized by looking through them and by reflection because of the irregular nature of the light deflection (Figure 67 on Table I), while machined glass usually has drawing streaks in a longitudinal direction (Figures 68-70).

The exposures in Figures 68, 69 and 70 on Table II are taken from the same glass plate (plate size 25 x 25 cm, 4/4 glass). The lattice constant of the colored lattice diaphragm used was $2a = 3 \text{ mm}$ for

/383

NASA

Figures 68 and 69 with a focus depth of the concave mirror used K_2 of $f' = 350$ cm (cf. Figure 30). In this way the occurrence of the first color (red or reddish-brown) of a deflection of $\epsilon = 2a/f' = 3/3,500 \approx 3$ min. Now the diaphragm in Figure 68 is oriented vertically and it is seen that the deflection of 3 min is reached only in small areas at the upper edge of the plate. The same plate is the subject of Figure 69, but the diaphragm is oriented horizontally. The deflections are essentially greater and extend into the third order; the direction of drawing is strongly marked. The plate in Figure 70 was taken with a round lattice diaphragm so that here the absolute value of the light deflections were made visible independent of direction. By a direct comparison of Figures 68 and 69, it is found that practically only deflections perpendicular to the drawing streaks are present. Therefore, Figure 70 must agree almost completely with Figure 69, and this is indeed the case except for a different color sequence.

Sheet glass is divided into three quality classes today:

1. Structural Glass, First Type: defined by DIN 1249:

The glass may only contain small inconspicuous defects and faults which cannot be completely avoided during production. When looked through at an angle equal to or greater than 35° , perceivable waves, streaks and schlieren must not distort the image. Blisters and scratches may only appear in isolation, but not rather large scratches.

(4th)

This type is specified for glazing in higher-class residences, public buildings, store furnishings, etc.

2. Structural Glass, Second Type:

The glass may contain larger numbers of defects produced by the manufacturing process and in greater size than with structural glass, first type. The waves and schlieren may occur more significantly than in structural glass, first type. If special requirements are not levied upon it, this type can be used for glazing factories, shops, simple dwellings, etc.

Glass which does not meet the requirements of the second type is not fitted for buildings. It is designated as greenhouse glass and may only be used for nursery purposes.

Up to the present time no exact method for distinguishing these classes of quality has been introduced. Numerous measurements¹ of glass coming from a number of German companies have shown that the maximum mean light deflections for penetrating light amounts to $1 \frac{3}{4}$ min for structural glass, first type and $2 \frac{1}{2}$ min for structural glass, second type.

¹Carried out by G. Stamm at the Ballistic Institute of the Air War Academy.

The "greenhouse glass" quality occurs often because under certain conditions locally intense drawing streaks, schlieren, etc. occur while large areas of the same plates can be otherwise very good. In Figures 71, 72 and 73 on Table II three typical representatives of these three types of glass are compared. In order to make visible the absolute value of deflection, a round lattice diaphragm was used again (lattice constant $2a = 3$ mm, $f' = 350$ cm, i.e., red = 3 min; yellow = 6 min). In Figure 71 (structural glass, first type) no colors, but only a darkening, occur; this corresponds to a deflection of $1\frac{1}{2}$ min. However, with structural glass, second type (Figure 72), angles of deflection of 3 min (i.e., red coloring!) are reached at some points, while the image of the greenhouse glass (Figure 73) appears quite variegated (angle of deflection up to 6 min). Thus on the basis of the colored schlieren image, one glance can definitely tell the quality of a plate glass and pure estimates are no longer necessary. Not only the maximal light deflection but also the distribution of the different large deflections on the plate, are conclusive in evaluation.

Cover Page Source

Just what is necessary for sheet glass and what must be tested? Schlieren methods directly furnish the angle of deflection ϵ . This is decisive if e.g., an optical measurement is to be taken with the glass. Integration of the curve of the angle of deflection provides the change in density of the plate. This is of importance in determining which defects exist in the machine when the glass is drawn. However, what particularly bothers the eye is neither the change in density of the glass directly nor the size of the deflection. For, if the plate had a very strong and constant wedge-shaped defect, this would be almost imperceptible to the eye and the plate would appear free of defects. From this we know that the change in the angle of deflection $d\epsilon/dx$ is important for an effect which disturbs the eye.

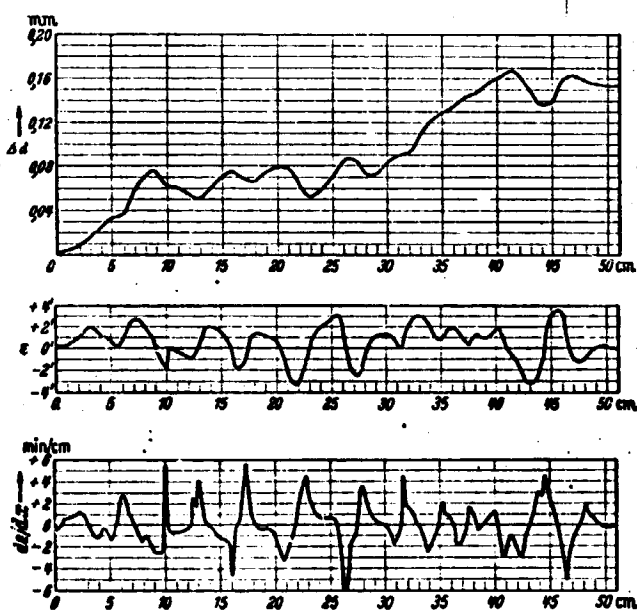


Figure 74. Alteration in Density Δd , Deflection ϵ and $d\epsilon/dx$ in Machine Glass.

NASA

We find de/dx by differentiation of the empirically obtained curve for the deflection. The change in density $\Delta\rho$, ϵ , and de/dx are plotted in Figure 74 for one case¹.

Several examples used in describing the various schlieren methods can also be used to investigate other objects made of glass. The examples provided there (Figures 5, 9, 42, 43) should be sufficient in this connection.

24. Thermo-Hydrodynamic Flow Phenomena in Gases

In enumerating several applications of schlieren methods, we shall first mention the best known. In setting up a schlieren arrangement, the quality of the optics used and of any built-in cells must be explained first. After this, the apparatus is generally tested, always with the aid of a flow process generated by heat in gases: a burning match, a candle, an incandescent bulb or the warm hand. The mean light deflections for these cases were given in numerical values on p. 340. The quality of the structure can be judged according to this.

The use of these processes as test objects is so appropriate because slight differences in temperature cause a relatively great change in density (see p.375).

But how can schlieren methods be applied to the scientific investigation of thermo-hydrodynamic processes?

One problem which has constantly stimulated new research because of its difficulty is the determination of heat exchange between solid bodies and fluids or gases².

Although mathematical solutions of the pertinent differential equations have already been found for heat exchange to perpendicular plates with free convection, in harmony with the test conditions, we are still far from having satisfactory solutions for complex bodies. The heat transfer to horizontal pipes of circular-cylindrical cross-section has special interest for practical application. Theories for this process have been advanced by Langmuir, as well as by others. (Cf. R. Hermann, *VDI-Forsch.*, No. 379) To experimentally validate theories of this type attempts have been made to measure the temperature field with thermocouples. Although it is certain that the temperature field in general will not be very affected by very thin wires running through it, right at the place where the measurement takes place, i.e., at the surface of the thermocouple, the velocity of the flow will be greatly retarded. It is difficult to judge defects caused by heat conduction and radiation; this is

¹The curves represent the evaluations made by Prof. Weidert for the glass plate shown in Figure 51. In this case the deflections were obtained according to F. Weidert's method described on p. 362.

²Cf. the thesis of Joh. Gaebler (Technical University, Berlin, 1935) from which some of the following data are taken.

particularly true in the immediate neighborhood of the pipe, where the temperature gradient can reach values of the order of magnitude of $600^\circ/\text{cm}$. Since a rather long time is also required to measure the temperature field, which must be done point-for-point, it is extremely possible that uncontrollable distortions of the temperature field often enter the measurements and falsify them.

For these reasons, the purely optical investigation, as is possible by using schlieren methods, offers considerable advantages because here the temperature field is not disturbed or affected at all and the measurement is assigned to only a single point in time.

In 1932 E. Schmidt used the direct shadow method as described on p. 358. The shadow image immediately provides the maximal temperature gradient and the limits of the temperature field.

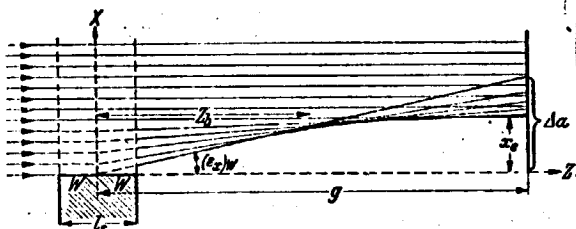


Figure 75. Light Deflection in the Vicinity of a Heat Radiating Body.

Let us again show the relationships schematically in Figure 75a. The parallel incident light is deflected most strongly at wall W of the heat radiating body (wall temperature T_w) (angle of deflection $[\epsilon_x]_w$). Deflection ϵ_x decreases when the distance x from the wall increases, until at x_e it is practically equal to zero.

The result of this is that the light rays overlap beginning at a certain distance from the process. If the light is collected at approximately a distance z_b , a sort of focus line is established there. At a greater distance g , the rays bypassing wall W lie farthest outside and therefore the deflection of these rays can be determined with complete reliability by the pure shadow method. Moreover, the area in which deflection takes place can be provided; on the exposures it projects a completely dark area around the body. Figures 76a and b show two examples taken by E. Schmidt¹.

The heat conductivity index can now be computed from exposures of this type. Let:

p_0, ρ_0, T_0, n_0 be respectively the pressure, density, temperature and refractive index of the gas (in regular air) at $T_0 = 273^\circ \text{ abs}$,

$p_\infty, \rho_\infty, T_\infty, n_\infty$, the corresponding magnitudes for the gas far removed from the heat radiating body,

¹Cf. also Figure 46.

p_w, ρ_w, T_w, n_w be the same magnitudes for the gas in the immediate neighborhood of the wall at the point in question.

Cover Page Title

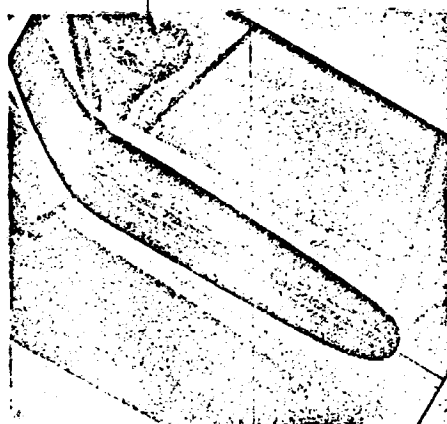


Figure 76a. Shadow Exposure of a Plane Heated Plate of 50 x 50 cm² Surface and 1 cm Thickness at 110-135°C (Without Diaphragm). Air Temperature About 25°C.

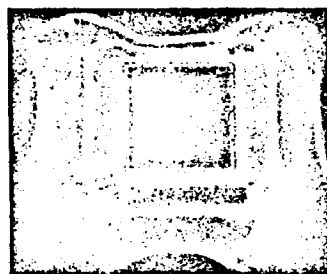


Figure 76b. Shadow Image of a Heated Square Pipe of 25 x 25 mm² Cross-Section With a Diaphragm at 52°C and 83°C. Air Temperature 23.7°C.

Equations (47) and (47a) are to be used for this case, and therefore the value experimentally determined for the vicinity of the wall:

$$\begin{aligned} (\epsilon_x)_w &= \frac{\Delta a}{g}, \\ \left(\frac{\partial n}{\partial x}\right)_w &= \frac{n}{l_s} \cdot \frac{\Delta a}{g}. \end{aligned} \quad (77)$$

First of all the disruptive effect of the ends was not considered. Only the temperature gradient $\delta T/\delta x$ in the immediate vicinity of the wall is desired. We used equations (59) and (60) to compute from $\partial n/\partial x$ to $\partial T/\partial x$:

$$\frac{n-1}{\epsilon} = \frac{n_0-1}{\epsilon_0}. \quad (78)$$

For air $n_0 = 1.000292$ (at $\lambda = 0.589 \mu$, $T_0 = 273$ abs., $p_0 = 760$ mm Hg)

$$n = 1 + (n_0 - 1) \frac{\epsilon}{\epsilon_0}. \quad (79)$$

c/ρ_0 can be replaced by $T_0 p/Tp_0$ by using gas equation (61):

NASA

/388

$$p_a = 1 + (n_0 - 1) \frac{T_0 p}{T p_0} \quad (80)$$

Here $p = p_w \approx p_\infty$.

Cover Page Title

Differentiated for x:

$$\frac{\partial n}{\partial x} = - \frac{(n_0 - 1) T_0 p_\infty}{p_0} \cdot \frac{1}{T^2} \cdot \frac{\partial T}{\partial x} \quad (81)$$

For air:

$$(n_0 - 1) T_0 = 0.000292 \cdot 273 = 0.080.$$

Therefore with (77)

Cover Page Source

$$\left(\frac{\partial T}{\partial x} \right)_w = - \frac{T_w^2}{(n_0 - 1) T_0} \cdot \frac{p_0}{p_\infty} \cdot \frac{n_w}{l_s} \cdot \frac{\Delta a}{g} \quad (82)$$

n_w can be posited as practically equal to n_0 . (If the process takes place between plane-parallel walls, n_w would be exactly equal to n_0 , so that the edge conditions must also be considered in other cases.)

If we insert the numerical values for air, we get

$$\left(\frac{\partial T}{\partial x} \right)_w = - 12,5 T_w^2 \cdot \frac{760 \text{ mm Hg}}{p_\infty} \cdot \frac{\Delta a}{l_s \cdot g} \quad (83)$$

Using this equation and a schlieren exposure made by the pure shadow method, the temperature gradient can be computed simply for every point of the surface.

If α represents the heat exchange index and λ the heat conductivity index of air at temperature T_w , the following equation can be considered a definition from which the heat exchange index can be computed

$$\alpha (T_w - T_\infty) = - \lambda \left(\frac{\partial T}{\partial x} \right)_w \quad (84)$$

However, determination of the total temperature field by the direct shadow method is not immediately possible. Such a determination was first

carried out by using an interference refractor (Kennard, 1932; Schardin 1933). But the schlieren methods also allow measurement of the total temperature field (Schardin 1934).

In measuring with thermocouples, the length of the heating pipes can be so extensive and their surface temperatures made so uniform by intensively heating the ends, that the flow process can be assumed as completely even inside the pipe. In this way the measurements are exactly valid for infinitely long pipes.

However, when optical methods are used, the pipe must be penetrated in its longitudinal direction, i.e., in the first place, pipes which are too long cannot be used and in the second place, not only the inside of the pipe, but also the flow process at the ends enters the evaluation. In his thesis, Joh. Gaebler tried to eliminate this edge defect by taking measurements on two pipes where all data were maintained equal except for pipe length.

/389

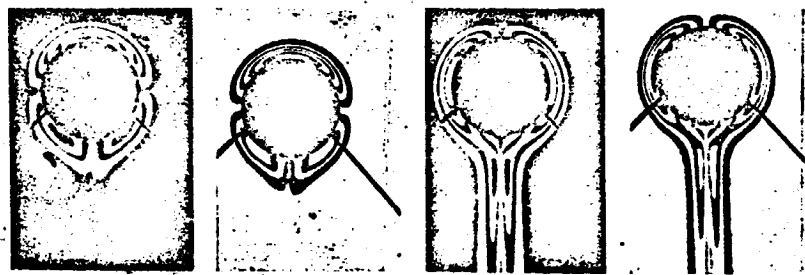


Figure 77. Exposures of a Heated Pipe With the Lattice Diaphragm Method. Left, Vertical Diaphragm; Right, Horizontal Diaphragm.

Naturally, this method by differentiation requires precise values and consideration of all defects present.

Figure 77 shows four evaluation exposures made with the lattice diaphragm method. The lattice was perpendicular for the first two and horizontal for the last two. At one time the undeflected image of the light source was in the middle of a slit and the second time it was between two slits. The heating pipe was 30 cm long, had a diameter of 4 cm and was heated to a temperature of 140°C. Figure 78 shows the evaluation of this exposure.

Every technical problem of heat loss from a solid body to a fluid or a gas has a hydrodynamic side. Even if it is impossible to make a quantitative evaluation of the total temperature field with schlieren methods in the most general cases, it is usually possible--at least in models--to create an image of flow phenomena. If it is desired to make the relationships in the model exactly fit those of the main process, it is necessary to adhere to Grashof's index:

NASA

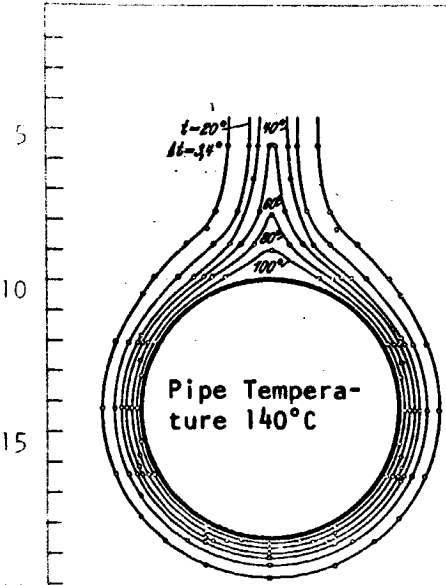
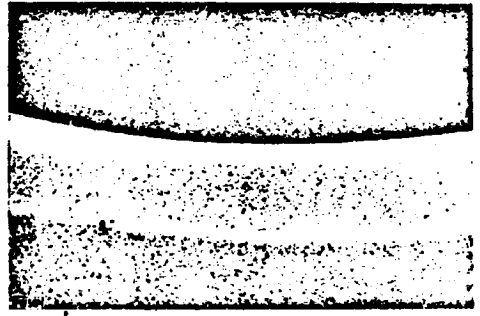


Figure 78. Temperature Field Taken From the Exposures in Figure 77.

the third power. This means that if the dimensions are cut in half, the temperature difference $T_w - T_\infty$ must be raised to eight times the value. Under some circumstances this may lead to prohibitive temperatures. A reliable compensation can be made in a closed container by raising the pressure (i.e., the density).



Figures 79a and b. Simultaneous Shadow Exposures of a Horizontal Heating Pipe at the Lower Stagnation Point (a) and at an Azimuth of 120° (b). Flow at the Lower Stagnation Point is Laminar, and the Focus Line of the Rays Near the Wall is Very Sharp. Flow in Figure 79b is Turbulent and the Focus Line is No Longer Recognizable. Wall Temperature 102°C, Room Temperature 18°C; $Gr = 10.2 \cdot 10^8$.

Page One Title

(85)

Cover Page Title

Here: l is a characteristic length, ρ is the density, β is the coefficient of volume expansion, T_w is a characteristic wall temperature, T_∞ is the room temperature, g is the acceleration due to gravity, and η is the absolute viscosity.

Especially for gases

Cover Page Source

$$Gr = \frac{\rho g^2 (T_w - T_\infty) g}{\eta^2 \theta_\infty} \quad (86)$$

It is inconvenient for the characteristic length to be concerned with

Figures 79a and b¹ may serve as examples for the importance of determining the kind of flow with the help of the schlieren method. These show whether the flow is laminar or turbulent and a decision can then be made whether to use laminar or turbulent heat exchange computations. R. Hermann has ascertained the contribution of turbulence with schlieren exposures on a perpendicular plate and a horizontal cylinder. Naturally this occurs at different Grashof's numbers, viz. at $Gr = 1.0 \cdot 10^9$ at the plate and $Gr = 3.5 \cdot 10^8$ on the cylinder, but with an equal Reynolds number of boundary layer flow, viz. $Re \approx 300$.

/391

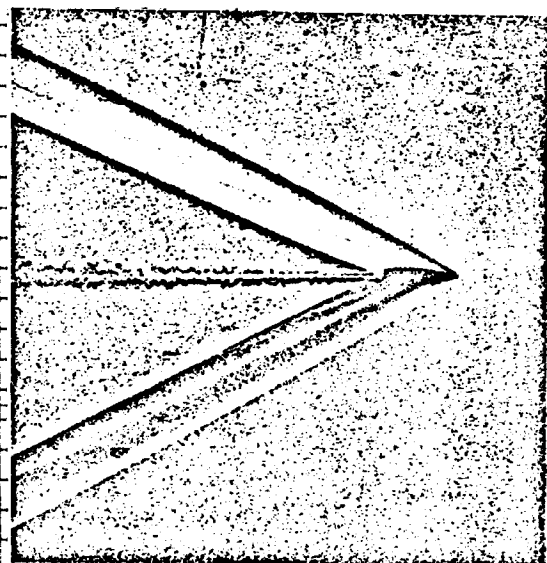


Figure 80. Schlieren Exposure of an unknown Bullet Flying at 785 m/sec. Horizontal Schlieren Diaphragm.

25. Application of the Schlieren Method in Ballistics

A very important field of application for schlieren methods is ballistics. Very early, mainly by E. Mach in 1887, the first schlieren exposures of flying bullets were made. In this way he demonstrated that a bullet flying faster than sound is accompanied by a head and tail wave (Figures 80 and 81). Later, numerous schlieren exposures of ballistic phenomena were made by C. Cranz; most of these were published in his well-known textbook of ballistics.

Schlieren exposures are chiefly used in ballistics to investigate the following phenomena:

1. Flow phenomena in the environment of the flying bullet,
2. Phenomena at the nozzle of a weapon,
3. The detonation of a bullet.

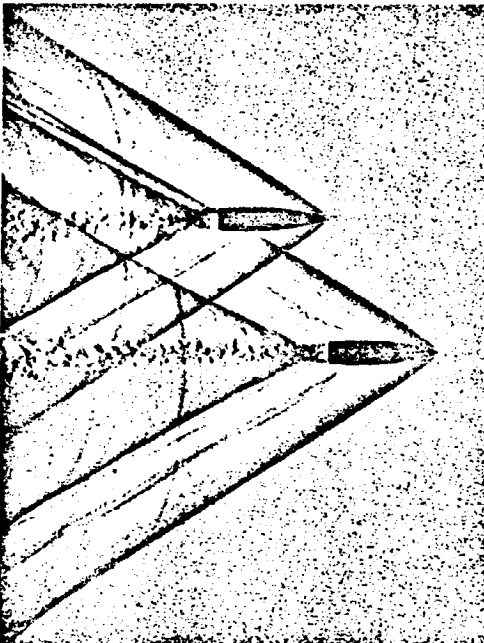
The chief matter here is investigation of the shape and propagation of shock waves. Here, there are finite pressure jumps at the leading edge of the shock wave so that rather large light deflections exist at the edge of the wave and very useful exposures can be made with the direct shadow method. Figure 80 shows the Toepler exposure of a Geschoss bullet flying with a muzzle velocity of 785 m/sec. Notice first its head wave which begins almost exactly at the tip of the bullet. At the beginning it is slightly curved. However, with increasing propagation its inclination approaches the Mach

/392

¹ Cf. R. Hermann: VDI-Forschgs. No. 379, p. 21.

$\sin \alpha = \frac{v_{\text{ph}}}{v}$

Cover



speed of sound there may be areas where supersonic velocity is still present and in which compression shocks can therefore occur (cf. Figure 83).

$$W = c_m \cdot \frac{\rho v^2}{2} \cdot F,$$

88
Even

where: c_w is the coefficient of resistance (adimensional); ρ is the density; v is the bullet velocity and F , the cross-sectional area of the bullet ($= \pi R^2$).

/394

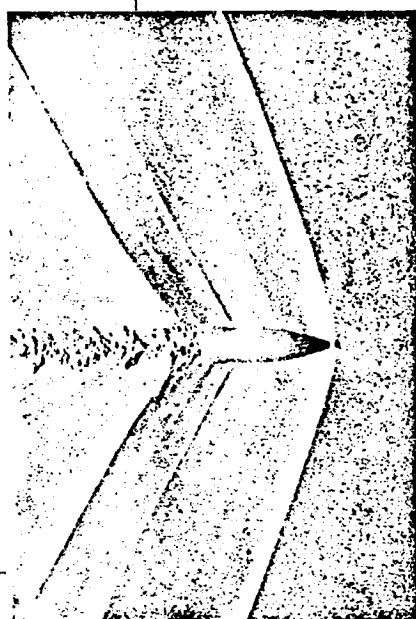


Figure 82. A S-Bullet Flying at 375 m/sec.

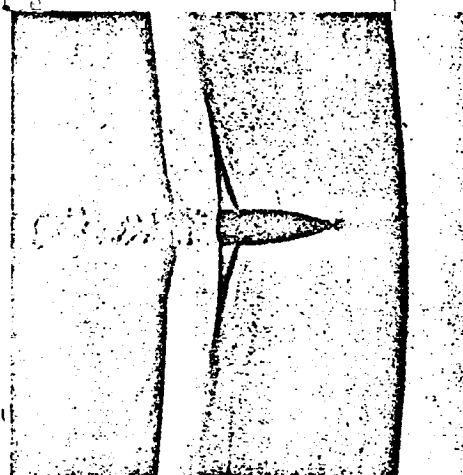


Figure 83. An S-Bullet Moving Almost Exactly at the Speed of Sound. Head and Tail Waves Have Separated From the Bullet. The Base of the Bullet is Still Accompanied by Two Compression Waves of Finite Extent.

In passing through the velocity of sound, a considerable rise in resistance therefore occurs. Although it has been known since Mach's schlieren exposures (1887), that the speed of sound is responsible for this, the phenomenon did not enter computations of external ballistics until after the World War. Up until that time, the coefficient of resistance was considered only as a function of the velocity and not, as it must be, as a function of the ratio of bullet velocity to the speed of sound. Sufficient attention to the schlieren exposures would thus have considerably improved precision firing during the World War in many cases! Still another very important consequence for troops is to be deduced from the schlieren exposures of a bullet flying at supersonic speeds:

The head and tail waves accompanying the bullet are detonation waves. When they hit the ear of an observer the latter perceives a detonation. Therefore, when a round is fired off, the following three detonations must be distinguished: 1, the muzzle detonation of the weapon, 2, the bullet detonation, and 3, the detonation report.

/395

NASA



Figure 84. S-Bullet Flying Below the Speed of Sound.



Figure 85. Explosive Particles Flying at 1,900 m/sec.

Only when the cone of the head wave being propagated with the bullet can be perceived spatially, can one understand that the direction from which the bullet intonation seems to come is essentially different from the direction of the muzzle detonation or detonation report. Now, if the bullet detonation is confused with the muzzle detonation, grave errors in judgement can occur under certain conditions.

TABLE 9.

α (°)	v (m/s)	α (°)	v (m/s)	α (°)	v (m/s)	α (°)	v (m/s)
0	∞	25	804,5	50	443,8	75	352,0
5	3901	30	680,0	55	415,1	80	345,2
10	1958	35	592,8	60	392,6	85	341,3
15	1344	40	528,9	65	375,1	90	340
20	994,1	45	480,8	70	361,8		

*Tr. Note: Commas in Table 9 indicate decimal points.

The head and tail waves of a bullet can be explained as envelopes enclosing the elementary waves caused by the flying bullet in the air. If we assume that the bullet represents a point, a series of these elementary waves exist, as in Figure 87, and the validity of the Mach ratio $\alpha = a/v$ is immediately perceived from the drawing.

The fact that this explanation corresponds to reality is demonstrated by Figure 88 which represents a round going through a pipe with slits in it. The parts of the head and tail wave protruding through the slits can be considered as elementary waves. Notice that these envelopes again produce either head or tail waves.

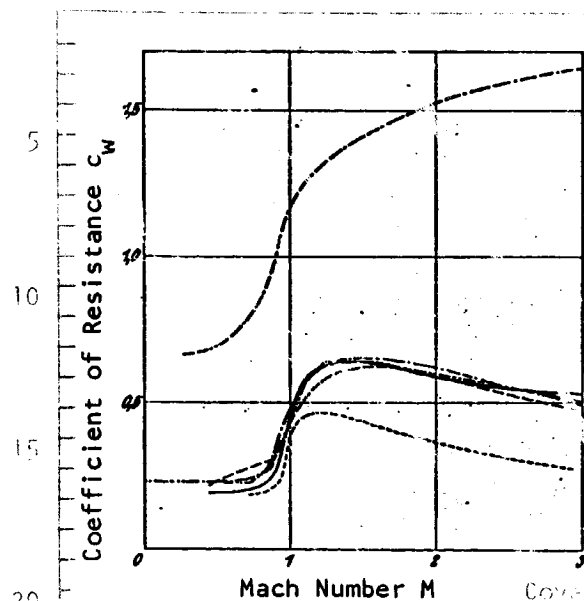


Figure 86. Coefficient of Resistance of Flying Bullets as a Function of the Mach Number. Ogive-Bullet With Two Cal. Contour Radii:

— Krupp, ---- Stacci,
 - - - - Vallier, ---- Mayewski-
 Sabudski, S-Bullet: ----- According
 to Cranz-Becker. Cylindrical Bullet:
 - · - - According to Krupp.

oscillation of the bullet. Thus, if one wishes to obtain an exact picture of the flight characteristics of a bullet, he must investigate the flow processes. From the point-of-view of gas dynamics, the head wave of a bullet is an oblique compression shock (see §26). At constant velocity and up to a certain angular aperture of the tip of the bullet, this compression wave begins right at the bullet and beyond this angle begins ahead of the bullet at a perpendicular tangent. In this way the pressure acting on the tip of the bullet also increases. It is greatest on a bullet with the tip removed at right angles. Around the tip of the ogive bullet is an expansion of the air compressed by the compression shock. This expansion phenomenon can be followed more closely by observing the Mach lines formed by the small irregularities at the surface. These can best be made visible with the pure shadow method, rather than with the Toepler method; for the shadow method provides only the changes in light deflection, while in the Toepler method the brightness is directly proportional to the absolute value of light deflection. Therefore the Mach lines can be projected much more clearly by the shadow method in connection with a photographic process adjusted for contrast (Figure 88).

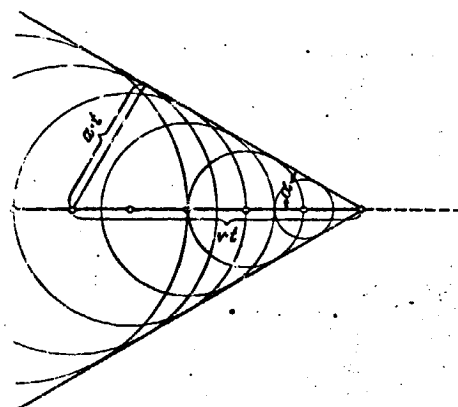


Figure 87. The Appearance of a Head Wave as an Envelope for the Elementary Waves Beginning at the Bullet. Validity of the Mach Relationship.

Now, since every bullet has finite dimensions, a flow about the body occurs; the passage of this flow is of considerable importance in regard to the forces acting on the bullet during flight. First of all, these forces cause air resistance and secondly, if the bullet is flying somewhat obliquely, a moment acting on it in connection with the gyroscopic effect contributes to the

/396

/397

REPRODUCIBILITY OF THE ORIGINAL PAGE IS POOR.

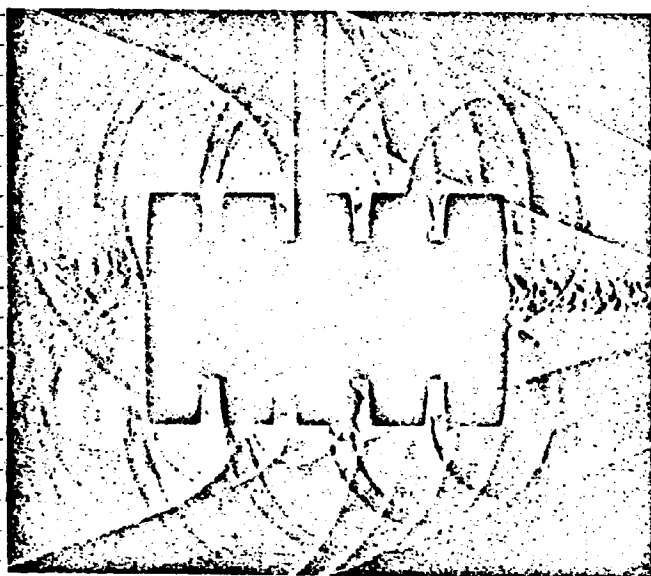


Figure 88. A Round Passing Through a Pipe With Slits In It.

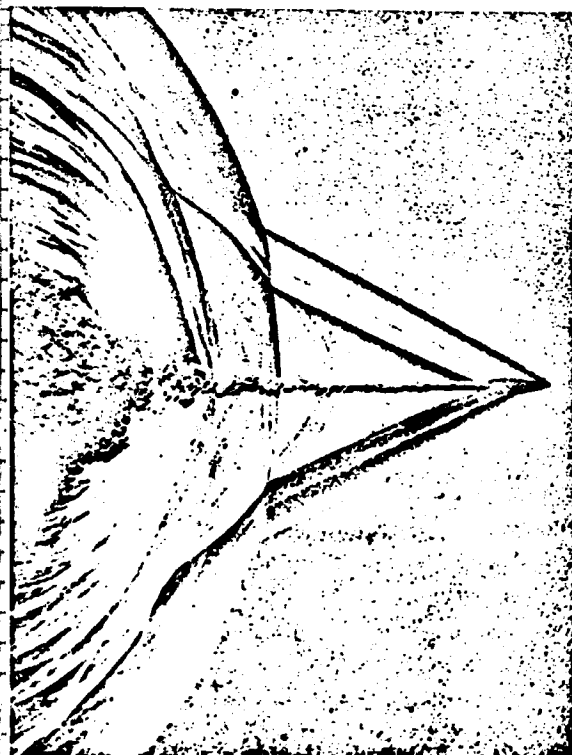


Figure 90. A Flying Gaschoss Bullet Has Just Overtaken the Muzzle Detonation Wave. The Cone of the Head Wave is Superimposed on the Muzzle Detonation Wave. The Path of Turbulence is Also Inside the Muzzle Detonation Wave.

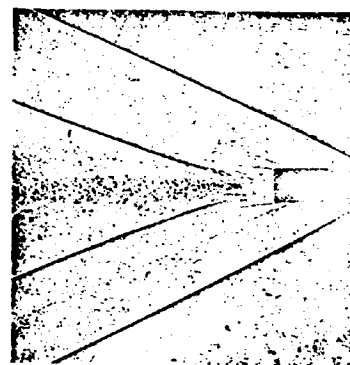


Figure 89. Shadow Exposure of a Flying S-Bullet.

We have an approximate parallel flow along the cylindrical part of the bullet. Particularly well marked Mach lines arise at the grooves, which are used to hold the shell and (with full bullets) at the rotating bands. Another expansion takes place around the base of the bullet. In the tail wave, also a compression wave, another transfer to parallel flow occurs. This does not begin immediately at the base of the bullet, but is only formed in the wake of the flow behind the bullet. Sometimes the opinion is expressed that the tail wave is a rarefaction wave. However, this is not the case. Evidence against this can be provided by the course of blackening in a Toepler schlieren exposure because it changes analogously with the head wave.

The space behind the bullet is filled with air flowing directly along the jacket surface of the bullet. This air is turbulent and heated by dissipation of kinetic energy. As a result of this the "path of turbulence" behind the bullet can be perceived for a great distance. The visible changes in density in the path retain its respective particles of air, in contradistinction to the change in density in the head and tail wave. Therefore in Figure 90 it is still possible to follow the path of turbulence after the muzzle detonation wave has passed by it, but one cannot do so with the head and tail wave. For within the muzzle detonation wave the bullet does not have supersonic speed everywhere in relation to the surrounding medium. The cone of the head wave is therefore always superimposed on the muzzle detonation wave, while the path of turbulence begins with the air particles found in the vicinity of the bullet when the bullet overtook the muzzle detonation wave.



Figure 91. Before the Bullet Leaves the Barrel, the Air in the Barrel Must be Forced Out. As a Result of this a Spherical Detonation Wave and Flow Phenomena are Formed in Front of the Muzzle. (Shadow Exposure).

Let us consider the processes of firing a bullet in more detail by using some schlieren exposures. In the forward movement of the bullet in the barrel, it must force the air in the barrel out. The leading edge of this moving air is a straight compression shock. As it leaves the muzzle, it expands into a spherical detonation wave (Figure 91). Air streaming behind it causes flow phenomena very similar to those of stationary flow from a cylindrical nozzle. After the bullet itself has left the muzzle, comes the expansion of the highly compressed powder gases. This produces the muzzle detonation wave which, because of its high pressure, has a greater velocity than that of the first wave caused by the expelled air; therefore the second wave catches up with the first. At first the velocity of the muzzle wave is also greater than that of the bullet. Still, due to spatial propagation, its intensity, and with it its velocity, must drop sharply. As distance from the muzzle increases, it approaches the normal speed of sound. With a great deal of accuracy the velocity of the bullet can be presumed constant in the vicinity of the muzzle. Therefore the bullet will overtake the muzzle detonation wave

after a certain flight distance (Figure 90).

/ 399

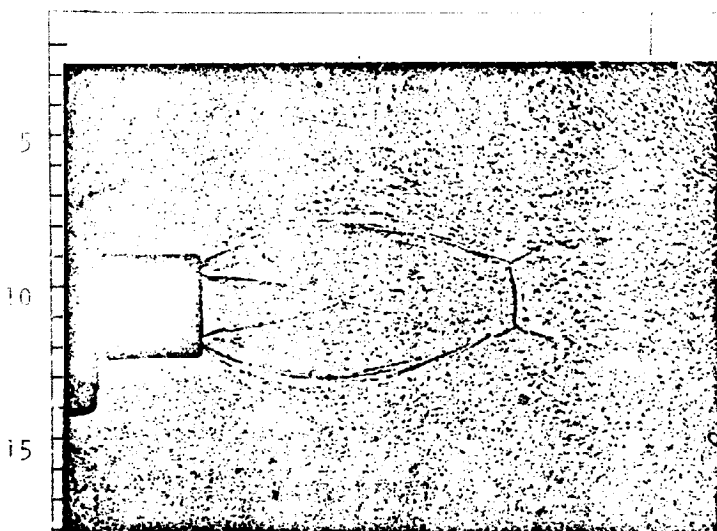


Figure 92. Flow in Front of a Rifle Muzzle After the Bullet Has Left the Barrel. (Shadow Exposure).

After the bullet has left the barrel, the combustion gases flow out of the muzzle. For this reason approximately the same relationships are seen in front of the muzzle as in front of a cylindrical nozzle through which a gas escapes from a pressure container. The only difference is that here the volume of the container (the inside of the barrel) is so small in comparison with the size of the effluent opening (muzzle cross-section), that the inside pressure changes very rapidly. Figure 92 represents the flow in front of a rifle muzzle after the bullet has flown approximately 1 m. In principle we can recognize the same compression shocks

already present before the exit of the bullet in Figure 91.

Even in the detonation or penetration of a bullet into the target, there are many problems where schlieren methods can be used advantageously.

Investigating the detonation of an explosive belongs alone in the problem area of "terminal ballistics". This will be covered in more detail in §28.

/400

When bullets penetrate translucent solid or fluid media, waves are generated which precede the bullet; this is because in this case the bullet velocity is almost always less than the speed of sound of the medium concerned. Besides this, when water and other fluids are penetrated, the bullet forms a hollow space which practically excludes the light (Figure 93).

In investigation of bombarded armor plates by flash moving picture devices, H. Schardin and W. Struth found supersonic waves on both sides of the plate under certain conditions¹; these waves arose in a spherical wave originating in the iron at the point where the bullet hit. This is reflected back and forth on both boundary surfaces of the plate and partially dissipates its energy into the air.

Many valuable conclusions can be drawn from exposures of this type.

NASA

¹Z. Techn. Physik, Vol. 18, p. 447, 1937.

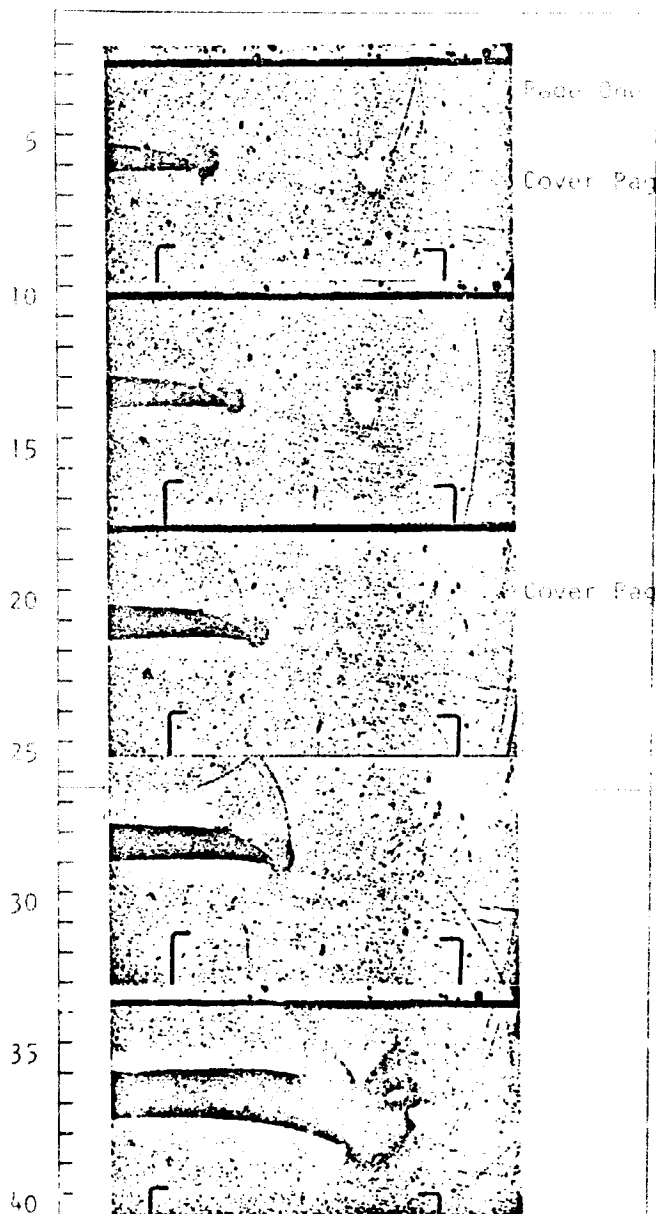


Figure 93. A Series of Exposures of Shooting Into a Container of Water. The Light Deflection of the Hollow Space Caused by the Bullet is So Large That It Appears Completely Black. The Sound Wave Ahead of the Bullet Can Be Seen in the First Images, and It Is Also Possible to See the Interference Waves Caused by the Base of the Bullet.

26. Applications in Flow Research

It is not possible to make flow phenomena directly visible at low velocities (up to about 100 m/sec in air) by using schlieren methods, since the changes in density present are not sufficient to cause an appreciable deflection of light (cf. p.375). In these cases smoke wind tunnels can be used advantageously and visualization of the flow lines are produced by smoke, oil vapor or, in the case of fluids, with dye solutions. Here it is important for the medium applied to follow the motions of the undisturbed flow flawlessly. This would be the case if it had the same density and viscosity as the flowing medium. When solid particles are mixed, especially with gases, this condition is not always sufficiently heeded. One might think of mixing a second gas to a gas or a second fluid to a fluid, and of selecting this second medium so that it is of exactly the same density and kinematical viscosity, but has a different refractive index than the flowing medium. In this case the flow lines could be made visible with the schlieren method with no possible disturbance of the flow process. Acetylene has been recommended for this purpose for flow processes in air. However, ether, carbon dioxide and heated air are also used in practice in many cases. Of particular advantage is the use of two gases when it is a matter of investigating how gas currents representing different states of rest affect each other. Among others F. Krueger and H. Casper [111] have investigated the turbulence of intersecting waves by having carbon dioxide stream through a slit against a wedge (see p.407).

If the flow lines are to be made visible in a uniform current,

/401

individual threads of the medium with changed refractive index must be allowed to flow in, just as with a smoke wind tunnel. L. Mach had already built a wind tunnel of this type in 1896 [15]. He worked with air which had been irregularly heated by a burner. H. Schardin and J. Pohl constructed a wind tunnel in which the air was heated by thin electrical heating wires at a standard distance directly in front of the object to be investigated. Figure 94 represents an exposure made with this tunnel. The stream lines here are in a downward current of 1.5 m/sec. An air compressor suctioned air from the air current (drawing rate 300 l/min). One can see how the flow lines run into the suction pump. /402

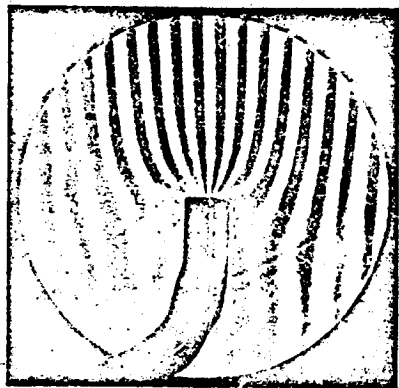


Figure 94. Visualization of Flow Lines of Air By Using Electrical Heating Wires (H. Schardin and J. Pohl). A Compressed Air Injector-Sucked Air From a Wind Tunnel in Which a Downward Flow of 1.5 m/sec Reigned.

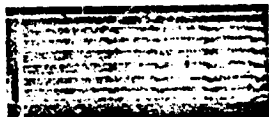


Figure 95. Visualization of Flow Lines of Air Using Electrical Sparks (Townend) Which Flash Periodically. Schlieren Diaphragm Parallel to the Flow Lines.

If the flow lines are made visible in a way similar to a smoke wind tunnel, a slight alteration in H. C. H. Townend's process also allows measurement of the current velocity. To slightly heat a thread of the current, H. C. H. Townend did not use an electrically heated wire, but a spark jumping between platinum electrodes. When a spark jumps, a warm air schlieren is produced and determines a definite point inside the flowing medium. If the sparks keep jumping for some time, the electrodes become warm so

that a thread of warm air is drawn between them at the same time.

If the stream is projected with a schlieren apparatus in which the direction of the edge of the schlieren diaphragm coincides with that of the flow of the thread, the schlieren image gets flow threads which contain enlarged spots (knots); if the position of the schlieren diaphragm is turned 90°, only the positions of the flashovers can be seen (cf. Figures 95 and 96). Now if the sparks jump at a constant time interval, the flow velocity can be determined for stationary currents from the interval between the knots with a single exposure. Similarly, if a spark is chosen as a light source and is controlled synchronously with the sparks in the current, a stationary image of the current is found on the ground-glass plate, and a slight difference in the frequency of the sparks provides an arbitrarily delayed reproduction of the flow passage.

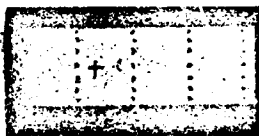


Figure 96. As in Figure 95. Schlieren Diaphragm Perpendicular to the Lines of Flow.

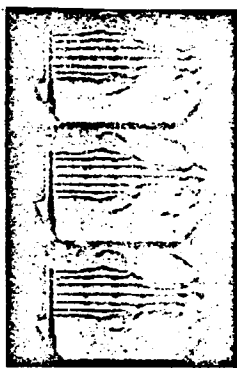


Figure 97. Stream of Air Flowing Into a Quiet Atmosphere. Visualization of Air Flow Lines According to Townend. Frequency of Exposure was Equal to the Frequency With Which the Rings of Turbulence Separate at the Ray Boundaries, and Therefore the Set of Images Provides an Apparently Static Process (cf. Also Figure 91).

furnish a free jet without distortion. The nozzles intended for use are first computed and then tested by providing the walls with grooves where disturbances originate and which have an envelope corresponding to the head wave of a bullet (cf. p.392). In this case they are designated "Mach lines". Their inclination to the direction of flow is the "Mach angle". In accord with equation (87), the following formula is valid

$$\sin \alpha = \frac{a}{v},$$

where a is the speed of sound, and v is the flow velocity at the pertinent point.

NASA

If the flow process is turbulent in one region, the knots would not be seen under stationary observation. Therefore this process is very appropriate for investigating the transition from laminar to turbulent flow.

Nonstationary processes can be investigated in the same way if the exposures are taken with a slow motion camera and a sufficiently high frame rate (Figure 97). Otherwise the following more simple procedure is possible: the schlieren arrangement is set for a dark field, i.e., only the knots appear bright against a dark background. Then the sequential positions for the knots occurring at a definite point in time can be fixed on a single plate. Only one suitable sequence of illumination sparks need be chosen.

If, as we have seen, the use of the schlieren methods is very appropriate under certain conditions at subsonic velocities, it is still not usually used here. The situation is different with supersonic velocities. Here the schlieren methods represent the main means of investigation. The construction of a supersonic nozzle--the most essential part of a supersonic tunnel--cannot even be accomplished without continuous checking in a schlieren image. For one requirement of a good supersonic channel is that it

/403

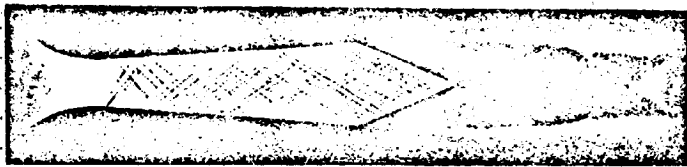


Figure 98. Effluence of Air at Supersonic Speed from a Tapered Jet. Mach Lines Begin Behind the Narrowest Cross-Section.

α can be considered as an equation of state, just as are pressure, temperature, density and flow velocity. Against the wall α can be taken directly from the schlieren exposure, since the flow direction is known there (assuming that no separation of flow occurs). Inside the current α can be

determined for all points at which two Mach lines, originating on opposite sides, cross. Their intersecting angle is equal to 2α . Therefore two intersecting Mach lines furnish the direction of flow (cf. Figure 98).

In investigating flow around a profile at supersonic speed, schlieren methods are particularly suitable because finite differences in density occur in the flow and the change in density is primarily responsible for the light deflection in the schlieren apparatus. Compression shocks are also involved in supersonic flow. Here the density jumps practically discontinuously to a somewhat higher value so that the density gradient assumes unusually high values at the leading edge of the shock. Since according to equation (41) the light deflection depends on n -degree and n in turn is related to ρ according to (59), the shock fronts can be made very obvious even if the absolute alteration in density is only very slight.

/404

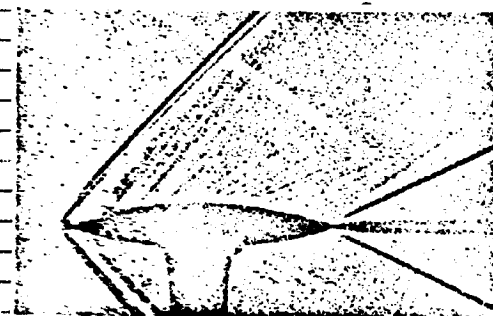


Figure 99. Plane Supersonic Flow Around a Strut. The Oblique Compression Shocks Before and Behind Waves of a Flying Bullet.

In discussing the schlieren image of a supersonic flow, the orientation of the schlieren diaphragm must also be considered and attention paid to the fact that the direction and magnitude of the light deflection depends on the entire course of the n -degree along the light ray, as well as on the exterior shape limiting the process. It is seldom as simple as is sometimes read in gas dynamic treatises, e.g., that darkening of the schlieren image represents an area of pressure and brightening an area of rarefaction.

With proper discussion, such as results from the data introduced into Part II of this paper, a great deal can be derived from the schlieren image of

a supersonic flow. In some cases under certain conditions a quantitative evaluation is also possible.

NASA

Several practical examples are shown in Figures 98-100.

For the supersonic nozzle with a rectangular cross-section, shown in Figure 98, a pressure chamber is to be assumed on the left with gas flowing from it through the nozzle. In practice this pressure chamber is generally just the free atmosphere; then a flow goes into a vacuum chamber. It is very visible in Figure 98 that at first supersonic flow is only present beyond the narrowest cross-section, since it is here that the Mach lines first begin. Their angle of inclination is large at first and then becomes smaller, i.e., the flow velocity increases with the increase in nozzle cross-section--a situation which can only occur with supersonic speed. It can also be perceived in Figure 98 that the upper and lower boundaries of the nozzle end are only effective within the Mach angle. Depending on the pressure behind the nozzle, there is an expansion around the ends of the nozzle or an oblique compression shock proceeds from them; if the counter pressure is too high, a straight compression shock enters the nozzle.

Expansion proceeds adiabatically and has been computed exactly by Th. Meyer [37] for the plane case.

The oblique compression shock can be presented as a normal straight one if it is considered as coming from a system moving parallel to the front of the compression wave.

Th. Meyer has computed the events at a Laval nozzle by using expansion flow and oblique compression shock. The correctness of his observations has been proved by Magin [36] with schlieren exposures.

Figure 99 shows the flow around a plane profile. If the mount were not visible, it might be believed that a flying bullet were involved. The oblique compression shocks of the head and tail waves are present. Along the profile numerous Mach lines can be seen; they diverge from one another, i.e., the entire flow between the head and tail wave is an expansion flow.

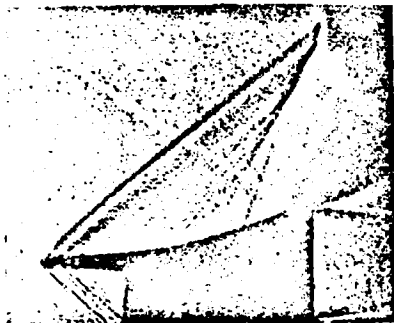


Figure 100. Schlieren Exposure of a Compression Flow. Formation of a Compression Shock Where Mach Lines Meet.

A compression flow is shown in Figure 100. The upper part of the plane profile is concave. The result of this is a convergence of the Mach lines. Intersection of them, however, is physically impossible; for this would mean that multiple pressure is present at one point at the same time. It can be perceived from Figure 100 that nature solves this difficulty with the appearance of a new compression shock.

In this way plane supersonic flow can be understood quite well

and also computed quantitatively for the most part; spatial problems present considerably greater difficulties. It is true that here graphic methods are partially successful, but the correctness of the figuring must usually be proved by direct schlieren exposures.

27. Origin and Propagation of Waves

Although wave propagation processes in fluids and gases are not distinguishable in principle from hydrodynamic processes--the whole area of acoustics is included in the basic hydrodynamic equations--, presentation of the problems is essentially different. Particularly, nonstationary processes are considered in the origin and propagation of waves, while hydrodynamics is usually concerned with stationary phenomena.

One problem which has been treated in a number of works (F. H. Tufts, 1902; R. Wachsmuth, 1904; F. Krueger and H. Casper, 1936) and for which schlieren methods have been successfully used is the generation of the Aeolian mode, the slit tone and the strident tone. This generation can be attributed to the formation of turbulence behind a bar or flowing through a slit. The regularities of a turbulent path were first investigated in a purely experimental manner (also in principle with a schlieren method) by H. Benard in 1908 and were later treated theoretically by Th. v. Karman (1912).

F. Krueger sets the frequency of the dissolution of this turbulence as equalling the frequency of the sound resulting from it. Then a dependency of the sound pitch on the flow velocity and the width of the slit must be proved in accordance with the laws of the turbulent path.

And therefore it must be 1.

$$\frac{ND}{U} = \text{const}, \quad (89)$$

where N is the pitch, D the diameter of the bar (with Aeolian tones) or the width of the slit (with slit tones) and U the flow velocity of the air.

2. The constant must agree numerically with the values produced in a purely hydrodynamic fashion.

In the case of strident sounds, the pitch is influenced by the distance f of the tooth from the slit in such a way that the pitch drops to a definite value as distance increases and then suddenly rises about an octave, only to drop again. This phenomenon can also be explained by theory of turbulence if a reciprocal connection of the turbulent distance with the tooth interval is assumed. At the smallest tooth interval, this corresponds to the distance between two eddies; after the first jump in frequency, which at f is approximately equal to double the amount of the turbulent interval in free flow, the turbulent interval becomes equal to half the tooth interval; Accordingly after the next jump in frequency, three turbulent intervals correspond to one tooth interval.

The fact that this theory is in accord with the facts can now be proved with the help of the schlieren method. Wachsmuth used ether vapor to make the flow of air from a pipe visible. F. Krueger and H. Casper let carbon dioxide flow through the slit; here the dissolution of turbulence was plainly visible. Resolution in time was made with a slow motion camera.

Figure 101 shows the formation of turbulence on the left side of the tooth. In Figure 102 the turbulent interval is equal to half the tooth interval and is equal to a third the tooth interval in Figure 103. The Toepler method was used in a shape where the image of a circular light source L (perforated diaphragm, 4 mm diameter) was completely stopped down by a round schlieren diaphragm. Therefore in Figures 101-103 the light deviations in each direction are perceived as brightening on a dark background. Since no deflection occurs in the middle of the beam, a black streak appears here and it looks as if the beam were split. This should not lead to any false conclusions. By narrowing the aperture with a straight edge parallel to the course of the ray, one side would become brighter and the other darker than the background. Since in the previous case it was a matter of proving dissolution of turbulence, the use of a straight schlieren diaphragm, perpendicular to the direction of the ray would also be very appropriate; for then the stationary, straight line path of the ray would not be visible at all, but rather only the deviations from its path, i.e., the lateral fluctuations and turbulent dissolution. In similar cases the author has taken a simultaneous exposure of light deflection in two directions perpendicular to one another¹.

/407



Figure 101. Generation of a Strident Sound. Visualization of Flow With the Use of Carbon Dioxide. Formation of Turbulence on the Left Side of the Tooth.

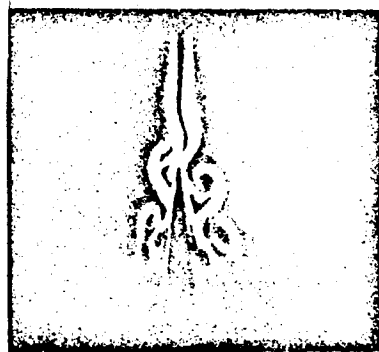


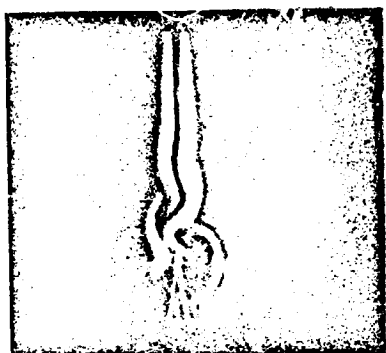
Figure 102. As in Figure 101. Turbulent Interval Equal to Half the Tooth Interval.

The sensitivity of schlieren methods is generally not capable of making sound waves of normal frequency and sound intensity visible. The light

/408

¹ VDI-Forsch., No. 367, p. 22.

deflection caused by a sound field, however, increases proportionally to $v^2 \cdot A$ (v = frequency, A is the amplitude of the physical movement in the sound wave)¹, so that it should be possible to make them visible at a sufficiently high frequency and sufficient amplitude. However, the maximum amplitude which can be reached in practice is not independent of the frequency, but it may be assumed that A is proportional to $1/v$. In this way the light deflection would increase with the frequency v .



For example, for $v = 20,000$ Hz and $A = 5 \mu$ in air (practically attainable) at a penetrated layer density of 5 cm

$$\epsilon = 10^{-5}$$

and can therefore be made visible (cf. with values of Table 2).
Cover Page Source

Figure 103. As in Figure 101. Turbulent Interval Equal to One Third the Tooth Interval.

In any case it is noted that ultrasonic waves can be made visible without any difficulty, as was achieved in 1930 by E. P. Tavil [70]. To make sound waves in air visible R. Pohlman uses the Boas coincidence method (cf. p.317).

It is even easier to make detonation waves visible. Their front consists of a compression shock (cf. p.404). The light deflection caused in it is so large that no sensitive schlieren method is necessary and even the shadow method alone produces very useful exposures (Figure 104). If it is a matter of following the propagation of sound waves, it is therefore appropriate to experiment with detonation waves.

Making an exposure of a sound field is of practical importance for room and building acoustics. In the model of a room an electrical spark gap is set up to produce detonation waves at the location of sound sources (speakers' platforms, orchestras, etc.); these waves are reflected from the individual objects and walls of the room. The appearance of the reflected waves can be registered at any arbitrary point in time and conclusions about audibility can be drawn from them for the various positions in the room. Investigations of this type have been carried out by Sabine and F. M. Osswald [116].

Two exposures taken by Osswald (with the shadow method) are shown in Figures 105 and 106. Figure 105 shows the effect of a fold in a wall on sound propagation in a room. Here there is an intense intermixture of the sound waves behind the primary wave front. Figure 106 represents a study profile for channeling. Its purpose is to obtain good sound distribution.

¹ VDI-Forsch., No. 367, p. 28.

NASA

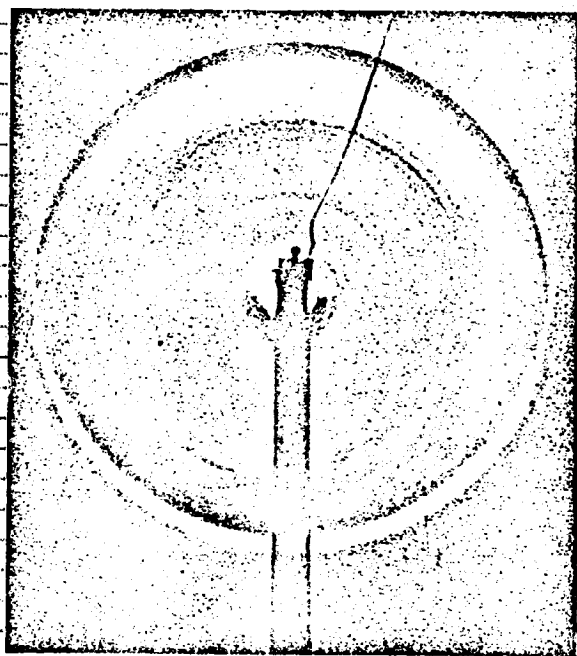


Figure 104. Spark Detonation Waves in Air. Schlieren Diaphragm (Toepler Arrangement) Horizontal.

New findings in the investigation of detonation wave propagation can also be obtained physically by using schlieren methods. One might think that the propagation of waves has been so thoroughly explained by classical wave theory that nothing more remains to be resolved from the physical point of view. This is not the case. If we begin by disregarding nonlinearities which occur with intensive detonation waves, and consider the limiting case of small amplitudes, propagation in a continuum certainly does not present any problems, but as soon as boundary surfaces between two different media are present, phenomena occur which have only been recognized recently.

Here let us look at a few schlieren images taken in the Ballistics Institute of the Air War Academy by O. v. Schmidt.

In Figure 107 we see a glass cuvette which contains two fluids in separate layers, on the bottom a solution of NaCl (sound velocity 1,600 m/sec) and on the top Xylol (sound velocity 1,175 m/sec). In the boundary layer between the two fluids a spark detonation wave is now produced. This wave must therefore be propagated in both fluids at the same time like a hemisphere.

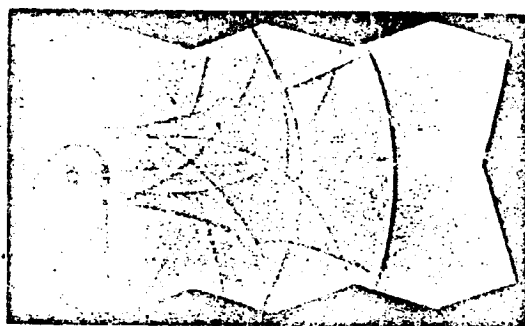


Figure 105. Effect of Folding the Wall of a Chamber on Sound Propagation.

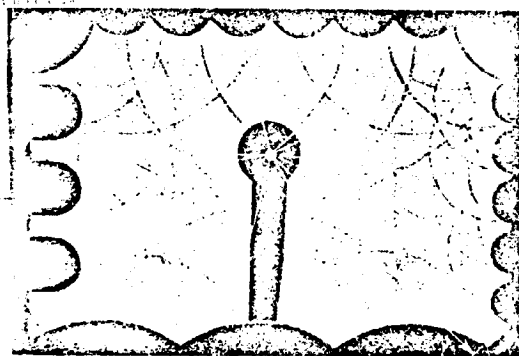


Figure 106. Study Profile for Channeling.

/410

/411

The radii of both hemispheres must behave like the sound velocities, i.e., a smaller hemisphere must be seen on the top than on the bottom at the time of exposure. Figure 107 does show--as expected--these two hemispheres, but in addition, starting at the intersection point of the large circle with the boundary layer, there is seen a straight wave front tangent to the small circle. This front represents a perfectly new type of wave propagation. It is also present if the detonation spark does not jump in the boundary layer (Figure 108), and is then tangent to the wave reflected at the boundary surface.

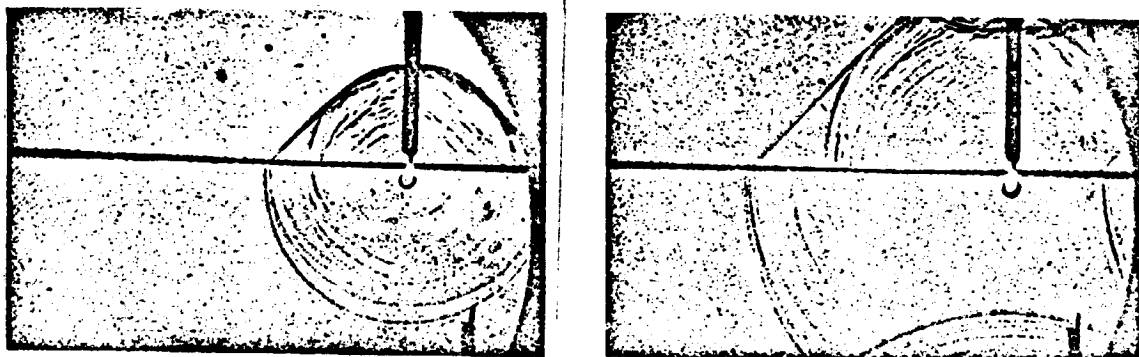


Figure 107a and b. Propagation of Detonation Waves at the Boundary Layer Between Two Fluids of Different Sound Velocity.

After looking at the schlieren exposures, it is not difficult to find an explanation of this new kind of process: the spherical wave in the "faster" medium (let this expression be accepted for the medium with the higher sound velocity) runs along the boundary layer with supersonic speed in reference to the "slower" medium; for this reason--just as in the formation of the head wave of a flying bullet (see p.395)--the elementary waves originating at the boundary layer in the "slower" medium will have an envelope and thus form the new type of wave front. If the head wave angle is checked in Figures 107 and 108b, we find, in exact correspondence with the Mach formula (87)

$$\sin \alpha = \sin 47^\circ = \frac{a_1}{a_2} = \frac{1175}{1600}, \quad (90)$$

where a_1 means the sound velocity of the upper and a_2 the sound velocity of the lower medium. However, if we represent this fact acoustically, we find the following: the sound from sound source Q can reach a point P in the "slower" medium in the following three ways (Figure 109):

1. The direct path across the primary wave. The time necessary for this

$$t_1 = \frac{PQ}{a_1} \quad (91)$$

2. The path across the reflected wave with a travel time of

/413

$$t_2 = \frac{QA + AP}{a_1} = \frac{PQ'}{a_1} \quad (92)$$

3. The path across the head wave with travel time

$$t_3 = \frac{QB}{a_1} + \frac{BC}{a_2} + \frac{CP}{a_1} \quad (93)$$

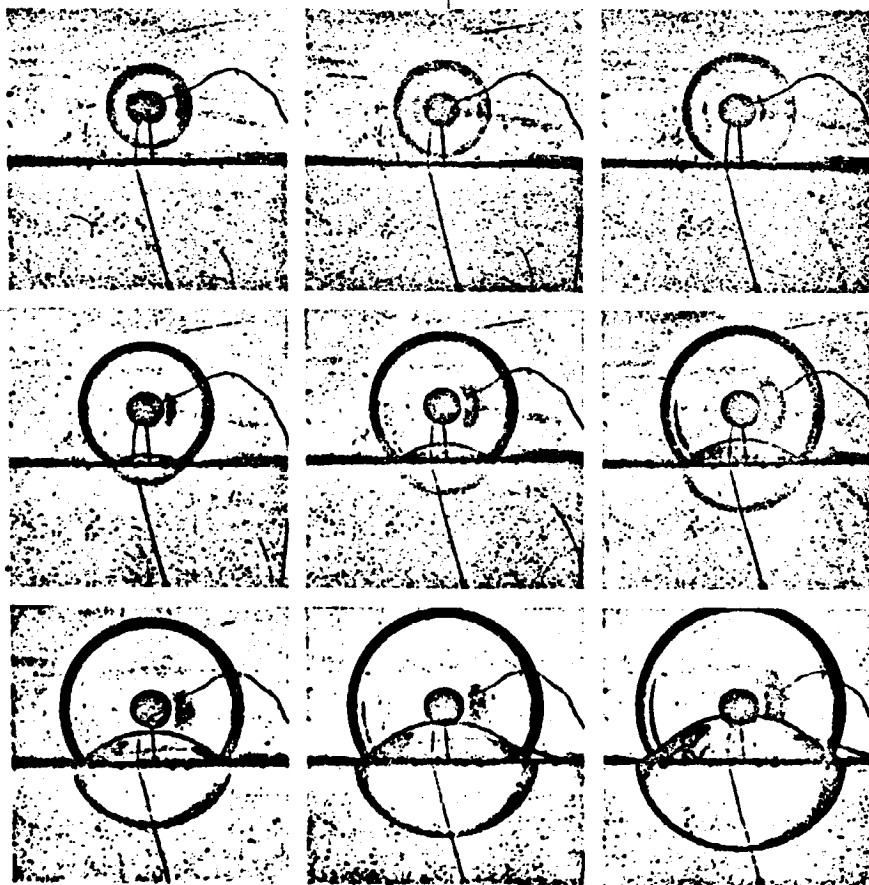


Figure 108a. Propagation of a Spherical Wave at the Boundary Layer Between Two Media With Different Sound Velocities (Carbon Tetrachloride and Water). The Wave Center (In This Case a Small Amount of Detonating Lead Azide) Does Not Lie in the Boundary Layer.

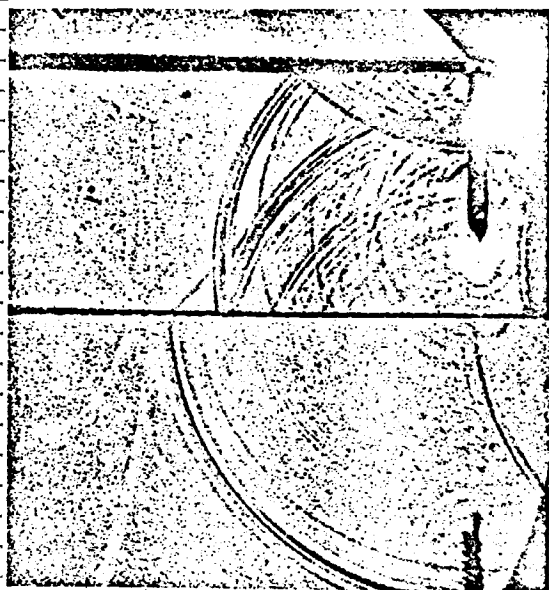


Figure 108b. Formation of the "v. Schmidt" Head Wave in the Propagation of a Spherical Wave at the Boundary Layer Between Media With Different Sound Velocities (Xylol and Table Salt Solution).

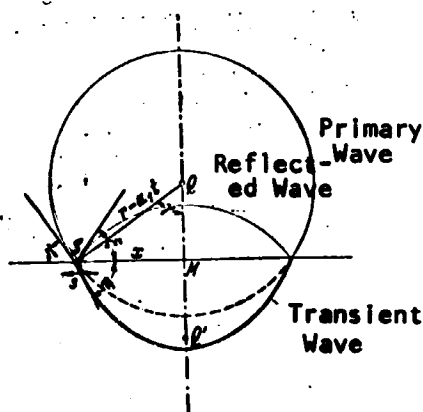


Figure 110. Outline of the Propagation of a Spherical Wave at the Boundary of Two Fluids.

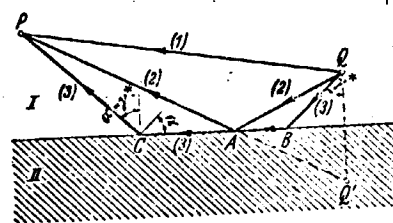


Figure 109. Sound Path From Q to P At the Boundary of Two Fluids.

Although this path is the longest, it still requires the shortest time ($t_3 < t_1 < t_2$), since the distance BC is traversed with the higher velocity a_2 .

This fact about the three different sound paths is new in regard to acoustics. It was first determined in seismology when time measurements were taken at the time of blasting at the surface of the ground (Mintrop, 1919). In the beginning, this phenomenon could not be explained until O. v. Schmidt presented the theory repeated here in 1928. This theory was at first rejected in physics circles, although in mineralogical research the speed of sound was constantly used according to method number 3 (see Figure 109) in deep stone layers to determine the ground composition. This area, somewhat remote to physicists, was not given sufficient attention. Only in 1938 did the schlieren exposures made by O. v. Schmidt conclusively prove the existence of the head wave.

Let us discuss the exposure in Figure 108 in somewhat more detail. If the primary detonation wave strikes the boundary surface, the point of intersection S of the wave front with the boundary surface moves at infinite

velocity at the moment of contact. The "intersection velocity" then subsides, producing (see Figure 110):

Page One Title

$$s = \frac{dx}{dt} = \frac{r}{x} \cdot \frac{dr}{dt} = \frac{r}{\sqrt{r^2 - c^2}} \cdot a_1 = \frac{a_1}{\sin \gamma} \quad (94)$$

(where $e = QM$).

At first s has a value indicating supersonic velocity for both media. Therefore it is quite reasonable to ask whether intersection point S does not produce head waves in both media; actually they are present but are identical with the penetrating or reflected wave.

/414

Proof for the reflected wave:

Let ξ designate the head wave angle of the head wave determined by S in the "slow" medium, and in a purely formal way, based on the Mach relationship (87):

Cover Page Source

$$\sin \xi = \frac{a_1}{s} = \frac{a_1}{a_1/\sin \gamma} = \sin \gamma, \text{ i.e. } \xi = \gamma. \quad (95)$$

However, γ is the angle at which the reflected wave strikes the boundary layer at every point in time.

Proof for the penetrating wave:

Let η be the head wave angle determined by S in the "fast" medium, and in a purely formal manner according to (87)

$$\sin \eta = \frac{a_2}{s} = \frac{a_2}{a_1/\sin \gamma}, \quad (96)$$

i.e.

$$\frac{\sin \gamma}{\sin \eta} = \frac{a_1}{a_2}. \quad (97)$$

However, this is nothing but the Snellius law of refraction according to which the penetrating wave is computed anyway.

Thus, we may consider the principle of head wave formation as a superior principle referring to both reflection and refraction, as well as representing the new "v. Schmidt ray".

MACH

If $s = a_2$ has taken place, there will be no further head wave developed in the "faster" medium. Then Page One Title

$$\text{Cover } s' = \frac{a_1}{\sin \gamma^*} = a_2,$$

and

$$\sin \gamma^* = \frac{a_1}{a_2}. \quad (98)$$

In this case according to (97), $\eta = 90^\circ$, i.e. γ^* is the angle of total reflection. The wave front in the "faster" medium lies perpendicular to the boundary layer and in its continuation becomes independent of S , since it proceeds at constant velocity a_2 while the velocity of S constantly decreases to the limiting value $s = a_1$ (for $\gamma = 90^\circ$).

Because of its constant velocity in the "slow" medium, the wave front in the "faster" medium now drags the head wave, limited to straight lines, with head wave angle α ; this is (cf. equation (90))

$$\sin \alpha = \frac{a_1}{a_2} = \sin \gamma^*, \quad (4'') \quad (99)$$

i.e. the head wave angle is identical with the total reflection angle.

/415

All of these phases can be seen very clearly in the schlieren exposure of Figure 108.

In spite of this explanatory demonstration, the following situation is still not clear from a physical point-of-view: the ray occurring in the "faster" medium below the angle of total reflection should be without energy on the basis of the Fresnel equations. As the schlieren exposures show, the energy present in the boundary layer is completely capable of continuing to provide energy in the "slow" medium in the form of the head wave. In order to elucidate this fact, a transverse effect, i.e. a movement of energy in the wave front in the direction of the boundary layer, must be presumed and this is not considered in the Fresnel equations. In addition, it is known from optics, that modifying the interior structure of a boundary layer makes it possible to change the distribution of energy between the penetrating and the reflected light within wide limits (reflex diminishing layers). Although an ideal boundary surface is fundamental for the Fresnel equations, such surfaces never occur in practice.

Figures 107 and 108 illustrate the processes of wave propagation at the boundary layer of two fluids. The same phenomena also occur in other media. Thus, e.g., Figure 111 shows the wave propagation at a boundary layer of water

and plexiglass. The wave penetrating the plexiglass can be seen very well in the schlieren image. This wave also pulls the "v. Schmidt" head wave into the water again. If the solid body (plexiglass) were opaque, it would naturally be impossible to see the wave progressing through it, but the occurrence of the head wave in the other medium (water in this case) now gives the possibility of investigating sound wave propagation in opaque bodies. This methodology should be of great importance for physical technology.

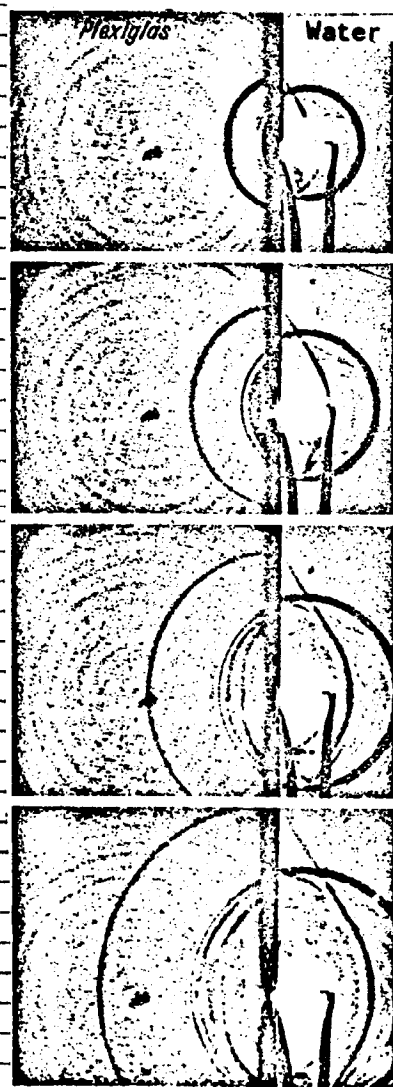


Figure 111. Propagation of a Spherical Wave at the Boundary Between Plexiglass and Water.

Figure 112 shows the processes in bars made of various materials. The bars are in water and are struck by the spark detonation wave. The head waves produced by the longitudinal sound wave develop on both sides of the bars. However, other waves with a more acute angle are also found. Further investigation shows that they are caused by transverse waves. This provides an opportunity of determining the magnitude of elasticity of a material: both velocities can be taken from the head wave angle of the longitudinal and transverse angle and from this the elastic magnitudes can be computed.

(411)

The exact structure of the oscillation mode produced in the water by the transverse wave has still not been explained.

Under certain conditions the head wave theory is capable of bringing a series of problems in other areas closer to a solution. O. v. Schmidt particularly believes that the silent zone related to sound propagation and the short wave circuit of the earth can be explained by it. The fact that the head wave phenomenon also occurs in surface waves is demonstrated by colored image Figure 113 (Table II). This was exposed with the lattice diaphragm method and represents the shape of a water surface above which surface waves propagate from point C (see the schematic diagram in Figure 114).

/417

The water vessel used had two different depths: the left half was shallower than the right half, so that speed of

passage on the right had to be greater, for it is approximately determined by

Page One Title

$$c = \sqrt{g \cdot h} \quad (100)$$

Cover Page Title

(h is the water depth). Therefore two sets of semicircles ($a_1, a_2 \dots$ and $b_1, b_2 \dots$, cf. Figure 114) also had to be expected in this case; the semicircles terminate at the point of discontinuity of water depth (at points $S_1 \dots$ and $T_1 \dots$). However, it can be seen from Figure 113 that here, too, a head wave ($c_1, c_2 \dots$) is described proceeding from the end of the larger circle ($S_1 \dots$) and into the smaller circles. The fact that the exposure of Figure 113 is not on the same scale as the diagram provided in Figure 114 must be based on the additional amplitude dependence of the surface wave velocity and a disturbance caused by capillary waves.

Cover Page Source

At the same time Figure 113 may be used as an example of the fact that schlieren methods are also suited for investigating the propagation processes of surface waves. Although model tests are often carried out with surface waves in experimental lectures (e.g. experiments of R. W. Pohl are well-known), quantitative test results referring to amplitude at the same time do still not exist. In the opinion of the author the schlieren methods appear to be the only useful method of attacking such questions experimentally. Stereophotomoving pictures would seem to be the only other possible method.

While up until now we have only been concerned with the propagation of waves with a small amplitude, the investigation of waves with a finite amplitude presents a field of work particularly reserved for the use of schlieren methods. Since these are of special importance for explosive processes, the next section shall deal with them in more detail.

/418

28. Combustion and Detonation Phenomena.

Combustion phenomena in gases involve considerable change in density. First of all the initial products of the chemical transformation (e.g., hydrogen and oxygen mixed with the nitrogen of the air) differ from each other in density and refractive index, and the combustion products also have different values for both magnitudes; considerable differences in temperature result from the liberation of combustion heat and give rise to a further difference in density. For this reason the schlieren methods are an appropriate tool for studying combustion processes.

We are concerned with stationary combustion phenomena if a combustible mixture of gases flows through an aperture into the open air and the flow velocity lies between two definite limits. If the flow velocity is too small, the flame flashes back and if it is too large the flame is blown out.

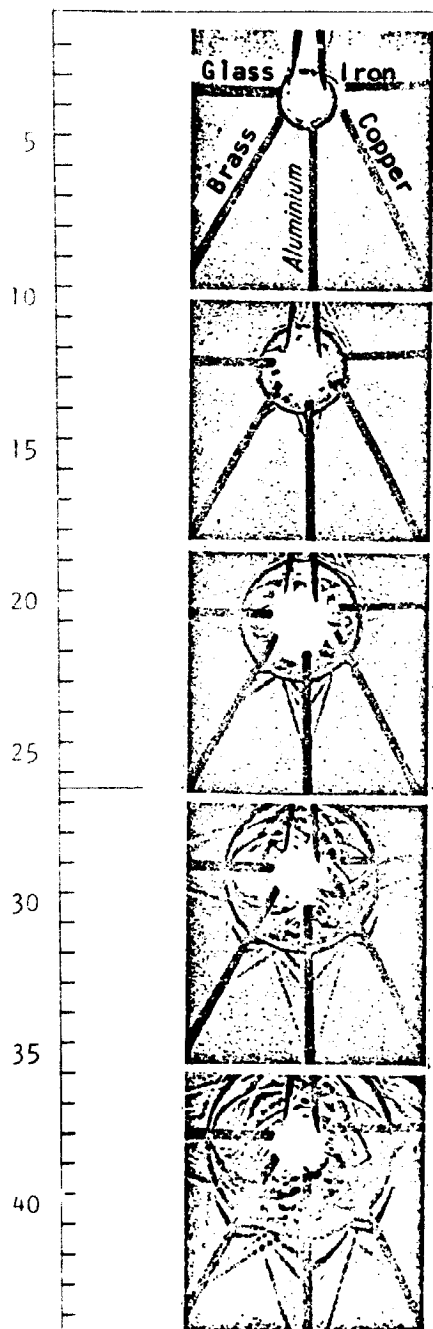


Figure 112. Bars of Different Material In Water Are Struck by a Spark Detonation Wave. The Longitudinal and Transverse Waves in the Bars Draw Out a "v. Schmidt" Head Wave in the Water.

Page One Title

Cover Page Title

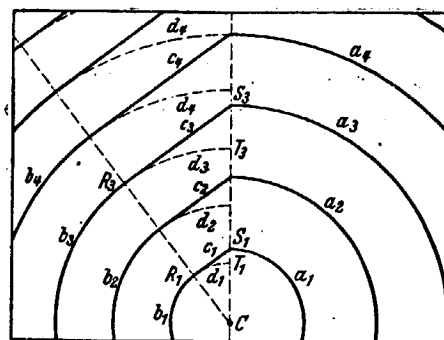


Figure 114. Schematic Representation of the Propagation of Surface Waves in a Container Which Has Deeper Water on the Right Than on the Left.

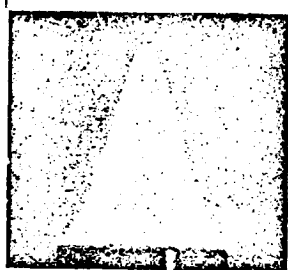
Cover Page Source

The theory has been presented by A. Gouy¹ that the standard component of flow velocity in the combustion plane equals the combustion velocity. Therefore it should be possible to compute the combustion velocity from an exposure of the combustion plane. Here, however, discrepancies arise if we begin with the combustion plane obtained from a simple photographic image of the burning flame. A. N. van de Poll and T. Westerdijsk [139] have compared a combustion cone taken with its own light with the combustion cone provided by a schlieren exposure and have determined that the visible shining surface does not coincide with the hydrodynamic discontinuity surface (resulting from the schlieren exposure). An example of this is given in Figure 115. This pertains to a butane-air flame with an excess of air where a secondary combustion is therefore missing. The combustion pipe was sufficiently long for a parabolic distribution of velocity to be set up inside it. Figure 115a shows the optical combustion plane and Figure 115b the hydrodynamic one. On the optical level the base of the cone is broader than

¹Gouy, A., *Ann. Chim. Physique*, Vol. 87, p. 29, 1879.

the lip of the burner and the tip of the cone is rounded off. (Neither describes the case for the schlieren cone). Since these phenomena contradict the Gouy theory, the result is that the schlieren exposure provides a more useful image of the combustion front than does the optical image.

Cover Page Title



Cover Page Source



Figures 115a and b. Butane-Air Flame With an Excess of Air. a, Optical Combustion Plane; b, Hydrodynamic Combustion Plane (Schlieren Image).

Van de Poll and Westerdijk also demonstrate the further advantage of using schlieren methods: lighting times of the order of magnitude of 1 sec are necessary for photographic exposures because the flame is not very bright. However, lighting times of 1/100 to 1/1,000 sec can be obtained with schlieren exposures by using a carbon or tungsten arc lamp. When an electrical spark is used as the light source the exposure time is only 10^{-6} to 10^{-7} sec. Thus no nonstationary phenomena in the flame front can be photographed directly, although it is possible without difficulty by using schlieren methods.

/419

Figure 116 gives an example of a nonstationary flame front. Photographing the optical image in this case would result in a thoroughly fuzzy image.

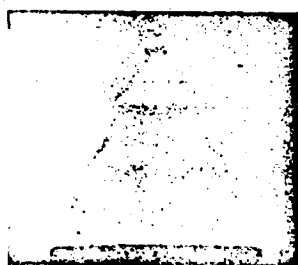


Figure 116. Butane-Air Flame With a Nonstationary Flame Front.

Combustion velocity is not a constant, but depends on current conditions. Therefore it can happen that when a mixture is burned in a closed container, in which the pressure and temperature (because of adiabatic compression) of the still unburned part increase because of the expansion of the burnt component, combustion velocity suddenly assumes high values and gives rise to extreme local pressure peaks. With certain mixtures of gases the increase in combustion velocity can lead to explosions. Knowledge of these phenomena is of great importance, for instance if one wishes to understand the course of combustion

in an internal combustion engine. Schlieren methods are also useful for solving this question since they do not have any influence on the process itself, as does, e.g. a probe. Still there are considerable difficulties in obtaining schlieren exposures of the activities in the cylinder of a running engine. This has been tried by K. Scheffler [104]. Some exposures of combustion in a bomb have been taken by W. Lindner [69] and [80]. However, it would be more expedient to create the simplest possible relationships. We would like to present several exposures by Payman and Shepherd which provide a relatively clear image [125].

/420

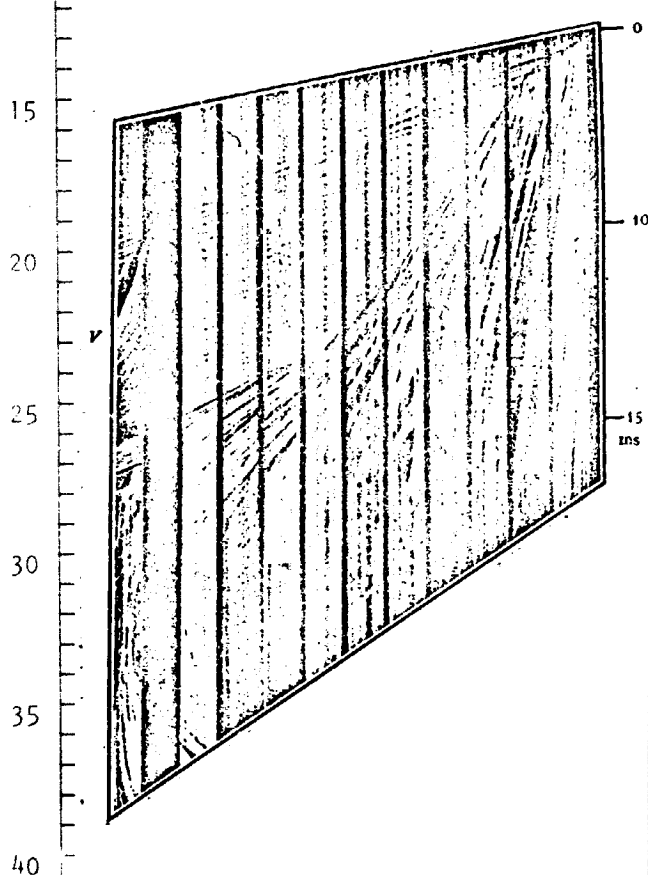


Figure 117. Explosion of a Mixture of Methane and Air in a Pipe (Pipe Length 3.65 m). Ignition on the Right, the Left End of the Pipe Open. V, Turbulent Ring.

Payman and Shepherd investigated the course of an explosion in a pipe 3.65 m long (diameter 30.5 cm). The pipe has been provided with slits and is divided into 10 single fields each of which serves as the object in a Toepler schlieren arrangement. Since the interesting thing here is the course in time, the exposure is made on a rotating film behind a slit. In this way the pressure and combustion fronts immediately provide the time-path curves. Figure 117 shows the explosion of a mixture of methane and air (9.1% methane).

Ignition takes place through a pipe filled with oxyhydrogen gas (125 cm long, 2.5 cm diameter), which is located at the right end of the large combustion pipe. An electrical spark initiates the process; the 10 different image strips for the individual fields of the pipe and one strip for the outside space have been fitted together in Figure 117. Starting at the right we see a detonation wave and the combustion front progress through the pipe.

The velocity of the detonation waves amounts to 360 m/sec and is constant. A turbulent ring is formed as it enters the free atmosphere, just as one forms in front of a rifle barrel during shooting (cf. Figure 91). Its

time-path curve is characterized by V. The first detonation wave front is followed by a large number of other waves which are somewhat flatter and therefore possess somewhat higher velocity. They proceed in a gas which has already

/421

been compressed (therefore heated) by the first detonation wave. The amount of precompression can be ascertained by the inclination of these straight lines.

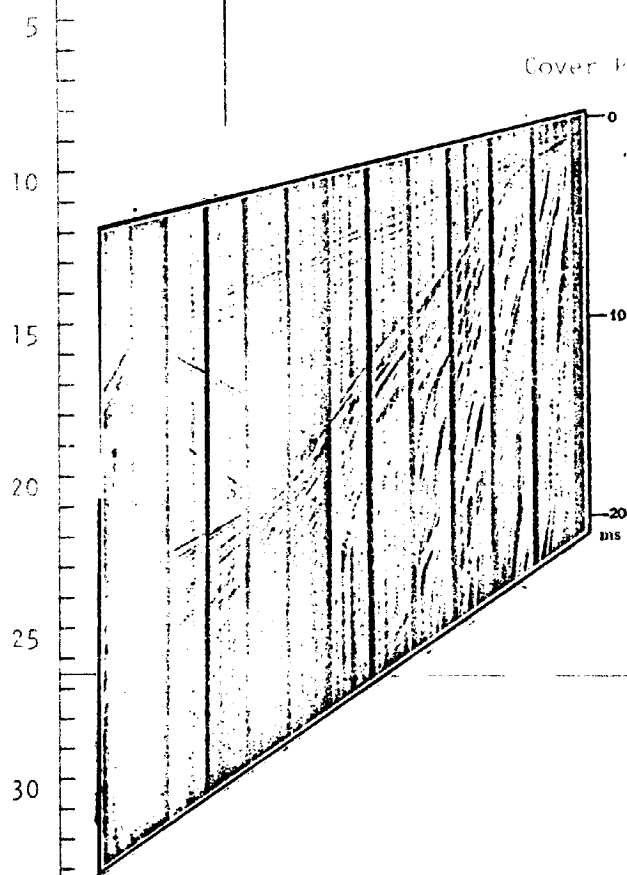


Figure 118. Like Figure 117. Left End of the Pipe Closed By a Paper Covering.

not immediately expand freely. First a pressure wave is reflected; its time-path curve can be seen well. Therefore, when this wave strikes the combustion front an apparent reduction in combustion velocity is caused, contrary to Figure 117. Thus this exposure is also a proof of the fact that the combustion phenomenon which has become stationary is first disrupted by the influence of the end of the pipe. The paper cover soon yields to the pressure of the detonation wave, rips and is pushed aside; then expansion can take place, again oppose the combustion front and cause its apparent acceleration up to the value of 520 m/sec.

The following quantitative statements can be made about combustion velocity; a value of 125 m/sec is measured during the stationary portion; the flow

The combustion velocity begins at almost the value of the detonation wave velocity, but drops immediately and from the third field on assumes the constant value of 120 m/sec for some time. From the seventh field on the combustion front is accelerated as high as 520 m/sec when it reaches the open end of the pipe. This acceleration is to be attributed to the influence of the open end of the pipe: the unburned gas compressed in front of the combustion front expands into the free atmosphere at the end of the pipe and consequently a rarefaction wave enters the pipe and adds further velocity toward the left through the still uncombusted gas and the explosive vapor. Therefore the extreme rise in combustion velocity is deceptive. Right at the end is found a recessive movement at the open end of the pipe since the pressure in the pipe decreases as a result of cooling.

Figure 118 has been taken under the same conditions but the open end of the pipe has been closed with a paper cover. Thus at first the process takes place just as in Figure 117. However, when the detonation wave reaches the paper cover it can-

/422

velocity u of the uncombusted gases before the front and toward the left is superimposed on the above value. How large is u ? The velocity of the first detonation wave (360 m/sec) is raised in contrast to the sound velocity of the unburned mixture of gas (340 m/sec). From this the material velocity immediately behind the wave front is found on the basis of gas dynamic functions. If the condition between the detonation wave and the combustion front were constant, this value would be set as equal to u . Constancy can be checked on the basis of the waves which can be seen in the entire range or the range is to be corrected from the inclination of these waves. A further possibility of determining u is offered by the wave reflected onto the paper cover. No supersonic velocity is to be assumed for it, because its velocity amounts only to 290 m/sec as a result of the flow; therefore the material velocity u of the uncombusted gases would be equal to 50 m/sec, even though the sound velocity of 340 m/sec were to be assumed in the gas between the detonation wave and the combustion front. Even this lies rather high and must be accordingly corrected.

Therefore the combustion velocity of 125 m/sec becomes only about 75 m/sec for the observer, if reference is made to the uncombusted gas before the combustion front.

Correspondingly the "apparent" combustion velocity increases considerably with expansion into the free atmosphere. For flow velocity u at later points of time it is also possible to determine values with the waves passing from right and left through the region before the combustion front. The waves entering from the left originated in the parts of the paper cover by reflection.

Figure 119 shows the example of a completely closed container: the left end of the combustion pipe is tightly sealed and the other conditions are the same as for Figures 117 and 118. In this case the first shock wave is completely reflected at the end¹. Instead of recoiling at 290 m/sec as in Figure 118, it recoils at 310 m/sec. When it passes through the combustion front its velocity is increased up to about 1,000 m/sec (as a consequence of the higher temperature), at the right end it is reflected again and for a second time passes through the combustion front. This has a very great effect upon the propagation of the combustion front. During the first passage it reverses its apparent direction of motion and after the second passage resumes its positive direction at high velocity. This process is repeated until the gas has been completely combusted. It is also worthy of note that a partial reflection takes place when the shock wave passes through the combustion front the second time². In this way a new shock wave of lesser intensity is formed and continues its course which may be followed for several reflections at the end of the pipe.

¹Concerning computation of the physical state behind the reflected wave front, see H. Schardin, *Physik. Z.*, Vol. 33, pp. 60-64, 1932.

²The reason for this is the lower density of the vapors. Correspondingly, a rarefaction wave must be reflected at the first passage of the shock wave, but this is difficult to prove because of its unmarked front.

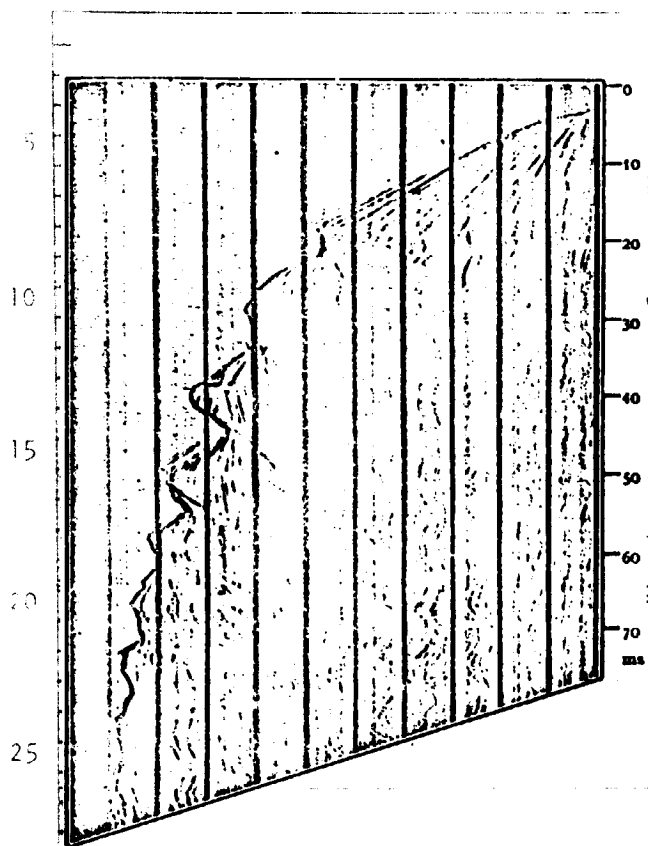


Figure 119. Like Figure 117. Left End of the Pipe Tightly Sealed.

ways by using an immediate optical exposure with its own light. The intensity of illumination of a detonation front is essentially greater, so that air brightness is usually sufficient to provide enough blackening on a rotating film. In addition, solid explosives and no gases are partially used for explosive experiments, so that visualization of the detonation front would not be directly possible using a schlieren method. A schlieren method, on the other hand, is suitable for major investigations where combustion using an explosive mixture of gases turns into an explosion.

In the case of an explosion it is extremely important to know what happens in the vicinity of the explosive after the explosion. In particular, measurement of the velocity of the air shock wave and of the vapors is important. Here again a schlieren arrangement is necessary, since the air shock wave is not immediately visible. Exposures of this type have been made by M. Patry [96] among others.

Since this division of the shock waves reoccurs at every passage through the combustion front, the process naturally becomes very complicated.

These examples should suffice to show how valuable the use of the schlieren methods is in investigating combustion processes. Insights of a major nature, scarcely possible by any other method, can be obtained.

An explosion is different in principle from combustion. While the combustion velocity lies in the order of magnitude of several meters per second, explosive velocities amount to several thousand meters per second. In combustion the vapors have a lesser density than the uncombusted substance, while in an explosion the situation is just the reverse; correspondingly the vapors in combustion move away from the combustion front and in an explosion move in the direction of the detonation wave. The distance-time curve of a combustion front can be reproduced very well with a schlieren image, but not al-

/424

/425

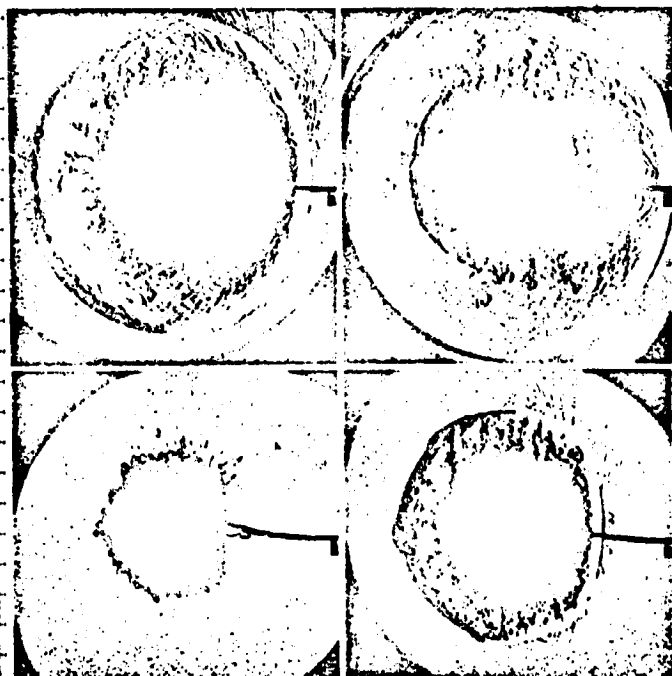


Figure 120. Four Successive Schlieren Exposures of a Lead Azide Pellet in Air.

An example for the use of schlieren methods in explosive phenomena are provided by Figures 120 and 121.

This concerns the explosion of about 1 g of lead azide. Figure 120 shows four successive stages in the schlieren image. In the first part of the image the detonation wave is hardly separate from the vapors, but innumerable solid particles have broken through the wave front. Each creates its own head wave. In the third part of the picture, the vapor front is already far from the wave front which becomes smoother and smoother. In the fourth part of the picture the new formation of a second detonation wave is distinguishable. Figure 121 shows the same process as a time-distance curve. The propagation of the two detonation waves and of the

vapors, the latter with a rough boundary because of the flying particles, can be seen.

By differentiation the course of a velocity w of the first air shock wave can be found, whence the Hugoniot equation yields:

$$\Delta p = \frac{2\pi}{\pi-1} \cdot \frac{w^2 - a_1^2}{a_1^2} \cdot p_0 \quad (101)$$

representing the pressure rise behind the wave front so that it is also indirectly possible to measure the pressure of a detonation wave in this way.

29. Diffusion

A further area of schlieren method application for measurements is diffusion. Already in 1893, O. Wiener [13] published an exhaustive work on this subject. The possibility of application is based on the connection between the concentration of a solution and the refractive index.

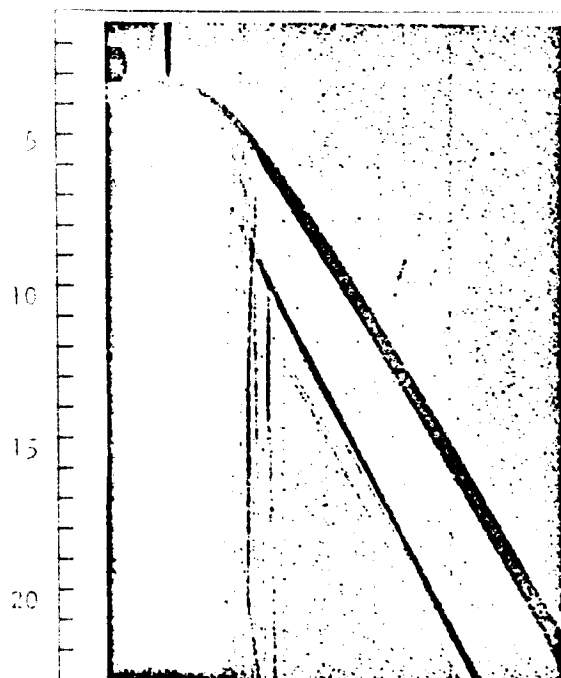


Figure 121. Time-Distance Schlieren Exposure of the Explosion of a Lead Azide Pellet in Air.

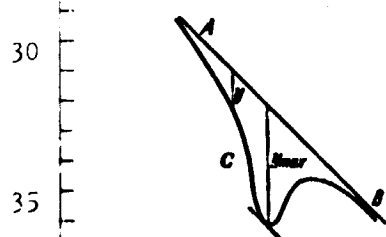


Figure 122. Light Deflection at Diffusion Between Two Layers of Liquids According to O. Wiener.

The general differential equation for diffusion is

$$\frac{\partial c}{\partial t} = D \cdot \Delta c. \quad (102)$$

Here c is the concentration, t the time and D the diffusion coefficient.

In most cases linear problems are involved; the following equation is valid for these

$$\frac{\partial c}{\partial t} = D \frac{\partial^2 c}{\partial y^2}. \quad (103)$$

Now if we posit

$$c = A + D n, \quad (104)$$

then

$$\frac{\partial c}{\partial t} = D \frac{\partial n}{\partial t},$$

and

$$\Delta c = D \cdot \Delta n,$$

whence

$$\frac{\partial n}{\partial t} = D \cdot \Delta n, \quad (105)$$

this means that in (102) c can be simply replaced by n if a linear relationship exists between c and n .

It is now within the scope of the schlieren methods to determine the spatial and temporal course of n (i.e., Δn and $\partial n / \partial t$) so that its course can be used to experimentally determine the diffusion constant and its dependence upon concentration and other magnitudes. Since considerable light deflection is handled here, the arrangement need not have a great deal of sensitivity, and more emphasis can be placed upon simple apparatus. The direct shadow

method is sufficient, e.g., according to O. Wiener, in a shape where the image of a slit inclined less than 45° is projected onto a screen into whose path is placed a cuvette with parallel walls in which the fluids under investigation exist in two layers. Light deflection into the area of diffusion then picks up the image of oblique slit AB (Figure 122) in a shape corresponding to curve C from which the deflection for the individual peaks inside the cuvette are to be taken.

Equation (49) is valid for limitation of the object by plane-parallel walls, i.e.,

$$\epsilon_y^* = \left(\frac{\partial n}{\partial y} \right)_y \cdot \frac{l_s}{n_0} = \frac{Y}{E}, \quad (106)$$

where ϵ_y^* is the deflection of a light ray in arc measurement after passing through the cuvette at height y . l_s is the thickness of the fluid layer, Y is the deflection onto the screen in the same scale as the distance E of the object from the screen and n_0 is the refractive index of the air (practically equal to 1).

Computation of the diffusion constants now takes place in the following way: solution of the diffusion equation (105) for the linear case is: /427

$$n = \frac{1}{2\sqrt{\pi Dt}} \int_{-\infty}^{+\infty} f(\xi) e^{-\frac{(y-\xi)^2}{4Dt}} d\xi, \quad (107)$$

where $f(\xi)$ is the given initial condition for distribution of the refractive index at time $t = 0$. Where two fluid layers are superposed, this produces:

$$n = \frac{n_1 - n_2}{2} \left(1 - \frac{2}{\sqrt{\pi}} \int_0^{\frac{y}{2\sqrt{Dt}}} e^{-\tau^2} d\tau \right) + n_2, \quad (108)$$

$$\frac{\partial n}{\partial y} = -\frac{n_1 - n_2}{2\sqrt{Dt}} \cdot \frac{1}{\sqrt{\pi}} e^{-\frac{y^2}{4Dt}} = \frac{Y}{E} \cdot \frac{n_0}{l_s}. \quad (109)$$

For $y = 0$, the maximum deflection Y_{\max} is obtained and from this for D

$$D = \frac{E^2 l_s^2 (n_1 - n_2)^2}{4\pi n_0^2 Y_{\max}^2}. \quad (110)$$

Since the time point $t = 0$ is not known exactly, it is advisable to transform equation (110) so that it contains only the time difference between the two last points of time and the maximum pertinent deflection:

$$D = \frac{E^2 P_1^2 (n_1 - n_2)^2}{4 \pi n_0^2 (l_2 - l_1)} \left(\frac{1}{Y_{1\max}^2} - \frac{1}{Y_{2\max}^2} \right); \quad (111)$$

D was presumed to be a constant and equation (109) makes it possible to determine whether this assumption holds: arbitrary values of t and y should always furnish the same D .

If D is a function of concentration, we should proceed from the following differential equation:

$$\frac{\partial c}{\partial t} = D(c) \frac{\partial^2 c}{\partial y^2} + \frac{dD}{dc} \left(\frac{\partial c}{\partial y} \right)^2. \quad (112)$$

The solution of this equation entails serious mathematical difficulties¹.

In addition a further modification of the initial equation must be carried out if the influence of gravity or centrifugal force is to be considered.

30. Results of the Ultracentrifuge Technology

In 1934 the author wrote in the *VDI-Forsch.*, No. 367: "Rough calculation has shown that the difference in concentration in the solution of high molecular material (e.g., sugar) in a circulating tray with a sedimentation equilibrium is large enough to be measured. The schlieren method should present an indirect possibility of determining the molecular weight of such materials." At that time the author did not know that a development was already in progress which would lead to great success today in the field of organic colloid research. An excellent summary of this subject is found in the book *Die Ultrazentrifuge* [The Ultracentrifuge] by The Svedberg and K.O. Pedersen [137]. The success obtained is to be attributed mainly to the development of the rapid centrifuge, the so-called ultracentrifuge, with which it is possible today to reach 750,000 g (g = acceleration due to gravity) in a fluid. The differences in concentration found in this way in colloidal solutions are sufficient to be measured on the basis, first, of different light absorption and, second, of light diffraction.

The light absorption method cannot always be used, so that success obtained is largely to be attributed to the refraction method, i.e., the schlieren methods.

¹Cf. Boltzmann, *Wiedemanns Ann.*, Vol. 53, p. 959, 1894.

In ultracentrifuge technology a distinction is made today between the "scale method" and the "slit method". Both are schlieren methods, the slit method with and the scale method without optical exposure of the object. The special names have their basis in their special arrangements.

Cover Page Title

The scale method is represented in Figure 123. An illuminated scale L is photographed with lens O. Between L and O the ultracentrifuge tray is so that the light deflection caused in it results in a distortion of the image of the scale at L'. If ϵ is the light deflection at one point, this corresponds to a displacement

$$\Delta a = \epsilon \cdot b$$

at the location of the scale and a shift

$$\Delta a' = G \cdot \epsilon \cdot b$$

Cover Page Source

in the image of the scale, if G represents the scale of the exposure;

$$G = \frac{z'}{z}$$

$\Delta a'$ can be read off for each point from the photograph of the distorted scale, and then

$$\epsilon = \frac{1}{f} \frac{\Delta a'}{b}$$

(113)

This angle is valid for that position of the cell from which the displaced light beam comes. If the distance Y of the displaced point of the scale from the optical axis is measured, this corresponds to the distance

$$y = \frac{1}{f} \frac{l-b}{l} \cdot Y = \frac{l-b}{f} \cdot Y$$

(114)

in the object.

However, in practice the scale is photographed twice in succession under the same conditions with and without deflection. In order for the displaced scale to appear sharply as small an aperture as possible is necessary; otherwise light deflection of various sizes will pertain to the individual light rays of one bundle.

/429

NA 31

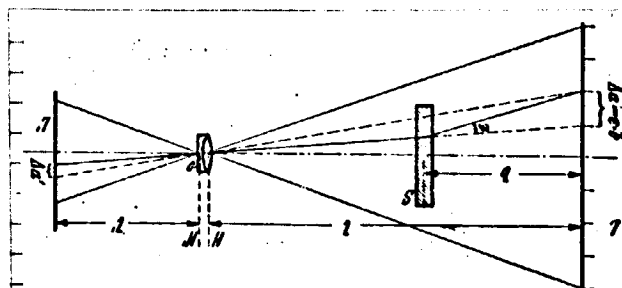


Figure 123. Schematic of the Scale Method.

Essentially this method corresponds to schlieren arrangement number 2, but with exposure of the scale and not of the object (cf. below 364).

The slit method was introduced into ultracentrifuge technology by O. Lamm. By means of a schlieren head a line of light is projected through a slit-shaped schlieren diaphragm. Now the line of light, measurable with a micrometer, is displaced

with light deflection until the spot in the object to be measured is exposed again. Observation takes place visually. Naturally adjustment of the light source requires time so that only measurement of the sedimentation equilibrium can be carried out in this way.

Cover Page Source

The lattice diaphragm method described as method number 7 basically accomplishes more than the slit method since it furnishes the pertinent location for several light deflections at the same time; therefore this should also be of value in the service of ultracentrifuge technology. It would particularly permit changes of light deflection in time to be recorded simply by making a photographic registration of the isophots behind a slit onto paper rotating at a suitable velocity.

Direct registration of the light deflection as a curve is possible with a method of J. Thovert [49], which has been somewhat modified by Philpot (cf. p. 348).

The cells for the fluid in the ultracentrifuge have the shape of a sector with the point at the center of rotation in order to avoid disruptive convection currents. Sensitivity increases with increasing thickness of the liquid layer. Difficulties occur if the thickness is too great when the scale method is used, because with this method the cell is radiated by divergent light; then the use of a parallel ray pencil is necessary, e.g., as in the investigation of a horizontal heating pipe with a lattice diaphragm method.

/430

It is beyond the scope of this paper to go into the physical fundamentals of evaluating the measured results. The centrifugal force $m\omega^2 r$, operating on a particle of mass m at a distance r from the center of rotation and angular velocity ω , causes a separation of the particles according to their mass, while diffusion has a tendency to mix them (cf. §29). Now, the sedimentation velocity or the sedimentation equilibrium can be measured in order to obtain molecular data where determination according to the otherwise normal chemical and physical methods is extremely uncertain.

In particular the native albumen bodies or proteins represent an area of organic chemistry which has not been well investigated.

It is true that the approximate analytical composition (50 to 55% C; 6.5 to 7.3% H; 15 to 18% N; 21 to 24% O; 0 to 2.4% S; ash) are known, as well as a few amino acids from which the proteins are constructed. However the kind and amount of the individual building blocks is very different and the multitude of protein species extremely great.

Above all, the determination of molecular size was uncertain up to now.

Svedberg and his colleagues investigated a large number of animal and plant proteins with the aid of the ultracentrifuge. Only a small part of these is contained in the following tables in which the sedimentation constants are given (for 20°C; the numerical values have been multiplied by a factor 10^{13}). The hemoglobin of amphibians and reptiles has two components.

TABLE 10. HEMOGLOBIN.

Man	4.48
Horse	4.41
Rabbit	4.4
Chicken	4.2
Pigeon	4.4
Fish	4.1—4.5
Amphibian	4.5—4.8; 7.0—7.7
Reptile	4.5—4.8; 7.43

TABLE 11. ERYTHROCRUORIN.

Arenicola marina	57.4
Lumbricus terrestris	60.9
Planorbis corneus	33.7
Daphnia pulex	16.3

Tr. note: Commas indicate decimal points.

Although the individual kinds of hemoglobin are chemically different, as demonstrated by determination of the isoelectric point, they show considerable agreement in their sedimentation constants. In all of them the molecular weight amounts to about 68,000. In the case of amphibians and reptiles proteins of various molecular weights were found next to one another.

In contradistinction to the blood pigments included in blood particles, those directly dissolved in the blood plasma (Erythrocruorins) have higher sedimentation constants and therefore a higher molecular weight of about 3,000,000.

One peculiarity of proteins, their stability in the presence of various pH values, has been studied in more detail in several Erythrocruorins. These stability diagrams demonstrate the range where the individual protein molecules are durable, at what H concentration dissociation occurs, and in what range several materials are stable next to one another.

Sedimentation constants of $16 - 100 \cdot 10^{-13}$ were found in the hemocyanines

TABLE 12. HEMOCYANINES.

	$s_{20} \cdot 10^{13}$	M
Palinurus vulgaris	16,4	447000
Homarus vulgaris	22,6	803000
Calocaris macandreae	34	1329000
Octopus vulgaris	49,3	2785000
Helix pomatia	98,9	6630000

Tr. note: Commas indicate decimal points.

Svedberg's extremely numerous investigations go all the way from serum proteins to the proteins of muscles, milk and plants, as well as including enzymes, hormones and many other substances.

In conclusion it should be stated that the ultracentrifuge has produced surprising results. The native, soluble proteins are thus shown to consist of one individual or several small molecular types of well-defined mass and shape; it seems that only a limited number of weight classes occur, multiples of a basic mass unit. If the basic unit is selected as 17,600, it must be multiplied by 2, 4, 8, 16, 24, 48, 96, 192, 384, and 576 to produce the weights which occur. A few proteins are compared in the following table in order to clarify this theory:

TABLE 13.

	$s_{20} \cdot 10^{13}$	M _{found}	M _{comp.}
Lactalbumin	1,9	17400	17600
Pepsin	3,3	35500	35200 = 2 · 17600
Hemoglobin (Horse)	4,4	68000	70400 = 4 · 17600
Myogen A	7,86	150000	140800 = 8 · 17600
Excelsin	13,3	295000	282000 = 16 · 17600
Hemocyanine (Palinurus)	16,4	450000	422000 = 24 · 17600
(Nephrops)	24,5	820000	845000 = 48 · 17600
(Rossia)	56,2	3300000	3380000 = 192 · 17600
(Helix pomatia)	98,9	6600000	6760000 = 384 · 17600

Tr. note: Commas indicate decimal points.

Even though deviations occur with some proteins, the regularity observed cannot be accidental. Deviations may appear because the individual molecules are not chemically equal, but consist of larger and smaller amino acids. Even the presence of other organic bodies may be involved.

/432

In addition, the ultracentrifuge method did not only lead to the fact that the existence of the molecules is related to a certain pH range, but has also allowed exact measurement of this range and determined the existence of other components.

Even the influence of salt solutions, the effect of ionic valances, the reciprocal influence of proteins, splitting of gigantic molecules by ultraviolet light and ultrasound were able to be investigated with this method.

Finally this method has confirmed the findings of X-ray studies that proteins are really unit molecules and not an association of smaller molecules.

Clarification of experimental observations on proteins is supported by being able to consider them as consisting of spherical or nearly spherical particles.

This is not the case with linear high polymers, particularly with fibroid macromolecules.

Rubber, cellulose and other organic materials consist of fibroid molecules which have a thickness of a few Å units and are 100 to 1,000 times as long. In suitable solvents they are dispersed into individual molecules. Still, we are compelled to work in very dilute solutions (0.4 g/l) because otherwise considerable deviations would occur. This is because the osmotic pressure is greater than that which corresponds to the number of particles.

Other difficulties which occur in investigating these materials are the following:

Neither the natural nor the synthetic materials possess a unit molecular weight, but always consist of adjacent molecules of differing magnitude, and are therefore polydisperse.

Sedimentation velocity is disturbed by the shape of the molecule. Whether a molecule has the shape of a lengthy fiber or whether it is more or less coiled up into a ball is not immaterial.

The ultracentrifuge still has a large role to play in research on these macromolecules.

The requirement of working in sufficiently dilute solutions can be better met with the ultracentrifuge than with the osmometer in determining molecular size.

NASA

Even

Roman

125
Odd

If sedimentation velocity is sufficiently high and diffusion sufficiently low, a complete determination of type and amount of adjacent particles of varying sizes can be obtained in the centrifuge cell, while otherwise only the mean molecular weight can be ascertained with no expression of the type of polydispersion.

Cover Page Title

If other experimental data are called upon, the ultracentrifuge method can also facilitate determination of molecular shape. For example, the fibroid shape of nonsolvated particles, which involve a considerable volume of solvent in their movement, can be identified by the fact that with an increase in concentration they produce a sedimentation velocity of essentially smaller dimensions.

/433

31. Other Applications

The foregoing discussions have shown by means of example how indispensable the schlieren methods are for many types of physical research. Naturally the range of application has not been exhausted with the summary given above, and many interesting papers dealing with schlieren methods are scattered through the literature. Quite often their authors think that they have found an especially suitable optical arrangement and are not conscious of having constructed a schlieren method. In many cases the light deflections occurring are so large that the lens mountings work like schlieren diaphragms. For example, in the arrangement which lead Benard to discover the laws of a turbulent path, he used a water container. Light penetrating it was used to make the surface waves visible and the deflected light fell completely out of the projecting lens. Naturally if a correct schlieren arrangement had been used, the sensitivity would have been considerably greater.

An interesting suggestion for large projection by television is made by F. Fischer [132]. A cathode ray tube contains a thin layer of oil whose surface is deformed by a pulsing and modulated cathode ray corresponding to the television image. The schlieren image of the oil layer is expected to illuminate a large moving picture screen.

In a similar way the author tried some time ago to transform an ultrared image into a visible picture: the ultrared light causes schlieren in a suitable layer and the schlieren serve as the object of a schlieren arrangement. For example, it was possible in this way to make the flame of a Bunsen burner visible.

Bergmann [109] uses the schlieren of continuous supersonic waves in liquids to measure the speed of sound by bringing the schlieren image to a stop with a rotating mirror.

H. Schardin and W. Struth [121] found the origin of "implosion pressure waves" in water in the sudden vacuum phenomenon of air bubbles (Figure 124). A similar process is also produced in cavitation; here too the existence of such pressure waves was assumed and they were held responsible for excessive

corrosion phenomena, but could not be directly detected (cf. P. de Haller [133], among others).

In optical laboratory practice the sensitive detection of schlieren serves to measure refractive relationships between small glass splinters by placing them into a fluid whose refractive index can always be varied by mixing two different parts of the fluid.

/434

F. Klauer, E. Turowski and T. v. Wolff have used the schlieren method to investigate the magnetic properties of oxygen [143]¹.

If a heating wire surrounded by oxygen is put into an inhomogeneous magnetic field, magnetic convection currents are added to the normal currents and, if both have the same direction, they lead to a faster cooling of the wire. A determination of oxygen can be physically carried out on the basis of this cooling.

Figures 125a and b provide an example for the influence of current in the inhomogeneous magnetic field. The left picture shows the heat field in the vicinity of the heating wire if no magnetic field is present between the poles to be identified at the contours. The right-hand picture shows how the heated gas is directed downward after the magnet is switched on. In this case both convection currents flow in opposite directions.

Until now schlieren methods were generally considered a measurement process which could be applied only in a few cases and which therefore remain somewhat beyond general laboratory practice. The purpose of these remarks would be achieved if they contributed to eliminate this prejudice. Today the schlieren methods are a tool of experimental physics with more general importance.

/435

Figure 124. Propagation of Implosion Pressure Waves in Water From Air Bubbles Which Had Been Attached to a Wire at the Moment of a Sudden Drop in Pressure When a Bullet was Fired Into the Water Container.

¹Cf. also H. Rein: "Determination of Oxygen by a Physical Method," *Schriften, Dtsch. Akad. Luftfahrtforsch.*, No. 11, 1940.



Figure 125a.



Figure 125b.

Figures 125a and b. Schlieren Exposures in the Vicinity of a Heating Wire in an Inhomogeneous Magnetic Field. a, Without Field; b, With Field.

In conclusion I have the pleasant duty of thanking Mr. G. Stamm, D. Ph., for the help he has provided me in writing this report.

REFERENCES

(41)

1. Foucault, Leon, *Ann. de l'Observatoire Imp. de Paris*, Vol. 5, p. 197, 1859.
2. Toepler, A., *Beobachtungen Nach einer Neuen Optischen Methode* [Observations According to a New Optical Method], Bonn, 1894; *Poggendorfs Ann.*, Vol. 127, p. 556, 1866; Vol. 128, p. 126, 1866; Vol. 131, p. 33, 180, 1867; Vol. 134, p. 194, 1868.
3. Mach, E., *Poggendorfs Ann.*, Vol. 159, p. 330, 1876.
4. Mach, E., and G. Gruss, *Wiener Berichte*, Vol. 78, p. 467, 1878.
5. Foucault, Leon, *Recueil des Travaux Scientifiques* [Summary of Scientific Works], Paris, 1878.
6. Dvorak, V., *Wiedemanns Ann.*, Vol. 9, p. 502, 1880.
7. Exner, S., *Repert. d. Phys.*, Vol. 21, p. 555, 1886.
8. Czapski, S., *Z. f. Instrumentenkle.*, Vol. 6, p. 139, 1886.
9. Thiel, E., *Arch. Artillerie- und Ingenieur-Offiziere d. Dtsch. Reichsheeres*, Vol. 94, p. 485, 1887.
10. Mach, E., *Wiener Berichte*, Vol. 95, p. 764, 1887; Vol. 98, pp. 41, 1303, 1310, 1327 and 1333, 1889.
11. Mach, E., *Ann. Physik u. Chemie*, Vol. 41, p. 140, 1890.
12. Boys, Z. *Phot. Soc.*, p. 119, 1892.
13. Wiener, O., *Wiedemanns Ann.*, Vol. 49, p. 105, 1893.
14. Boys, *Nature*, London, Vol. 47, p. 415, 1893.
15. Mach, L., *Z. Luftschiffahrt u. Physik der Atmosphaere*, Vol. 15, p. 129, 1896.

16. Obermayer, A. v., *Z. Luftschiffahrt u. Physik der Atmosphaere*, Vol. 15, p. 120, 1896.
17. Mach, L., *Wiener Berichte*, Vol. 105, p. 605, 1896.
18. Obermayer, A. v., *Mitt. Gegenstaende des Artillerie- und Genie-Wesens*, p. 815, 1897.
19. Mach, L., *Wiener Berichte*, Vol. 106, p. 1025, 1897.
20. Vielle, *Mem. des Poudres et Salpêtres*, Vol. 10, p. 177, 1899.
21. Emden, R., *Wiedemanns Ann.*, Vol. 69, pp. 264, 426, 1899.
22. Wood, R. W., *Philos. Mag.*, Vol. 48, p. 218, 1899; Vol. 50, p. 148, 1900; Vol. 52, p. 589, 1901.
23. Rieckeherr, *Kriegstechn. Z.*, Vol. 3, pp. 383, 439, 513, 1900.
24. Cranz, C., and R. Koch, *Ann. d. Phys.*, Vol. 3, p. 247, 1900.
25. Cranz, C. and R. Koch, *Anwendung der Elektrischen Momentphotographie auf die Untersuchung von Schusswaffen*, [The Use of Electrical Instantaneous Photographs in Weapons Research], Halle, Wilhelm Knapp, 1901.
26. Wierz, Melchoir, *Beitraege zur Theorie der Lichtbahnen und Wellenflaechen in Heterogenen Isotropen Medien*, [Contributions to the Theory of Light Paths and Wave Surfaces in Heterogeneous Isotropic Media], Dissertation Rostock, 1901.
27. Allen, H. S., *Proc. Roy. Philos. Soc.*, Glasgow, Vol. 33, p. 71, 1902.
28. Tufts, T. H., *Physic. Rev.*, Vol. 14, p. 57, 1902.
29. Wachsmuth, R., *Physik. Z.*, Vol. 4, p. 745, 1903.
30. Wachsmuth, R., *Ann. d. Phys.*, Vol. 14, p. 469, 1904.
31. Wood, R. W., *Physical Optics*, London, McMillan and Co., p. 94, 1905.
32. Toepler, A., "Observations According to a New Optical Method," *Ostwalds Klassiker der Exakten Wissenschaften*, No. 157, Leipzig, 1906.
33. Toepler, A., "Observations According to the Schlieren Method," *Ostwalds Klassiker der Exakten Wissenschaften*, No. 158, Leipzig, 1906.
34. Straubel, R. and Winkelmann's *Handbuch der Physik*, [Handbook for Physics], Vol. 6, p. 485, Leipzig, Johann Ambrosius Barth, 1906.
35. Dvorak, V., *Z. Physik. Chem. Unterricht*, Vol. 21, p. 17, 1908.
36. Magin, *Optische Untersuchungen ueber den Ausfluss von Luft Durch eine Lavalduese*, [Optical Investigations of the Efflux of Air Through a Laval Nozzle], Dissertation, Gottingen, 1908.
37. Meyer, Th., *Ueber Zweidimensionale Bewegungsvorgaenge in Einem Gas, das Mit Ueberschallgeschwindigkeit Stromt*, [Two Dimensional Movement Phenomena in a Gas Streaming at Supersonic Velocity], Dissertation, Gottingen, 1908.
38. Weinhold, *Z. Physik. Chem. Unterricht*, Vol. 21, p. 281, 1908.
39. Benard, H., *C. R. Acad. Sci.*, Paris, Vol. 147, p. 970, 1908.
40. Toepler, N., *Ann. d. Phys.*, Vol. 27, p. 1043, 1908.
41. Tanakadate, A., *C. R. Acad. Sci.*, Paris, Vol. 151, p. 211, 1910.
42. Lafay, A., *Techn. Aeron.*, Vol. 3, p. 169, 1911; Vol. 4, p. 91, 1911.
43. Lafay, A., *C. R. Acad. Sci.*, Paris, p. 694, 1911.
44. Cranz, C. and P. A. Guenther, *Z. Ges. Schiess- u. Sprengstoffwesen*, Vol. 7, p. 317, 1912.
45. Foley, and Sonder, *Physic. Rev.*, Vol. 35, p. 373, 1912.
46. Cranz, C. P. A. Guenther and F. Kuelp, *Z. Ges. Schiess- u. Sprengstoffwesen*, Vol. 9, p. 61, 1914.

47. Cranz, C. and B. Glatzel, *Ann. d. Phys.*, Vol. 43, p. 1186, 1914.
48. Cranz, C. and F. Kuelp, *Angewandte Phys.*, Vol. 88, p. 251, 1914.
49. Thovet, I., *Ann. de Physique*, Vol. 2, p. 369, 1914.
50. Ray, B., *Proc. Indian Ass. Cult. Sci.*, Vol. 6, p. 95, 1920.
51. Pramanik, S. Ch., *Proc. Indian Ass. Cult. Sci.*, Vol. 7, p. 115, 1922.
52. Quayle, Z. *Franklin Inst.*, Vol. 19, p. 193, 1922.
53. Cranz, C. and E. Barnes, *Z. Angew. Chem.*, Vol. 36, p. 76, 1923.
54. Wartenberg and Kannenberg, *Z. Physik. Chem.*, Vol. 105, p. 205, 1923.
55. Nelson, R. A., *Physic. Rev.*, Vol. 23, p. 94, 1924.
56. Terazawa, K. Yamazaki, Y. Akishino, *Rev. Aeronaut. Res. Inst.*, Tokyo, Vol. 1, p. 213, 1924.
57. Quayle, *Nature*, London, Vol. 115, p. 765, 1925.
58. Humphrey, R. H. and R. S. Jane, *Trans. Faraday Soc.*, Vol. 22, p. 420, 1926.
59. Payman, W. and H. Robinson, *Safety in Mines Research Bord Paper*, Nos. 18 and 29, 1926.
60. Cranz, C., *Lehrbuch der Ballistik*, [Textbook of Ballistics], Vol. 3, Second Edition, pp. 259, 264, Berlin, Springer, 1927.
61. Auerbach, F. and W. Hort, *Handbuch der Physikalischen und Technischen Mechanik*, [Handbook of Physical and Technical Mechanics], Vol. 5, p. 486, Leipzig, Johann Ambrosius Barth, 1928.
62. Lamm, O., *Z. Physik. Chem. A.*, Vol. 138, p. 313, 1928.
63. Payman, W., *Proc. Roy. Soc., London. A.*, Vol. 120, p. 90, 1928.
64. White, Z. *Chem. Soc.*, p. 1159, 1928.
65. Cranz, C. and H. Schardin, *Z. Physik.*, Vol. 56, p. 147, 1929.
66. Kohlrausch, Fr., *Lehrbuch der Praktischen Physik*, [Textbook of Practical Physics], 6th Edition, p. 504, Leipzig and Berlin, Teubner, 1930.
67. Schrott, P., *Kinotechn.*, Vol. 12, p. 40, 1930.
68. Schmidt, F., *Z. VDI*, Vol. 74, p. 1487, 1930.
69. Lindner, W., "Multiple Spark Exposure of Explosive Processes According to the Toepler Schlieren Method," *VDI-Forsch.*, No. 326, Verlag Berlin, VDI 1930.
70. Tawil, E. P., *C. R. Acad. Sci.*, Paris, Vol. 191, pp. 92, 998, 1930.
71. Kieser, K., *Phot. Ind.*, Vol. 28, p. 729, 1930; *Z. Angew. Chem.*, Vol. 43, p. 587, 1930.
72. Laffitte, P. and Patrie, *C. R. Acad. Sci.*, Paris, Vol. 191, p. 1335, 1930.
73. Vauthier, *Ann. de Physique*, Vol. 14, 1930.
74. Townend, H. C. H., "On Rendering air Flow Visible by Means of Hot Wires," *Reports and Memoranda*, p. 1349, 1930. British Aeronautical Research Committee.
75. Tietjens, O., in W. Wien and F. Harms' *Handbuch der Experimentalphysik*, [Handbook of Experimental Physics], Vol. 1, p. 695, Leipzig, 1931.
76. Gawthrop, D. B., W. C. F. Shepherd and G. St. Perrolt, *J. Franklin Inst.*, Vol. 211, p. 67, 1931.
77. Payman, W. and D. B. Woodhead, *Proc. Roy. Soc. Inst.*, Vol. 2, p. 522, 1931.
78. Nadai, A., *Proc. Amer. Soc. Test. Mat.*, Vol. 31, p. 2, 1931.
79. Klug, H., *Ann. d. Phys.*, Vol. 5, No. 11, p. 53, 1931.

/437

80. Lindner, W., *Entzündung und Verbrennung von Gas- und Brennstoffdampf-Gemischen*, [Ignition and Combustion of Gas and Fuel Vapor Mixtures], Berlin, VDI-Verlag, 1931.
- 5 81. Busemann, in W. Wien and F. Harms' *Handbuch der Experimentalphysik* [Handbook of Experimental Physics], Vol. IV/I, 1931.
82. Gawthrop, D. B., *J. Franklin Inst.*, Vol. 214, p. 647, 1932.
83. Bucerius, W., *Betriebsführung*, Vol. 11, No. 33, 1932.
84. Schmidt, E., *Forsch. Ing.-Wes.*, Vol. 3, p. 181, 1932.
- 10 85. Bucerius, W., *Schornsteinfeger und Technik*, [Chimney Screens and Technology], pp. 57, 65, Berlin, 1932.
86. Schardin, H., *Heizung und Lueftung*, [Heating and Air Conditioning], p. 167, 1932.
87. Malz, Hermann, *Die Grenzen der Schneidegeschwindigkeit beim Brennschneiden*, [The Limits of Cutting Velocity in Flame Cutting], Dissertation, Berlin, 1932.
- 15 88. Malz, Hermann and Conrady, *Autog. Metallbearb.*, Vol. 25, p. 117, 1932.
89. Shepherd, W. C. F., *Bur. Mines Bull.*, No. 354, 1932.
90. *Annual Report of National Physical Laboratory for 1932.*
- 20 91. "Hot Wire or Spark Shadowgraphs of the Airflow Through an Airscrew," *Philos. Mag.*, Vol. 14, p. 700, 1932.
92. Erk, S., *Z. VDI*, Vol. 77, p. 1119, 1933.
93. Gregor, C. W. M., *Metals and Alloys*, Vol. 4, p. 19, 1933.
94. Gregor, C. W. M., *World Power*, Vol. 19, p. 75, 1933.
- 25 95. Lamm, O., "A New Method for Determination of the Concentration Gradient in the Ultracentrifuge," *Nature*, London, Vol. 132, p. 820, 1933.
96. Patry, *Verbrennungen und Detonationen von Festen Sprengstoffen*, [Combustion and Detonation of Solid Explosives], Munich, 1933.
97. Taylor-Maccoll, *Proc. Roy. Soc. Lond. A.*, Vol. 139, p. 838, 1933.
- 30 98. Taylor, H. G. and J. M. Waldram, *J. Sci. Instrum.*, Vol. 10, p. 378, 1933 plus three letters, Vol. 11, p. 31, 1934.
99. Luft, F., *Photo-Woche*, Vol. 24, No. 2, 1933. Reference *Kinotechn.*, Vol. 16, p. 27, 1934.
100. Townend, H. C. H., "Improvements in the Schlieren Method of Photography" *J. Sci. Instrum.*, Vol. 11, p. 184, 1934.
- 35 101. Townend, H. C. H., "Statistical Measurements of Turbulence in the Flow of Air Through a Pipe," *Proc. Roy. Soc. Lond. A.*, Vol. 145, 1934.
102. Schardin, H., "The Toepler Schlieren Method," *VDI-Forsch.*, No. 367, July-August, 1934.
- 40 103. Townend, H. C. H., "Flow Induced by a Jet of Air," *Reports and Memoranda*, p. 1634, 1934. British Aeronautical Research Committee.
104. Scheffler, Karl, *Thesis*, Technical inst., Berlin, 1934.
105. Pohlmann, R., "Visualization of Ultrasound in Gases and Measuring Its Intensity," *Naturwiss.*, Vol. 23, p. 511, 1935.
- 45 106. Payman, W. and H. Titman, *Proc. Roy. Soc., Lond. A.*, Vol. 152, p. 418, 1935.
107. Payman, W., *Nat. Phys., Rep. for the Year 1934*, London: His Majesty's Stationary Office, 1935. Ref. *Z. VDI*, Vol. 80, p. 702, 1936.
- 50 108. Gaebler, Joh., *Thesis*, Technical Institute, Berlin, 1935.

/438

109. Bergmann, L., "Recent Problems in the Ultrasonic Field," *Z. Techn. Physik*, Vol. 17, p. 512, 1936.
110. Hermann, R., "Heat Exchange in Free Flow on a Horizontal Cylinder and Diatomic Gases," *VDI-Forsch.*, No. 379, 1936.
111. Krueger, F. and H. Casper, "Turbulent Formation in Strident Sounds," *Z. Techn. Physik.*, Vol. 17, p. 417, 1936.
112. Krumm, E., "Heat Movement in Fluids and Gases," *Unterrichtsbl. f. Math. Naturw.*, Vol. 42, p. 96, 1936.
113. Townend, H. C. H., "A Method of Air Flow Cinematography Capable of Quantitative Analysis," *J. Aeron. Sci.*, Vol. 3, p. 343, 1936.
114. Try, S., "The Sensitivity of the Schlieren Camera," *Etz.*, Vol. 30, p. 683, 1936.
115. Zobel, Theodor, *Erhoehung der Schneideschwindigkeiten beim Brennschneiden Durch Neue Duesenformen*, [Raising the Cutting Velocities in Flame Cutting by New Nozzle Shapes], *Dissertation*, Technical Institute Berlin, 1936.
116. Osswald, F. M., *Z. Techn. Physik*, Vol. 17, p. 561, 1936.
117. Bone, W. A.; R. P. Fraser and H. W. Wheeler, *Phil. Trans. Roy. Soc. Lond. A.*, Vol. 235, p. 29, 1936.
118. Jensen-Marwedel, Hans, *Glastechnische Fabrikationsfehler*, [Manufacturing Defects in Glass Technology], Berlin, Springer, 1936.
119. Tiselius, A.; K. O. Pedersen and S. B. Eriksson Quensel, "Observation of Ultracentrifugal Sedimentation by the Toepler Schlieren Method," *Nature*, London, Vol. 139, p. 546, 1937.
120. Schaeffs, W., "A Schlieren Test on the Oscillation Mode of a Thin Quartz Disk," *Z. Physik.*, Vol. 105, p. 57, 1937.
121. Schardin, H. and W. Struth, *Z. Techn. Physik*, Vol. 18, p. 474, 1937.
122. Klassen, Tatjana, *Technical Physics USSR*, Vol. 4, p. 448, 1937.
123. Malsch, I., *Ann. Physik.*, Vol. 30, p. 534, 1937.
124. Zeiss Patent 26 Aug. 1937: *Geraet zum Pruefen der Oberflaechenbeschaffenheit Gekruemmter Spiegelnder Koerper im Reflektierten Licht*, [Device For Testing the Surface Condition of Curved Mirror Bodies in Reflected Light].
125. Payman, W. and W. C. F. Shepherd, *Journ. Roy. Soc. London*, Vol. 158, p. 348, 1937.
126. Seddon, E., *Journ. Soc. Glass Techn.*, Vol. 21, p. 281, 1937.
127. Philpot, G. St. L., *Nature*, London, Vol. 141, p. 283, 1938.
128. Schmidt, O. v., *Z. Techn. Physik.*, Vol. 19, p. 554, 1938.
129. Andersson, K. G. I., *Nature*, London, Vol. 143, p. 720, 1939.
130. Svensson, H., *Kolloid- Z.*, Vol. 87, pp. 181-186, 1939.
131. Weidert, Franz, *Glastechn. Ber.*, Vol. 17, p. 167, 1939.
132. Fischer, F., *Schweizer Arch. Angew. Wiss. Techn.*, Vol. 6, p. 89, 1940.
133. De Haller, P., *Schweizer Arch. Angew. Wiss. Techn.*, Vol. 6, p. 61, 1940.
134. Hansen, G., *Zeiss- Nachrichten*, Vol. 3, p. 302, 1940.
135. Schmidt, O. v. and A. Kling, *Physik. Z.*, Vol. 17-18, p. 407, 1940.
136. Tuttle, Clifton and Randle Cartwright, "A Method for the Measurement of Flatness of Polished Surfaces," *J. Opt. Soc. Amer.*, Vol. 30, p. 348, 1940.

NASA

/439

5	137. Svedberg, The and Kai O. Pedersen, <i>Die Ultrazentrifuge Theorie. Konstruktion und Ergebnisse</i> [The Ultracentrifuge Theory, Construction and Results], Dresden "Theodor Steinkopff, 1940 equals <i>Handbuch der Kolloidwissenschaft in Einzeldarstellungen</i> , [Handbook of Colloidal Science in Individual Presentations], Vol. 7.
	138. Reil and Lerch, <i>Glastechn. Ber.</i> , Vol. 18, p. 113, 1940.
10	139. Van de Poll, A. N. I. and T. Westerdijk, <i>Z. Techn. Physik.</i> , Vol. 2, p. 29, 1941.
	140. Schardin, H. Short Review in <i>Opt. Rdsch, u. Photo-Optiker</i> , Vol. 31, 1941.
	141. Springer, L., <i>Glashuette</i> , Vol. 71, pp. 169, 193, 1941.
	142. Jebesen-Marwedel, G., <i>Glashuette</i> , Vol. 71, pp. 362, 527, 1941.
15	143. Klauer, F., E. Turowski and D. V. Wolff, <i>Z. Techn. Physik.</i> , Vol. 22, p. 223, 1941.
	144. Schardin, H. and G. Stamm, "Testing Flat Glass Using a Colored Schlieren Method," <i>Glastechn. Ber.</i> , Vol. 20, p. 249, 1942.
20	Cover Page Source
	Translated for the National Aeronautics and Space Administration under contract No. NASw-1695 by Techtran Corporation, P.O. Box 729, Glen Burnie, Md. 21061.
25	(4'')
30	
35	
40	
45	
50	NASA

Plate I

Page One Title

5
10
15
20
25
30
35
40
45
50



Figure 7

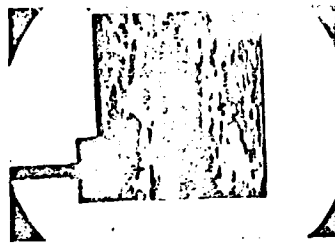


Figure 32

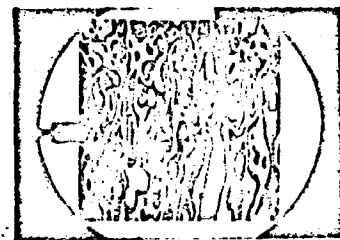


Figure 67



Figure 36

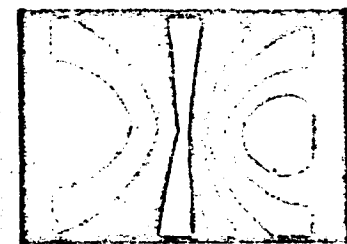


Figure 126

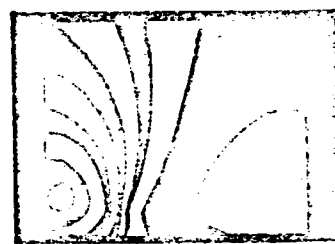


Figure 127

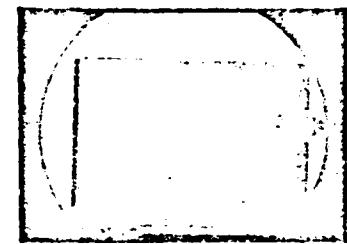


Figure 64

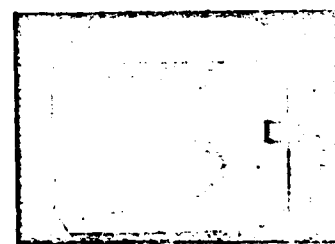


Figure 65

Colored Photographs Taken With the Lattice Diaphragm and Prism Methods

NASA

Plate II

Page One Title

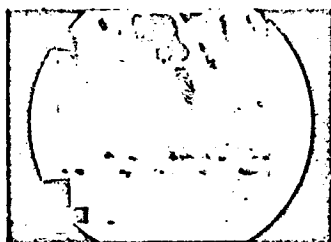


Figure 68

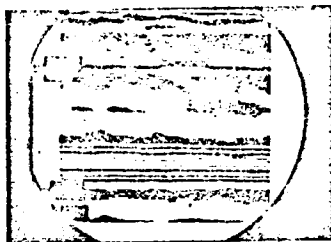


Figure 69

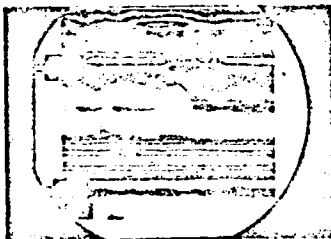


Figure 70

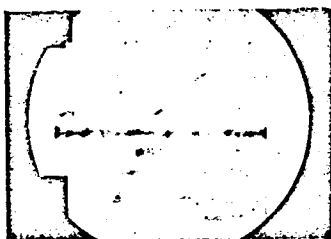


Figure 71

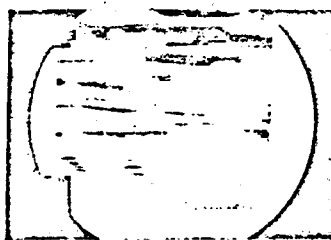


Figure 72

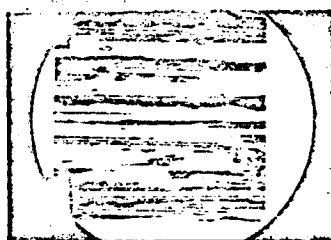


Figure 73



Figure 113

Figures 68 to 73. Colored Photographs of Structural Glass Taken With the Lattice Diaphragm Method.

Figure 113. Colored Photographs of Surface Waves.

NASA